UNIVERSITÀ DEGLI STUDI DI TRIESTE

DIPARTIMENTO DI SCIENZA DELLA VITA
School of Molecular Biomedicine

Translational Approach for the Study of Metabolic Dysfunction-Associated Steatotic Liver Disease (MASLD): A Wide Spectrum Disease

A thesis submitted for the degree of Doctor of Philosophy in Molecular Biomedicine (Ph.D.)

– XXXV Cycle –

Ph.D. Student:
Noel C. Salvoza

Ph.D. Coordinator:
Germana Meroni, Ph.D.
Università degli studi di Trieste

Supervisor:
Claudio Tiribelli, M.D., Ph.D
Fondazione Italiana Fegato

Co-supervisor:
Natalia Rosso, Ph.D.
Fondazione Italiana Fegato

Academic Year 2021/2022

TABLE OF CONTENTS

LIST OF FIGURES

LIST OF TABLES

SUMMARY

Metabolic dysfunction-associated steatotic liver disease (MASLD) is a major cause of chronic liver disease worldwide. It encompasses a wide spectrum of conditions, ranging from simple steatosis (MAFL) to the more severe metabolic dysfunction-associated steatohepatitis (MASH). At present, diagnosis still depends on liver biopsy, an invasive procedure with some risks for the patient. Furthermore, to date, there is no approved pharmacological treatment. Consequently, there is an urgent need to develop non-invasive diagnostic biomarkers and to identify new therapeutic targets for MASLD. Further studies are also necessary to study the crosstalk of the liver with other organs to provide a more extensive view of its pathogenesis. In general, we aimed to fulfill the existing scientific gaps in terms of therapy, diagnosis, and pathophysiology of MASLD using a translational approach. Firstly, we assessed the effect of novel therapeutic compounds in reverting the MASLD-related pathophysiological mechanisms. Then, we identified and validated new non-invasive biomarkers for liver fibrosis in MASLD patients. Lastly, we investigated the potential role of omentin-1, a novel adipocytokine expressed by visceral adipose tissue (VAT) in obesity-related MASLD.

Therapy: Triterpenic acid and acteoside, the major components of APPLIVER and ACTEOS respectively, have been reported to exert hepatoprotective effects but the molecular mechanisms remain elusive, particularly in the MASLD context. We assessed their effects in an *in vitro* model resembling the MASLD-related pathophysiological mechanisms. ACTEOS reduced both the TNF-α and reactive oxygen species (ROS) production and, most importantly, attenuated collagen deposition elicited by the excess of free fatty acids (FFA) in the co-culture model. APPLIVER also showed inhibition of both TNF-α production and collagen deposition caused by FFA accumulation. The compounds in the absence of FFA did not induce any cellular effects.

Diagnosis: Several reports indicate fibrosis as the strongest predictor of long-term clinical outcomes in MASLD patients. We assessed the performance of plasma ficolin-2 (FCN-2) as a biomarker of fibrosis identified by an *in silico* discovery strategy. The plasma level of FCN-2 was inversely correlated with the stage of liver fibrosis, independently of steatosis, inflammation, and ballooning. Moreover, FCN-2 level decreased significantly in a stepwise fashion from minimal- (F0/F1) to moderate/advanced- fibrosis (F2-F3) and in cirrhotic subjects (F4). The diagnostic performance of FCN-2 in detecting $F \geq 2$ was higher than other non-invasive fibrosis algorithms (APRI, FIB-4). The diagnostic accuracy improved when combined with AST to Platelet Ratio Index (APRI) score and high-density lipoprotein (HDL). Overall, FCN-2 plasma level can accurately

discriminate liver fibrosis status (minimal *vs.* moderate/advanced), thereby significantly improving fibrosis diagnostic algorithms.

Pathophysiology: Through our simple *in silico* analysis, we identified omentin-1, a novel adipocytokine expressed by VAT, and we explored its role in obesity-related MASLD. In clinical validation, the obese groups showed significantly lower VAT expression (mRNA and protein) and plasma level of omentin-1 as compared to the lean group. Interestingly, within the MASH group, fibrosis did not affect omentin-1 expression. Likewise, VAT of mice fed with a high-fat diet, showing histological signs of MASH, showed decreased omentin-1 (mRNA and protein) as compared to control diet mice. *In vitro,* omentin-1 addition on fat-laden human hepatocytes showed no effect in steatosis but significantly decreased TNF-α levels, ER stress, and oxidative stress. The same results were obtained using *ex vivo* VAT explants from obese subjects upon omentin-1 supplementation. In addition, omentin-1 reduced nuclear factor kappa B (*NF-κB*) mRNA expression in both *in vitro* and *ex vivo* set-ups. In VAT explants, D-glucose and insulin significantly reduced omentin-1 expression (mRNA and protein level). Altogether, our findings suggest that reduced levels of omentin-1 contribute to MASLD development. Omentin-1 supplementation reduces inflammation, ER stress, and oxidative stress probably via inhibiting the NF-κB pathway and might also play a role in the regulation of glucose-insulin metabolism.

Our data highlight the importance of translational research in understanding the pathophysiology, diagnosis, and therapy in the context of MASLD. *In silico* strategy allowed us to identify potential diagnostic/therapeutic targets of MASLD. Then, *in vitro* and *ex vivo studies* paved the way to understand the role of APPLIVER, ACTEOS, and omentin-1 as promising therapeutic compounds in counteracting MASLD-related pathophysiological mechanisms. Lastly, *in vivo* clinical validation demonstrated that FCN-2 could be a potential non-invasive biomarker for significant fibrosis. Altogether, these new findings lead to a better understanding of MASLD and could eventually facilitate new drug/biomarker development.

CHAPTER 1

INTRODUCTION

1. MASLD: Definition and Nomenclature

Nonalcoholic fatty liver disease (NAFLD) is an umbrella term used to describe a range of liver conditions characterized by the accumulation of fat in the liver, without significant alcohol consumption. NAFLD is becoming increasingly prevalent and is now considered the most common liver disease worldwide, affecting nearly 1 billion people [1]. It can range from simple steatosis (nonalcoholic fatty liver, NAFL) to a more severe form known as nonalcoholic steatohepatitis (NASH), which can eventually lead to fibrosis, cirrhosis, and liver cancer.

In 1845, Thomas Addison was the first to use the term “fatty liver” in individuals who consumed significant amounts of alcohol (Figure 1). Although alcohol-induced liver steatosis was already described at that time, the “non-alcoholic” counterpart was only coined in 1980 by Ludwig and colleagues to describe a group of patients with abnormal liver function tests without excessive alcohol intake [2,3]. Over the years, the definition of NAFLD has evolved, and a more standardized definition was introduced that required the exclusion of other causes of liver disease, such as the usage of steatogenic drugs, the presence of viral hepatitis, and autoimmune disorders [4].

However, substantial evidence has highlighted the close association between NAFLD and metabolic disorders such as obesity, type 2 diabetes mellitus (T2DM), hypertension, and dyslipidemia. In fact, primary NAFLD is now considered the hepatic manifestation of the metabolic syndrome (MS) [5]. As a result, there has been a push to rename NAFLD to better reflect its underlying pathogenesis and can help in patient stratification for its management. In 2020, an international expert panel recommended the term "metabolic associated fatty liver disease" (MAFLD) as a more accurate and clinically relevant term to describe the condition [6]. There are several reasons why NAFLD was renamed to MAFLD. First, NAFLD is a negative definition that does not account for the close association between the disease and metabolic disorders. Second, the term NAFLD is relatively broad and may include patients with different underlying pathophysiologies. Third, the term NAFLD has been criticized for its lack of clinical relevance, as it does not provide information on the severity or progression of the disease [6–8].

The new nomenclature MAFLD has sparked debate among experts in the field, but it reflects the growing recognition of the complex nature of the disease and its close association with metabolic disorders [7,9]. In fact, the latest clinical practice guidelines of Asian Pacific Association for the Study of the Liver (APASL) used and endorsed the term MAFLD [10]. The endorsement and

utilization of MAFLD in the guidelines reflected a growing recognition of the intricate association between metabolic factors and liver disease.

However, retaining the term "fatty" in MAFLD and the absence of a true international consensus on the nomenclature sparked discussions and deliberations among several prominent liver disease organizations, namely AASLD (American Association for the Study of Liver Diseases), ALEH (Latin American Association for the Study of the Liver), and EASL (European Association for the Study of the Liver). These organizations along with field experts and patient advocates recognized the need for a more comprehensive, universally accepted, and non-stigmatizing term that would better encompass the various metabolic aspects of the disease. Hence, multiple rounds of meetings were held to establish a final nomenclature that would address these concerns. During these meetings, the experts and stakeholders considered different perspectives and evaluated various options for the revised terminology. The goal was to create a name that would reflect the underlying metabolic nature of the disease while also being inclusive and easily applicable across diverse populations [11].

As a result of these extensive discussions, the consensus was reached to officially introduced the term steatotic liver disease (SLD) and its sub-categories (Figure 2). Under SLD, MASLD (metabolic dysfunction-associated fatty liver disease) is defined as the presence of hepatic steatosis in conjunction with one cardio-metabolic risk factors and no other discernible cause. A new category, outside pure MASLD, termed MetALD was selected to describe individuals with MASLD who consume higher amounts of alcohol than recommended per week. For those who do not exhibit metabolic parameters and have no known cause for their liver disease, they were categorized as having cryptogenic SLD [11]. The specific diagnostic criteria of the SLD schema will be further discussed in the diagnostic section of this paper.

The adoption of MASLD as the preferred term represents a significant step forward in the field of hepatology. It demonstrates the collaborative efforts of multiple liver disease organizations to establish a unified and more accurate terminology for this complex condition. The updated nomenclature is expected to facilitate better communication, research, and patient care, while also promoting a deeper understanding of the metabolic underpinnings of liver disease globally. The hope is that this new terminology will increase awareness of the condition and lead to more effective diagnosis, treatment, and prevention strategies.

Overall, whether it is referred to as NAFLD, MAFLD or MASLD, the underlying issue remains the same – a rapidly increasing prevalence of this disease that presents a significant health and economic burden on a global scale. In this PhD manuscript, we adhere to the updated nomenclature and will utilize the term MASLD, along with its corresponding subtypes, metabolic dysfuction-

associated steatotic liver (MASL) and metabolic dysfunction-associated steatohepatitis (MASH), to maintain consistency.

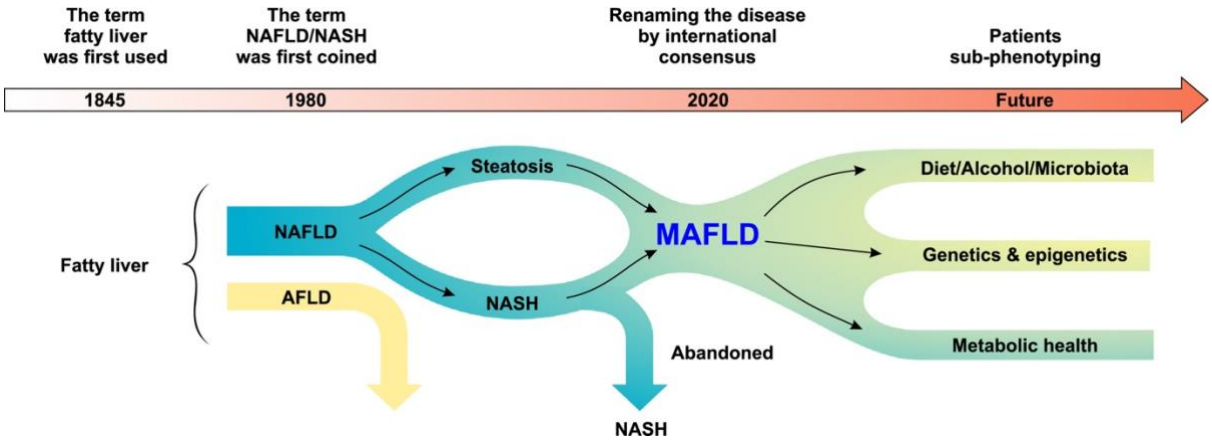

Figure 1. Past, present, and future perspectives of redefining fatty liver disease (Adapted from Fouad *et al., 2020)*

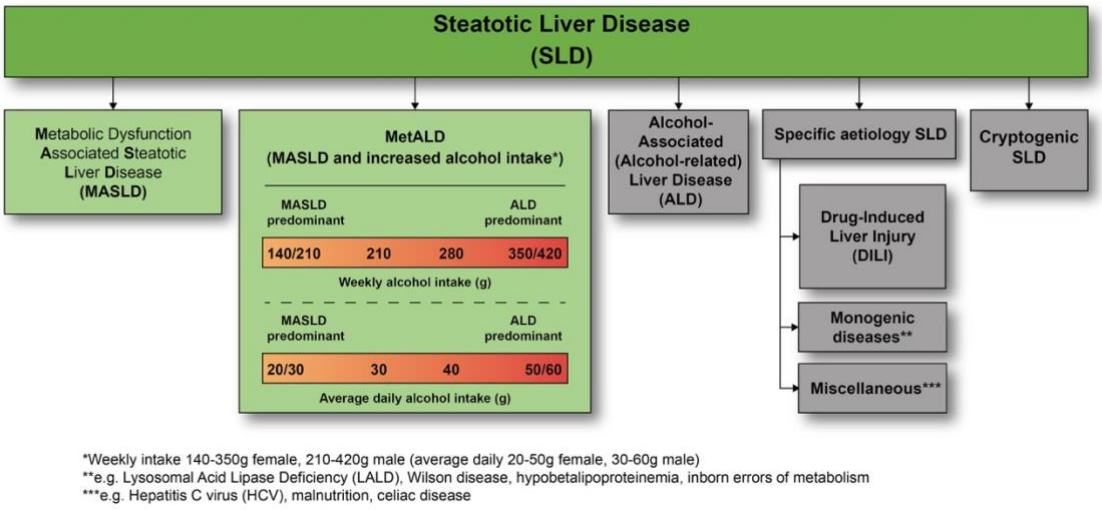

Figure 2. Steatotic Liver Disease sub-classification (Adapted from Rinella *et al.*, 2023).

2. MASLD Epidemiology: Prevalence, Incidence, and Outcomes

MASLD is a serious health issue and recent scientific publications have provided updated epidemiological data on the prevalence and incidence of MASLD worldwide, shedding light on the magnitude of this condition and its associated risk factors. The exact prevalence of MASLD is difficult to obtain since the gold standard for the diagnosis is histology-based. Therefore, the prevalence is only estimated using other diagnostic modalities, such as blood tests and imaging. A systematic review and meta-analysis by Younoussi *et al*. in 2016 [12] estimated that the global prevalence of MASLD is 25.24%, with the highest rates observed in the Middle East (32%) and South America (31%). Europe, North

America, and Asia stand at intermediate values (20-30%) while Africa was reported with the lowest prevalence at 14%. The prevalence of MASH, a more severe form of MASLD, is estimated to be around 7.6% [1,12]. Aside from differences in the geographic regions that are being studied, the prevalence of MASLD/MASH also varies with the diagnostic method used, clinical setting, age, sex, and race/ethnicity.

Most of the epidemiological studies reported that the prevalence of MASLD is higher in individuals with metabolic risk factors such as obesity, T2DM, dyslipidemia, and MS. The presence of obesity only, in the absence of other features of MS, increases the risk of developing MASLD. The WHO 2016 report revealed that there were more than 1.9 billion overweight adults, of which 650 million were obese. Hence, the introduction of the terms "obesity pandemic" and "globesity" to define the worrisome phenomenon. The numbers are also alarming in children and adolescents mainly due to more sedentary lifestyles and the consumption of less healthy diets [13,14].

The incidence of MASLD and MASH varies widely across populations and regions, with higher rates reported in developed countries. A systematic review and meta-analysis showed that the estimated incidence of MASLD is 47 cases per 1,000 person-years [15]. The highest incidence rates were observed in Europe and the Middle East. The study also reported that the incidence of MASH was 3.4 per 1,000 person-years. In the United States, the incidence of MASLD has doubled over the last two decades, affecting approximately 25% of the population [12,16]. Similarly, a study conducted in China reported a significant increase in the prevalence of MASLD from 15.31% in 2008 to 29.27% in 2018 [17].

The outcomes of MASLD and MASH are highly variable and depend on several factors, including the stage of liver disease, the presence of comorbidities, and lifestyle factors. In general, MASLD is associated with an increased risk of liver-related morbidity and mortality, cardiovascular disease (CVD), and all-cause mortality [18]. MASLD is an independent predictor for cardiovascular disease and mortality, and in turn, cardiovascular mortality is the most common cause of death among MASLD patients. MASH, the severe phenotype of MASLD, can progress to liver fibrosis, cirrhosis, and hepatocellular carcinoma (HCC). The prognosis of MASH is largely determined by the stage of fibrosis. Patients with mild fibrosis have a low risk of progression to cirrhosis, while those with advanced fibrosis have a higher risk of developing cirrhosis and its complications [19].

3. Natural History

MASLD covers a wide spectrum of liver diseases ranging from simple steatosis (or MASL) to MASH, fibrosis, cirrhosis, and HCC (Figure 3). The natural history and progression of MASLD have been extensively studied in recent years. However, there is a paucity of good quality data on the natural history of MASLD, with most existing studies relying on retrospective data.

Another challenge is that the classification of MASLD/MASH and its subtypes can only be diagnosed by liver biopsy. Despite these limitations, substantial evidence reported that the progression of MASLD is highly variable and depends on several factors, including age, gender, obesity, diabetes, and genetic predisposition. Patients with only MASL carry a very low risk of adverse outcomes, whereas the presence of MASH increases the risks of liver and possibly non-liver-related outcomes. The adverse liver outcomes associated with MASH comprise cirrhosis, liver failure, and hepatocellular carcinoma, while non-liver-related adverse outcomes are mostly linked to cardiovascular disease and malignancy [20]. However, the progression from MASL to MASH is not linear, and in fact, some patients with MASH, even those with fibrosis, may spontaneously regress [21,22]. On the other hand, MAFL, although very slow, do progress to MASH and even cirrhosis. Moreover, HCC can also develop in MASH patients even without evidence of cirrhosis [23].

A recently published prospective observational study, by Sanyal and colleagues [24], filled some important knowledge gaps in the natural history of MASLD. In a large population-based cohort followed for a median of 4 years, they identified important insights that advance our knowledge of MASLD. First, they reported that liver disease progression and the incidence of decompensation in patients with MASLD is relatively slow compared with other causes of liver disease. Secondly, the incidence of HCC in patients with MASLD was fairly low. Third, they provide a strong rationale that fibrosis stage (that ranges from F1 (centrilobular pericellular fibrosis) to F4 (cirrhosis)) was the most important predictor of clinical outcomes in MASH. Fibrosis stages F3 and F4 were associated with increased risks of liver-related complications and death as compared to lower fibrosis stages. In the 2023 AASLD guidelines, patients with MASH and at least stage 2 fibrosis (F2), referred to as "at-risk" MASH, have a demonstrably higher risk of liver-related morbidity and mortality [16].

Overall, these studies highlight the importance of early detection and risk stratification in patients with MASLD. Patients with advanced fibrosis or MASH should be closely monitored and may require more aggressive management to prevent progression to cirrhosis and HCC.

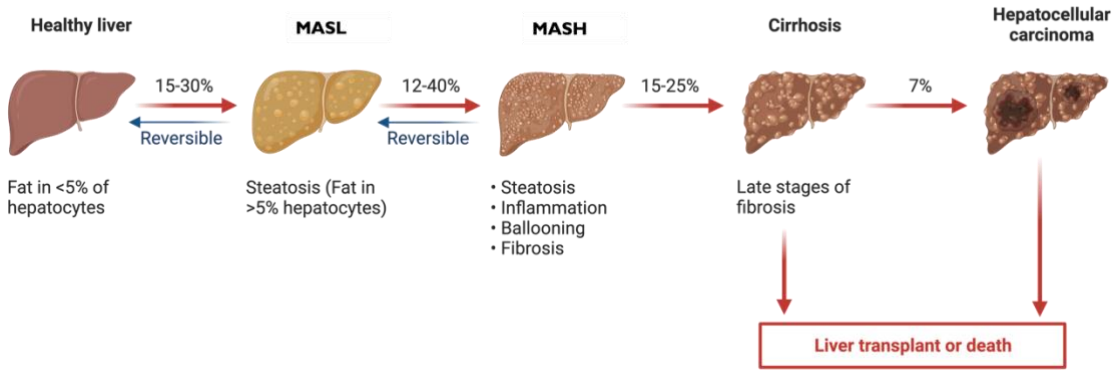

Figure 3. Natural history and progression of MASLD (modified from Fang *et al.*, 2022)

4. Risk Factors

Several risk factors contribute to MASLD development, and these factors can be broadly categorized into metabolic, genetic, epigenetic, environmental, age, sex, ethnicity, and the presence of comorbidities. The most significant risk is having metabolic abnormalities such as insulin resistance, dyslipidemia, central obesity, and hypertension, which often precede and are closely linked to MASLD. The presence of multiple metabolic abnormalities further increases the risk of histological progression of MASH and all-cause mortality. The interplay between MASLD and metabolic comorbidities may also stem from reciprocal interactions between the liver and other endocrine organs, such as the pancreas, adipose tissue, and muscle, through the secretion of hepatokines that regulate fatty acid metabolism, insulin action, and glucose metabolism, adipocytokines, and myokines.

The increasing prevalence of MASLD is thought to be primarily related to the obesity pandemic, especially during childhood and adolescence [25]. Obesity, characterized by adipose tissue (AT) mass expansion, is seen in 51% of MASLD and 81% of MASH patients globally [12]. However, there are lean, or low AT mass patients that also develop MASLD, suggesting that AT function rather than AT mass/obesity could be the key driver of the disease [26,27]. Aside from its role as the regulator of lipid flux to the liver, adipose tissue is also recognized as a major endocrine organ producing a large array of mediators, known as adipocytokines [26]. The role of adipocytokines in AT-liver crosstalk has become an important area of MASLD research because of its potential utility as a diagnostic and or/ therapeutic target.

Other components of the MS also increase the risk of developing MASLD. T2DM patients are insulin resistant, often obese, dyslipidemic, display increased liver enzymes, and tend to accumulate hepatic fat independently of BMI. Diabetes risk and T2DM closely associate with the severity of MASLD, progression to MASH, advanced fibrosis, and the development of HCC [28]. MASLD is often accompanied by hypertension, which is more prevalent in individuals with MASLD at all stages of the disease. The incidence of hypertension in early-stage MASLD is approximately 6.5 per 100 person-years, while in those with cirrhosis, it is around 14.5 per 100 person-years [24]. The coexistence of hypertension with other metabolic comorbidities significantly increases the epidemiological risk of MASH, and it has also been linked to fibrosis progression. It remains unclear whether hypertension contributes to the development of MASLD/MASH, or whether both conditions are manifestations of underlying metabolic disease drivers [16]. Moreover, CVD is the most common cause of death in patients with MASLD. However, the extent to which MASLD independently drives CVD is unclear. To decrease CVD in individuals at risk, it is recommended to promptly treat comorbid conditions such as hypertension, dyslipidemia, and hyperglycemia, and promote smoking cessation [10,16,28]. Chronic kidney disease (CKD) and obstructive sleep apnea

(OSA) are also closely related to MASLD and treatment of these disorders are recommended [29]. However, the extent to which the liver mechanistically contributes to the development of CKD and OSA independent of associated metabolic disorders remains unclear.

Age, sex, and ethnicity are also significant risk factors. MASLD is more prevalent in middle-aged and older individuals, males, postmenopausal females, and those of Hispanic or Asian descent [10,16]. We have recently published a comprehensive review [30] on the molecular mechanisms underlying the sex differences in MASLD, including steatosis, inflammation, fibrosis, and the role of gut dysbiosis. Our analysis reveals that the interplay of several factors, including sexually dimorphic genes and hormones, contributes to the disparity in MASLD development and progression between males and females. Therefore, it is essential not to disregard the role of sex differences in future experimental models, diagnostic algorithms, and clinical trials for MASLD.

Genetic factors have been associated to the prevalence and severity of MASLD. The I148M variant of patatin-like phospholipase domain containing-3 (PNPLA3) impairs lipolysis of triglyceride in lipid droplets. Polymorphisms in hepatocyte fat metabolism-associated proteins have also been linked to an increased risk of MASLD progression, including transmembrane 6 superfamily member 2 (TM6SF2), which may play a role in cholesterol metabolism, and membrane-bound O-acyltransferase domain-containing 7 (MBOAT7), which influences phospholipid metabolism. Recently, loss-of-function variants in HSD17B13, a gene that encodes an enzyme that also localizes to lipid droplets in hepatocytes, have been linked to protection against MASH, progressive fibrosis, and HCC. However, the presence of mutations in these susceptible genes in lean MASLD does not explain the risk of its progression to MASH [16,31].

Epigenetic factors, such as microRNAs (miR), DNA methylation, histone including modification, and ubiquitination alterations, can also influence the development of MASLD and are the subject of current research. Environmental factors such as high fructose corn syrup consumption, sedentary lifestyle, and exposure to toxins like pesticides and industrial chemicals can increase the risk of MASLD [16,31].

Moreover, lean MASLD is a subtype of MASLD that is characterized by the presence of liver fat in individuals with a normal body mass index (BMI). The prevalence of MASLD in lean individuals varies from 4.1% in the United States to as high as 19% in Asia [16]. Compared with healthy controls, lean MASLD patients have increased IR, metabolic comorbidities, and visceral adiposity [10,16]. The precise mechanisms behind lean MASLD are still unclear, but it may be related to genetic factors, altered gut microbiota, and other metabolic abnormalities.

Overall, the development of MASLD is a complex process that involves multiple risk factors, including metabolic disorders, genetic and epigenetic

factors, environmental factors, age, sex, ethnicity, and the presence of comorbidities. Understanding these risk factors can help identify individuals at risk and facilitate the development of effective prevention and treatment strategies. Additionally, lean MASLD warrants further research to understand its underlying mechanisms and develop targeted therapies.

5. Pathogenesis and the Molecular Mechanisms Involved in MASLD

MASLD is a complex and multifactorial disorder that develops because of several mechanisms including steatosis, inflammation, oxidative stress, endoplasmic reticulum (ER) stress, fibrosis, and insulin-glucose dysregulation. The pathogenesis of MASLD has evolved over the years, initially described by the "two-hit" hypothesis in 1998 that proposed the accumulation of fat in hepatocytes as the first hit followed by oxidative stress and inflammation as the second hit leading to the progression of the disease [32]. However, this hypothesis has been modified to the "multiple-hit" hypothesis, which suggests the involvement of various pathways and factors in the pathogenesis of MASLD, including insulin resistance, genetic and epigenetic factors, environmental factors, and non-hepatic players such as adipose tissue and gut microbiota [33]. A summary of the events in MASLD development and progression is shown in the schematic representation below (Figure 4).

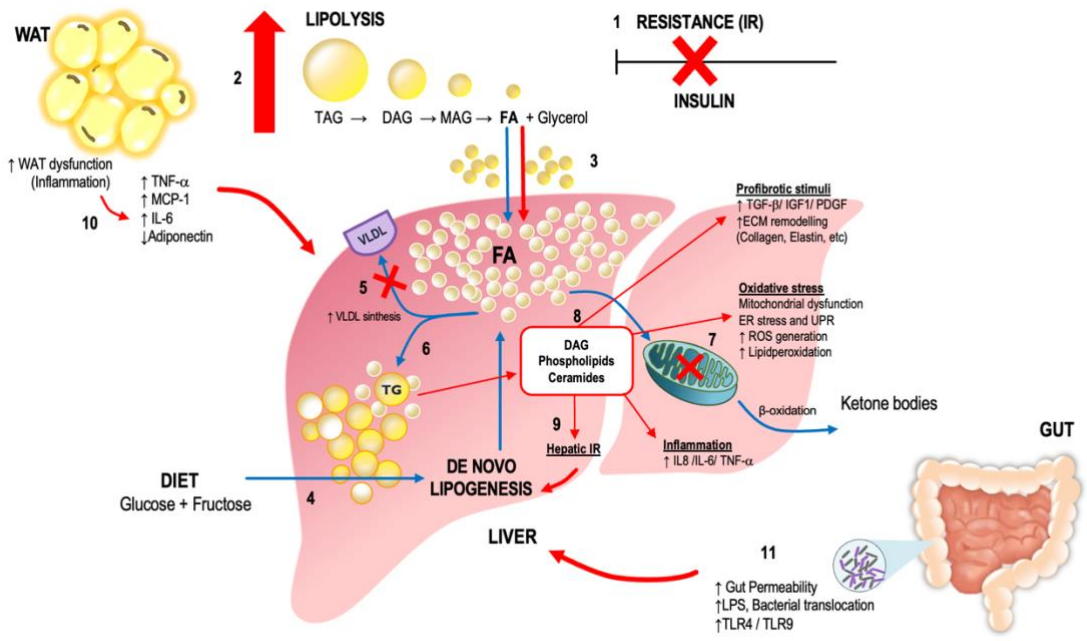

Figure 4. Dysregulation in hepatic FA supply during MASLD (figure and description adapted from Rosso and Bellentani, 2020) The normal processes are represented in blue, whereas the pathological-associated processes are evidenced in red. **1)** Insulin resistance (IR), is associated with **2)** an increased basal lipolysis in the WAT resulting in **3)** an excessive delivery of FA to the liver. On the other side consumption of sugar-enriched diets promotes **4)** an active hepatic FA synthesis (de novo lipogenesis). Impairment of

WAT lipolysis **5)** inhibits VLDL synthesis, and thus **6)** increasing the TG intrahepatic pool. **7)** Mitochondrial Dysfunction leads to impaired β-oxidation and subsequent oxidative damage. **8)** Accumulation of intermediate FA products (DAG, phospholipids, ceramides) account for the FA-induced toxicity triggering inflammation, profibrotic stimuli, and 9**)** hepatic insulin resistance. **10)** Expansion of WAT promotes the release of deleterious cytokines that induce a chronic inflammatory status that further compromise the hepatic functionality. **11)** Dysbiosis induces and enhanced gut permeability (leaky gut) with the subsequent bacteria/LPS translocation to the blood contributing to the hepatic inflammation.

5.1 Steatosis

The accumulation of triglycerides in hepatocytes, referred to as steatosis, is considered the hallmark of MASLD. The excess triglycerides in the liver are derived from increased lipolysis, *de novo* lipogenesis (DNL) and impaired fatty acid oxidation. One best example of impaired lipolysis is seen in patients who are obese. Obesity, characterized by visceral adipose tissue expansion, is associated with an increase in basal lipolysis, therefore, leading to an excess delivery of fatty acids in the liver. The events are further exacerbated due to an impaired sensitivity of adipocytes to the antilipolytic effects of insulin [31]. DNL is another source of fat accumulation in the liver. Consumption of saturated fats and excess sugar, especially fructose is associated with fat accumulation in the liver and with MASH [16]. Finally, impaired mitochondrial β-oxidation leads to lipid accumulation because of lipotoxic species such as diacylglycerol and sphingolipids. This fat accumulation in the liver can eventually cause cellular damage, leading to a vicious cycle of inflammation, oxidative stress, and other pathologic mechanisms [20,31].

5.2 Inflammation

Inflammation is a key driver of MASLD progression from simple steatosis to MASH. Inflammatory cells, including macrophages and neutrophils, infiltrate the liver and release proinflammatory cytokines, such as tumor necrosis factor-alpha (TNF-α), interleukin-6 (IL-6), and interleukin-1beta (IL-1β). These cytokines induce hepatocyte injury and apoptosis, leading to the progression of liver damage [33]. Aside from the liver, expansion of VAT in obesity promotes the release of deleterious cytokines that induce a systemic chronic inflammation. The activation of inflammatory pathways both in adipose tissue and distal tissues such as the liver and skeletal muscle is associated with convergence to other pathological events that drive the progression of MASLD [34].

5.3 Oxidative Stress

Oxidative stress is considered a major factor in the pathophysiology of inflammatory chronic liver diseases, including MASLD. Oxidative stress occurs when the balance between oxidants or ROS and antioxidants is disrupted. Chronic impairment of lipid metabolism is closely linked to oxidative stress, which affects metabolism-related organelles, leading to cellular lipotoxicity, lipid peroxidation, chronic ER stress, and mitochondrial dysfunction. Increased oxidative stress also triggers hepatocytes stress pathways, leading to

inflammation and fibrogenesis, contributing to the progression of MASH [35]. In MASH, mitochondrial DNA, and protein abnormalities are associated with the increase of oxidative stress [36,37]. A decreased oxidative capacity of the electron transport chain (ETC) and mutations in complex II could also lead to a condition of "electron leakage", meaning that the electron normal flow could be interrupted, binding with oxygen to produce ROS species such as superoxide or hydrogen peroxide [38]. Moreover, the levels of glutathione (GSH) peroxidase, superoxide dismutase (SOD), and catalase seem to be low in MASH, so the capability of the mitochondria to reduce ROS levels is reduced [39]. Aside from the liver, excessive adipose tissue seen in obese patients is a source of pro-inflammatory cytokines that increase ROS production and lipid peroxidation rate leading to oxidative stress. ROS further perpetuates inflammation via the activation of redox-sensitive transcription factors, such as NF-κB and activator protein-1, and the NADPH oxidase pathway [40]. Oxidative stress is a major driver of inflammation and fibrosis in MASLD. Therefore, modulation of the oxidant/antioxidant imbalance emerges as an interesting target to prevent MASLD development and progression.

5.4 Endoplasmic Reticulum Stress

Both inflammation and oxidative stress are involved in the induction of ER stress signaling pathways and subsequent unfolded protein response (UPR) activation to restore ER homeostasis [41]. Moreover, protein misfolding in the ER with associated ER stress causes hepatic steatosis, which is multifactorial and can occur via the regulation of lipogenesis, VLDL secretion, and FA oxidation [42]. These statements imply that steatosis, oxidative stress, ER stress, and inflammatory pathways somewhat converge at different stages of MASLD, and thereby creating a positive feedback loop that may promote disease progression (Figure 5). Under stress conditions such as FFA overload and lipotoxicity, misfolded and unfolded proteins accumulate in the ER lumen, leading to the activation of the UPR and ER stress. The activity of the UPR is primarily regulated by transmembrane stress transducer proteins which are activated by the release of glucose-regulated protein 78/binding immunoglobulin protein (GRP78/BiP) from the ER. Through these pathways, ER stress activates a myriad of downstream signaling cascades such as the transcription of CCAAT/enhancer-binding protein homologous protein (CHOP), which perpetuates oxidative stress and inflammation [43]. ER stress is also involved in the reduction of antioxidant mechanisms, such as downregulation of NFE2-related factor 2 (Nrf2) and depletion of glutathione (GSH) [39,43].

5.5 Fibrosis

In MASLD, fibrosis is the most important morbidity and prognostic factor, as it is associated with the progression of the disease to severe liver damage [19]. Accordingly, in the NASH CRN system, fibrosis can be classified in different

stages from stage 0 = no fibrosis; stage 1 = centrilobular pericellular fibrosis (or periportal fibrosis in children); stage 2 = centrilobular and periportal fibrosis; stage 3 = bridging fibrosis; and stage 4 = cirrhosis [44]. Patients with MASH and at least stage 2 fibrosis (F2), referred to as "at-risk" MASH, have a demonstrably higher risk of liver-related morbidity and mortality [16]. MASLD patients with fibrosis, are therefore in need of in-depth hepatological investigation and intensive therapies. Monitoring of fibrosis progression is also necessary at variable time intervals [28].

Fibrosis is an intrinsic response to alleviate liver damage but becomes pathologic in chronic states such as MASH. The molecular mechanisms underlying fibrosis in MASLD are complex and multifactorial, but the canonical principle emphasizes the activation of hepatic stellate cells (HSCs), which is mainly mediated by inflammatory cytokines, oxidative stress, and lipotoxic species. These factors trigger the transformation of quiescent HSCs into activated myofibroblast-like cells that produce excessive extracellular matrix (ECM) components, such as collagen, fibronectin, and laminin, leading to the disruption of the normal tissue architecture and function [45,46].

Upon the trigger of noxious stimuli such as toxic lipids, various signaling pathways are activated, including transforming growth factor-β (TGF-β)/Smad, platelet-derived growth factor (PDGF), and Wingless and Int-1 (Wnt)/β-catenin signaling. TGF-β/Smad signaling is considered the most important pathway in HSC activation and ECM production in MASLD. TGF-β stimulates the phosphorylation and activation of Smad proteins, which translocate to the nucleus and activate the transcription of genes involved in ECM production. PDGF and Wnt/β-catenin signaling also contribute to HSC activation and ECM production in MASLD [47].

Several other factors contribute to the development and progression of fibrosis in MASLD, such as the presence and severity of comorbid disease, gut dysbiosis, genomic profile, and environmental factors. Therefore, understanding the risk factors and molecular mechanisms underlying fibrosis in MASLD is crucial for developing effective therapies to prevent or treat liver fibrosis.

5.6 Insulin Resistance and Glucose Dysregulation

Insulin resistance is a key factor in the pathogenesis of MASLD and its associated metabolic disorders, including obesity, dyslipidemia, and hypertension. The molecular mechanisms underlying insulin resistance in MASLD are complex and multifactorial, involving various organs and tissues, including the liver, adipose tissue, and skeletal muscle.

One of the main contributors to insulin resistance in MASLD is the expansion of VAT, emphasizing the role of AT-liver crosstalk. VAT is a highly metabolically active tissue that releases proinflammatory cytokines which can impair insulin signaling in the liver and peripheral tissues [40]. These cytokines activate the c-Jun N-terminal kinase (JNK) pathway, which phosphorylates insulin receptor

substrate (IRS) proteins, inhibiting their ability to transduce insulin signaling downstream. In addition, free fatty acids released by adipose tissue can also impair insulin signaling by inducing the accumulation of diacylglycerols and ceramides, which activate protein kinase C (PKC) and inhibit insulin receptor signaling. These mechanisms can ultimately result in a decreased insulin-suppressing effect on VAT lipolysis, leading to a vicious cycle of steatosis and associated pathologic events [26,48,49].

Another factor that contributes to insulin resistance in MASLD is the dysregulation of gluconeogenesis. The liver plays a critical role in maintaining glucose homeostasis, and under normal conditions, it suppresses gluconeogenesis in response to insulin signaling. However, as mentioned above, the MASLD liver becomes resistant to the inhibitory effects of insulin, leading to the upregulation of gluconeogenic enzymes and the overproduction of glucose. The molecular mechanisms underlying the dysregulation of gluconeogenesis in MASLD are not fully understood, but they may involve the activation of transcription factors, such as the peroxisome proliferator-activated receptor-gamma coactivator 1-alpha (PGC-1α), Forkhead box protein O1 (FOXO1), and cAMP response element-binding protein (CREB) [50].

In addition to VAT and dysregulated gluconeogenesis, other factors that contribute to insulin resistance in MASLD include mitochondrial dysfunction, ER stress, and gut dysbiosis. Mitochondrial dysfunction leads to the accumulation of ROS, which can impair insulin signaling by inactivating protein phosphatases that dephosphorylate IRS proteins [33,49]. ER stress can also impair insulin signaling by activating the JNK pathway and inducing the expression of proinflammatory cytokines. Gut dysbiosis, which is common in MASLD, can also contribute to insulin resistance by promoting the release of bacterial lipopolysaccharides (LPS), which can activate toll-like receptor 4 (TLR4) and induce inflammation and insulin resistance [49].

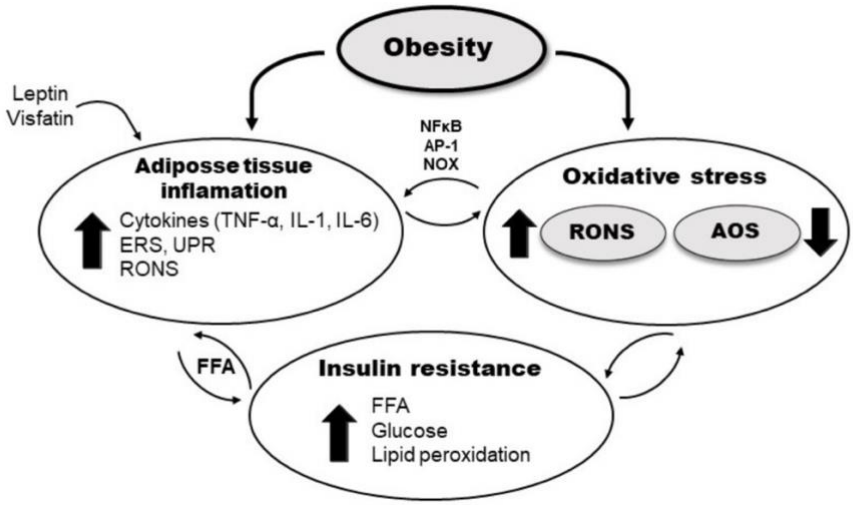

Figure 5. Schematic presentation showing the convergence of the different pathways involved in obesity-related MASLD (figure adapted from Panic *et al.*, 2022). Abbreviations: AP-1, activator protein-; ERS, endoplasmic reticulum stress; NOX, NADPH oxidase; UPR, unfolded protein response

To summarize, the pathogenesis of MASLD is multifactorial and involves multiple hits that act in parallel to initiate and perpetuate the disease. The factors described above, including steatosis, inflammation, oxidative stress, ER stress, fibrosis, and insulin-glucose dysregulation, are all interconnected and contribute to the complex pathogenesis of MASLD.

6. Diagnosis

MASLD is often asymptomatic, or only paucisymptomatic, meaning that affected individuals may not experience any noticeable symptoms or only have mild nonspecific symptoms such as fatigue or mild abdominal discomfort. As a result, many people with MASLD may not be diagnosed until advanced stages of the disease. Presently, the most common MASLD diagnostic approach requires a combination of clinical, laboratory, and imaging tests. However, they are not accurate and liver biopsy remains the gold standard for the definitive diagnosis of MASH.

Based on the 2016 EASL guidelines, the old term NAFLD, is defined by the presence of steatosis in >5% of hepatocytes according to histological analysis or by a proton density fat fraction (PDFF). NAFLD diagnosis also requires the exclusion of both secondary causes and of a daily alcohol consumption ≥30 g for men and ≥20 g for women. Examples of secondary causes of hepatic steatosis are viral infection and the use of steatogenic drugs [28]. Therefore, NAFLD is diagnosed by exclusion rather than by inclusion. As previously mentioned, NAFLD is highly heterogeneous, thus placing all patients with a diverse and differential array of disease drivers under the acronym NAFLD can negatively impact clinical decision-making. Of note, the overall impact of metabolic risk factors on the occurrence of steatosis appears to be higher than that of alcohol in these patients.

To address the challenges in NAFLD diagnosis, APASL endorsed the proposed new nomenclature for the condition: MAFLD. This proposed change shifts the focus towards an inclusive diagnosis based on the presence of metabolic dysfunction, which is the primary driver of the disease. APASL new diagnostic algorithm (Figure 6) is based on "positive criteria," regardless of alcohol consumption or other concomitant liver diseases [10]. This approach allows for the identification of a more homogeneous group of patients and facilitates the stratification of patients with MAFLD. Diagnosis of MAFLD is based on the detection of liver steatosis, which can be identified through liver histology, non-invasive biomarkers, or imaging. In addition, the presence of at least one of three criteria is required: overweight or obesity, T2DM, or clinical evidence of metabolic dysfunction, such as an abnormal lipid or glycemic profile or an increased waist circumference. The new criteria also recognize a special category for cases of cirrhosis where liver fat is no longer present [10].

On the other hand, the EASL 2016 guidelines [28] and the recently released 2023 AASLD guidelines [16] still retain the old nomenclature, NAFLD. With the

introduction of the newest nomenclature, MASLD, these two organizations, along with ALEH, outlined the new diagnostic criteria for MASLD [11]. The proposed criteria were designed to align with cardiometabolic risk factors that are believed to be associated with insulin resistance and have already been well-established and validated in the context of cardiovascular disease. It was agreed upon that patients exhibiting steatosis along with any one of the cardiometabolic criteria outlined in figure 7 would be diagnosed with MASLD. However, it is important to note that the diagnosis of MASLD does not imply that other causes of SLD should be disregarded. This is particularly crucial in children, where it is imperative to rule out other causes of hepatic steatosis before applying the MASLD diagnostic criteria to ensure that dual pathology is not overlooked [11].

Despite the slight differences in the naming and the diagnostic criteria of different liver societies, they still highlighted that patient with metabolic risk factors (i.e. obesity or metabolic syndrome) should undergo diagnostic procedures for the diagnosis of MASLD. As mentioned before, the definitive diagnosis of MASH requires liver biopsy, and it is the only procedure that reliably differentiates MASL from MASH, despite limitations due to sampling variability. The diagnosis of MASH requires the presence of all these histological features: steatosis, ballooning, and lobular inflammation. To improve the diagnosis of MASH, the NAFLD Activity Score (NAS) scoring system was developed by The NASH Clinical Research Network (NASH CRN). However, it should not be used for the diagnosis of MASH but rather for the evaluation of disease severity once the diagnosis has been established by the overall pathological assessment. Although NAS is correlated with aminotransferase and homeostasis model assessment of insulin resistance (HOMA-IR), they have a low prognostic value. Another alternative is the steatosis, activity, and fibrosis (SAF) score with good reproducibility and provides a more accurate and comprehensive description. For children, a specific histological score (Pediatric NAFLD Histological Score – PNHS) has been validated for better classification of MAFL/MASH. The diagnosis of MASH is also important for the approval of pharmacological treatment. As required by the European Medicines Agency and Food and Drug Administration (FDA), resolution of steatohepatitis and improvement in fibrosis remain key surrogate endpoints in phase 2b/3 MASLD trials [16,28,51].

Currently, liver biopsy is the only reliable method to diagnose MASH. However, this procedure involves risks such as bleeding, pain, and infection, and it is not available on a large scale. Therefore, non-invasive tests (NIT) are needed to identify MASH and its subtypes in MASLD patients. NIT not only reduce the number of liver biopsies needed, but can also be used to assess the likelihood of significant fibrosis, predict the risk of disease progression and decompensation, make management decisions, and, to some degree, assess response to treatment [16].

Emerging diagnostic tools for MASLD include advanced imaging techniques such as magnetic resonance elastography (MRE) and transient elastography (TE), which can detect liver fibrosis with high accuracy. In addition, there is growing interest in the use of non-invasive imaging-based techniques such as proton magnetic resonance spectroscopy (1H-MRS) and ultrasound elastography for the diagnosis and quantification of liver fat. MRI-based techniques such as MRI-PDFF and proton MRS are considered the gold standard to quantify liver fat [10,16,28].

Recent advances in non-invasive diagnostic tools for MASLD are also promising and may offer an alternative to liver biopsy. These biomarkers include serum levels of alanine aminotransferase (ALT), aspartate aminotransferase (AST), gamma-glutamyl transferase (GGT), and the ratio of AST to platelet count (APRI), as well as more advanced biomarkers such as fibrosis-4 index (FIB-4) and enhanced liver fibrosis (ELF) score. Many new serum markers such as Cytokeratin-18 fragments (CK-18) and Pro-C3 have shown acceptable diagnostic accuracies, but none of them is approved as of this writing. Thus, there is still a great need to develop novel non-invasive biomarkers particularly in establishing a diagnosis of MASLD, assessing disease severity, and monitoring disease progression and treatment response.

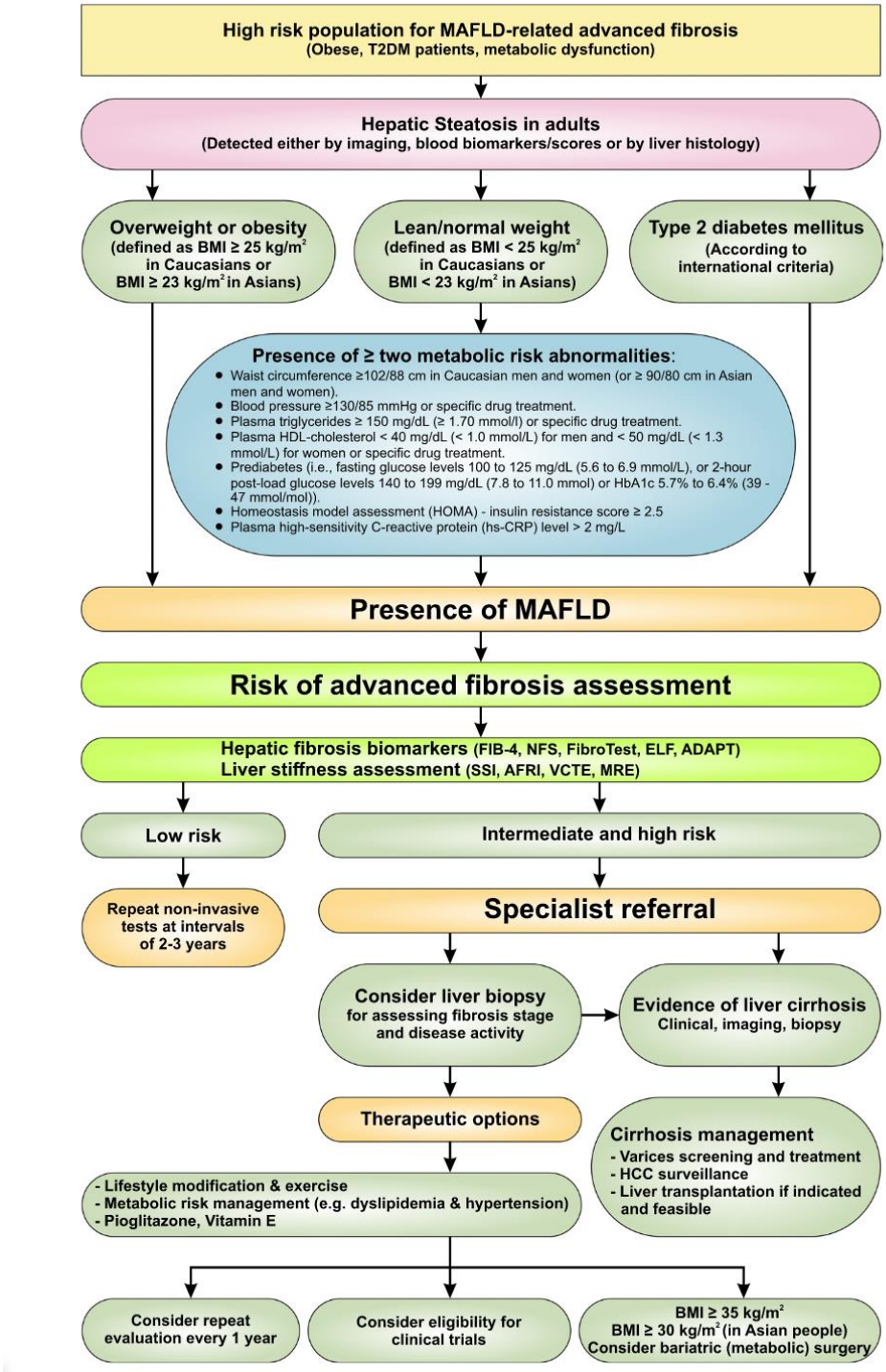

Figure 6. APASL recommended algorithm to diagnose, evaluate, and monitor disease severity in suspected patients with MAFLD and management approach for confirmed cases.

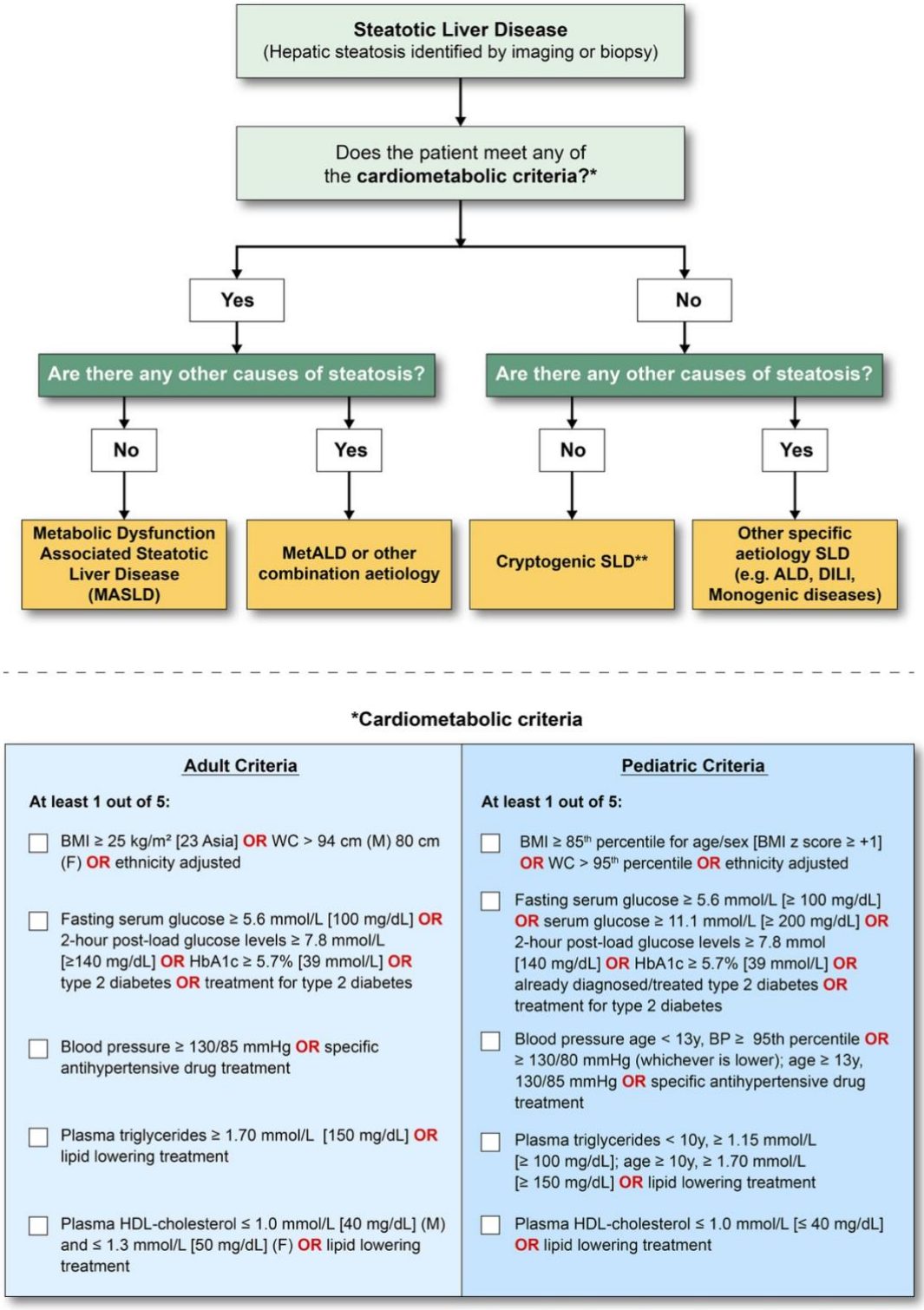

Figure 7. MASLD diagnostic criteria (Adapted from Rinella *et al.*, 2023)

7. Management

A desirable treatment should not only reduce liver steatosis and damage but also improve the metabolic complications and cardiovascular risks associated with MASLD. Therefore, lifestyle modifications are the first-line treatment for MASLD. Weight loss through diet and exercise is the cornerstone of treatment, as it has been shown to improve liver histology and reduce the risk of cardiovascular disease. According to the EASL and APASL guidelines, weight loss of at least 7% to 10% of initial body weight is recommended for patients with MASLD who are overweight or obese [10,28]. The AASLD guidelines recommend a similar approach, with a target weight loss of 5% to 10% of body weight [16]. Other lifestyle modifications that have been shown to be effective in improving liver histology and reducing liver steatosis include increased physical activity, a Mediterranean-style diet, and limitation of alcohol intake. The primary obstacles to the success of this regimen are patient non-compliance and the inability to maintain adherence over time. Therefore, it is recommended that a multidisciplinary approach with collaboration between different stakeholders, including government/policymakers, physicians, patients' associations, and researchers can effectively promote healthy lifestyles and benefit patients with MASLD.

Surgical options may be considered for the management of MASLD, especially for those who are unresponsive to lifestyle changes and pharmacotherapy. Bariatric operations are traditionally offered to patients with MASLD only if they qualify because of other obesity-related comorbidities (T2DM, hypertension, metabolic syndrome). Bariatric surgeries were reported to reduce liver fat and improve the histological lesions of MASLD, including fibrosis. Other surgical procedures such as the intra-gastric balloon and sleeve gastrectomy have also been shown to be effective in reducing liver fat and improving liver histology in MASLD patients but to a lesser extent. However, for MASH cirrhosis, the decision should be individualized due to the high risk of post-operative complications from bariatric surgery. Moreover, liver transplantation is an accepted procedure in MASH patients with end-stage liver disease (decompensated cirrhosis, HCC). The comparable overall survival, however, is similar to other indications, despite higher cardiovascular mortality [10,16,28].

Pharmacological therapy is another option for the treatment of MASLD. As the molecular pathogenesis of MASLD is being unraveled, there has been a steady increase in the number of drug targets available for the disease. However, to date, there is no FDA-approved drug specifically for the treatment of MASLD. At the end of 2019, it was estimated that there were 196 investigational candidate drugs for MASLD in various stages of development [52]. The drugs that have so far progressed to phase 3 development include obeticholic acid (OCA), elafibranor, selonsertib, cenicriviroc, resmetirom, and aramchol. OCA is a farnesoid X receptor agonist whose potential actions include decreasing hepatic

steatosis, inflammation, and fibrosis and an increase of insulin sensitivity [53]. Elafibranor, a dual peroxisome proliferator-activated receptor alpha/delta agonist (PPARα/δ) agonist was found to reduce steatohepatitis without worsening fibrosis [54]. Selonsertib, an inhibitor of apoptosis signal-regulating kinase-1 (ASK-1) showed reduction of hepatic inflammation and fibrosis in animal models and advanced to phase 3 but was discontinued because it was not superior to placebo in the trials [55]. Cenicriviroc, a CCR2/CCR5 chemokine receptor blocker aims to reduce the drivers of inflammation and fibrosis [56]. Resmetirom is a liver-directed, orally active, selective thyroid hormone receptor-β agonist designed to improve steatohepatitis by increasing hepatic fat metabolism and reducing lipotoxicity [57]. Aramchol, a cholic-arachidic acid conjugate that inhibits stearoyl-CoA desaturase, initially produced for treatment of gallstones and currently being tested in a phase 3/4 study to assess its efficacy and safety in subjects with steatohepatitis and fibrosis stages 2–3 [58].

Drugs approved to treat associated comorbidities with potential benefit in MASLD may be considered in the appropriate clinical setting. These include thiazolidinediones, glucagon-like peptide-1 receptor agonist (GLP-1RA), and sodium glucose cotransporter-2 inhibitors (SGLT-2i), as they confer cardiovascular benefit and improves MASH in patients with obesity/T2DM. Vitamin E, an antioxidant agent can be considered in certain individuals as it improves MASH in some patients without diabetes [10,16,28].

Despite significant advances in drug discovery, there are currently no FDA-approved medications available for the treatment of MASLD. This underscores the urgent need for novel therapeutic options, given the multifactorial pathogenesis of MASLD and its association with an increased risk of liver-related and cardiovascular morbidity and mortality, making it a pressing public health concern. The development of innovative drugs that can target the underlying mechanisms of MASLD and halt or even reverse its progression is vital to improving clinical outcomes for patients afflicted with this disease.

8. Translational Approach in MASLD Research

Given the complexity of MASLD, translational research has become increasingly important for understanding the underlying mechanisms and developing effective diagnostics or treatments. Translational research involves the translation of basic scientific discoveries into clinical applications, and vice versa, to improve patient outcomes [59]. In the context of MASLD, translational research involves the development and validation of experimental models that mimic the pathophysiology of MASLD and the translation of preclinical findings into clinical applications. Another important component of translational research is reverse translation. Reverse translation involves the translation of clinical observations and findings, back to the laboratory for further investigation [61]. In the context of MASLD, reverse translation involves the analysis of clinical data and samples to identify novel therapeutic or diagnostic

targets and validate preclinical findings in human subjects. The combination of translational research and reverse translation, also known as bidirectional translational research, has the potential to accelerate knowledge about MASLD. By integrating preclinical and clinical data, bidirectional translational research can unravel the pathogenesis, identify and validate promising diagnostic or therapeutic targets, optimize clinical trial design, and ultimately improve patient outcomes.

Several experimental models have been characterized in the field of translational research to recapitulate the molecular mechanisms involved in MASLD development. Currently, available *in vitro* models of MASLD include 2D systems (simple cell culture and co-culture) and 3D systems (organoids, precision-cut tissue slices, microfluidic devices, etc.). Each *in vitro* model has its advantages and disadvantages in studying MASLD. 2D cell culture systems are preferred because they provide useful and detailed information about the cellular response from fat overload. Moreover, 2D cell culture systems are simple and cost-effective and if two or more cells are combined (co-culture), they allow the study of cell-cell interactions and tissue-level responses. One of the promising co-culture models in MASLD is the combination of hepatic stellate cells and (HSCs) and hepatocytes. The crosstalk between these cells is necessary for the initiation of the fibrotic process, an important pathologic driver in MASLD progression [45].

3D cultures are emerging as a bridge between the easy-to-use 2D cell cultures and more complex *in vivo* models. The morphology, cellular heterogeneity, and spatial organization maintained within the 3D cell culture systems allow the preservation of natural adhesion between cells, interaction between cells and extracellular matrix, and key cellular signaling pathways [31,62]. Although promising, 3D cell culture systems can be challenging to handle and generate, and the experimental set-up has not been well standardized as of this writing, thus limiting their use among different laboratories. Therefore, the choice of *in vitro* model should be based on the research question and the specific advantages and limitations of each model.

Animal models are essential for studying the complex interactions between the liver, other organs, and the systemic environment in the development and progression of MASLD. In the last decade, several animal models were used to investigate the effects of gene mutations and environmental factors (diet and exercise) on the development and progression of MASLD, as well as the efficacy and safety of potential therapies. However, the translation of results to human scenario has been hindered by the complexity of disease pathogenesis. Several genetic models of MASLD have been developed but none of them fully recapitulate MASLD. Mice models like Lep^{ob}/ Lep^{ob} (leptin deficient) and Lep^{db}/ Lep^{db} (nonfunctional leptin receptor) are obese and present T2DM. However, these models do not present MASH and fibrosis [31,60]. Similarly, apolipoprotein ($ApoE^{-/-}$) and lipoprotein receptor ($Ldlr^{-/-}$) deficient mice present

some metabolic features of MASLD like dyslipidemia and obesity but do not develop MASH. Diet-induced obesity (High-fat diet, HFD; cafeteria diet, CAF) is widely used to examine metabolic syndrome and MASLD in animal translational models. Diet-induced obesity is a robust model that recreates obesity, glucose intolerance, dyslipidemia, MASH histology-like features, and to some extent, fibrosis [31,63,64]. Although each type of model has some limitations, the combination of genetic and diet models might be a valid platform to investigate MASLD pathogenesis and evaluate the efficacy of potential therapies.

Lastly, systems-oriented approaches involving integrated data generation and *in silico* models are emerging as the basis for experimental validation to address the current gaps in MASLD. The combination of 'omics' and experimental disease models has the potential in designing effective treatment or identification of predictive and prognostic biomarkers of MASLD. Moreover, the validation of novel diagnostic/therapeutic targets *in vitro* and *in vivo* can be identified and narrowed down first using *in silico* analysis. The integration of *in silico* data into the experimental models has been recognized for certain protein targets that have been useful in the preclinical testing of diagnostic/therapeutic targets of MASLD [65–68]. Moreover, *in silico* models can also help researchers optimize clinical trial design and predict the outcomes of clinical trials [69].

Taken together, the different models available for studying MASLD have specific advantages and disadvantages. Accordingly, the choice of model may depend on the particular context of use. In terms of future perspectives, there is a need for more sophisticated models that better reflect the complexity of MASLD. For example, the development of 3D liver organoid models that incorporate multiple cell types may be a promising avenue for studying MASLD. Additionally, the use of precision-cut liver slices (PCLS) and patient-derived induced pluripotent stem cells (iPSCs) may allow for the generation of personalized models of MASLD that reflect individual genetic and environmental factors. Finally, the integration of multi-omics approaches, such as transcriptomics and proteomics, may allow for a more comprehensive understanding of the pathogenesis of MASLD.

CHAPTER 2

AIMS OF THE Ph.D. RESEARCH

Metabolic dysfunction-associated steatotic liver disease is a major cause of chronic liver disease worldwide and is tightly associated with obesity. It is a spectrum of diseases that ranges from simple fatty liver to more severe forms, such as metabolic-associated steatohepatitis, cirrhosis, and hepatocellular carcinoma. Currently, liver biopsy, despite its invasiveness and limitations, remains the main method for diagnosis. Additionally, there is no approved drug for MASLD. Therefore, there is a pressing need to develop non-invasive diagnostic biomarkers and find new therapeutic targets for MASLD. Further research is also necessary to understand the crosstalk of the liver with other organs to gain a better understanding of the MASLD pathogenesis. This Ph.D. research aims to bridge these knowledge gaps using a translational approach. The study includes the evaluation of novel therapeutic compounds for MASLD, and the identification and validation of a new non-invasive biomarker for liver fibrosis. The study also includes the identification and characterization of a novel molecular target in VAT that is potentially involved in the pathogenesis of MASLD, using a combination of *in silico* analysis, *in vitro*, *ex vivo*, and *in vivo* experimental approaches. Below are the outlined specific objectives for each project:

PROJECT 1 (Therapy):

- To evaluate the therapeutic effects of APPLIVER (*Cydonia oblonga* cells extract, expressed in Triterpenic Acid) and ACTEOS (*Lippia citriodora* cells extract, expressed in Acteoside) in our *in vitro* model of hepatic steatosis. The study focused on evaluating the effects of these compounds on key molecular mechanisms associated with MASLD including steatosis, inflammation, and oxidative stress.
- To determine the *in vitro* antifibrotic effect of APPLIVER and ACTEOS using a simultaneous co-culture (SCC) model of hepatocytes and hepatic stellate cells.

PROJECT 2 (Diagnosis)

- To use a simple *in silico* strategy to identify potential protein biomarkers for liver fibrosis in the context of MASLD.
- To assess the performance of Ficolin-2 protein (FCN-2) as a putative novel biomarker of liver fibrosis.
- To investigate the utility of combining FCN-2 with other biomarkers and clinical parameters in a blood-based score test to improve the accuracy of diagnosing and predicting liver fibrosis.

PROJECT 3 (Pathophysiology)

- To identify a novel molecular target in VAT that is potentially involved in the pathogenesis of MASLD, using a simple *in silico* analysis.
- To determine the expression levels of omentin-1 (mRNA and protein) in VAT of MASLD patients and mice fed with a high-fat diet.
- To investigate the plasma levels of omentin-1 in obese groups with different stages of MASLD.
- To study the role of omentin-1 on MASLD-related mechanisms (steatosis, inflammation, oxidative stress, ER stress) in both *in vitro* model of hepatic steatosis and *ex vivo* VAT explants of MASLD patients.
- To determine the expression levels of omentin-1 (mRNA and protein) in VAT of MASLD patients supplemented with high levels of insulin and glucose.

CHAPTER 3

PROJECT 1 (THERAPY)

The beneficial effects of Triterpenic Acid and Acteoside in an *in vitro* model of metabolic-associated steatohepatitis (MASH)

Abstract

Triterpenic acid (TA) and acteoside (ACT), the major components of APPLIVER and ACTEOS respectively, have been reported to exert hepatoprotective effects but the molecular mechanisms remain elusive, particularly in MASLD/MASH context. We assessed their effects in our well-established *in vitro* model resembling the pathophysiological mechanisms involved in MASH. Human hepatocytes and hepatic stellate cells were exposed to free fatty acids (FFA) alone or in combination with APPLIVER and ACTEOS as mono- or co-culture. Steatosis, inflammation, generation of reactive oxygen species (ROS), and collagen deposition were determined. ACTEOS reduced both the TNF-α and ROS production and, most importantly, attenuated collagen deposition elicited by the excess of FFA in the co-culture model. APPLIVER also showed inhibition of both TNF-α production and collagen deposition caused by FFA accumulation. The compounds alone did not induce any cellular effects. The present study showed the efficacy of triterpenic acid and acteoside on pathophysiological mechanisms related to MASH. These *in vitro* data suggest that these compounds deserve further investigation for possible use in MASH treatment.

Publications:

- **Salvoza N,** Bedin C, Saccani A, Tiribelli C, Rosso N. The Beneficial Effects of Triterpenic Acid and Acteoside in an *In Vitro* Model of Nonalcoholic Steatohepatitis (NASH). International Journal of Molecular Sciences. 2022; 23(7):3562. https://doi.org/10.3390/ijms23073562
- **Salvoza N,** Giraudi PJ, Tiribelli C, Rosso N. Natural Compounds for Counteracting Nonalcoholic Fatty Liver Disease (NAFLD): Advantages and Limitations of the Suggested Candidates. International Journal of Molecular Sciences. 2022; 23(5):2764. https://doi.org/10.3390/ijms23052764

Poster Presentations:

- "International Conference on Fatty Liver". Vienna, Austria. February 17-22, 2022.
- "The Liver Meeting" by The American Association for the Study of the Liver Diseases (AASLD). Virtual Conference. November 12-15, 2021.
- "Digital NAFLD Summit" by the European Association for the Study of the Liver (EASL). Virtual Conference. September 16-17, 2021.
- "The International Liver Congress 2021" by The European Association for the Study of the Liver (EASL). Virtual Conference. June 23-26, 2021.

1. Introduction

The onset of MASLD is characterized by the accumulation of fat in the liver or steatosis, which triggers the release of lipotoxic species. This initiates a detrimental cycle involving inflammation, oxidative stress, and other pathological mechanisms [20,31]. On the other hand, the turning point of MASH progression is the activation of HSCs that can lead to fibrosis. Fibrosis is considered the most important morbidity and prognostic factor in MASLD development [19]. Fibrosis triggers the dysregulation in extracellular matrix production, which in turn initiates the release of noxious stimuli involved in inflammation and the progression of MASL to MASH [70,71]. The development of inflammation and fibrosis in MASH underlies cirrhosis and hepatocellular carcinoma (HCC) [28].

To date, despite many efforts to unravel MASLD pathogenesis, no pharmacological treatment is currently approved for this disease. Drugs available are often used to target the co-morbidities or the specific disease mechanisms involved in MASLD. Therefore, preclinical studies are important for the understanding of MASLD pathophysiology and future drug development.

Triterpenic acid is a triterpene isolated from various plants belonging to Rosaceae family, mostly from the leaves and whole herbs [72,73]. This compound was found to possess various pharmacological properties, including hepatoprotective effects [74,75]. On the other hand, the hepatoprotective effects of acteoside (ACT), a phenylpropanoid present in various species of Order Lamiales, were evaluated in LPS- and carbon tetrachloride (CCl4)-induced acute hepatic damage in mice. TA and ACT ameliorated the elevation of serum aspartate transaminase (AST) and alanine aminotransferase (ALT), as well as the depletion of endogenous antioxidants and oxidative stress markers [76,77]. Despite substantial evidence regarding the general hepatoprotective effects of both compounds in preclinical settings, the molecular mechanisms underlying the beneficial effects are still elusive.

Several models have been developed in an attempt to mimic the molecular mechanisms involved in the onset of MASLD and the progression of MASH [78]. Among these, two-dimensional cell culture models (monoculture and co-culture) provide the most advantages such as controlled conditions, are easy to handle, and offer reliable information about MASH development [78,79]. These characteristics make the system suitable for preclinical testing to evaluate drug efficacy and cellular tolerance.

We previously developed an *in vitro* human MASH model able to reproduce the initial phases of MASH development due to cell-to-cell interactions. Specifically, we reported that excess FFA accumulation in hepatocytes leads to increase inflammatory response, oxidative stress, and activation of HSCs, which are all key hallmarks of MASH [46,71,80].

In the present study, we assessed the effects of APPLIVER (*Cydonia oblonga* cells extract, expressed in triterpenic acid) and ACTEOS (*Lippia citriodora* cells extract, expressed in acteoside) in our *in vitro* model resembling the pathophysiological mechanisms involved in MASH. We demonstrated that APPLIVER and ACTEOS are promising therapeutic compounds in counteracting inflammation and ROS generation caused by excess of FFA in the hepatocytes. Most importantly, both compounds attenuated collagen production elicited by the excess of FFA in the co-culture model.

2. Results

2.1 Determination of Experimental Concentration

To assess the safety of the compounds in Huh7 monoculture and simultaneous co-culture (SCC) with or without FFA, a cell viability test (MTT assay) was performed for both compounds. MTT assay was also used to determine the effective treatment concentration of each compound needed for the succeeding experiments. Briefly, monoculture and SCC were exposed to 1200 μM FFA in the presence of increasing concentrations of the compounds at specific time points (24 hours for Huh7; 96 and 144 hours for SCC). Cells were also exposed to medium alone with increasing concentrations of compounds to assess their toxicity in monoculture and SCC without FFA.

The extent of cytotoxicity from each concentration of the compound was quantified as a percentage of cell viability relative to the vehicle control. According to ISO 10993-5 (*in vitro* cytotoxicity test on extracts), percentages of cell viability above 80% are considered as non-cytotoxic; within 60%–80% weak; 40%–60% moderate; and below 40% strong cytotoxic, respectively [81]. Results are shown in Table 1. No cytotoxicity was observed in Huh7 monoculture and SCC at 50 nM APPLIVER and 100 nM ACTEOS in all experimental conditions. We then selected 50 nM APPLIVER and 100 nM ACTEOS as the test concentrations.

Table 1. Cell viability after APPLIVER and ACTEOS exposure with or without FFA (% *vs* vehicle).

		Huh7 Monoculture	**Huh7 - LX2 Simultaneous Co-culture**	
		24h	**96h**	**144h**
		mean±SD	mean±SD	mean±SD
+FFA	**Vehicle**	100±0	100±0	100±0
	FFA	99±11	86±7	91±5
	APPLIVER 10 nM	89±18	83±2	97±5
	APPLIVER 50 nM	94±22	*69±28	111±8
	ACTEOS 100 nM	98±6	81±9	90±3
	ACTEOS 10000 nM	96±11	*75±7	88±1
- FFA	**Vehicle**	100±0	100±0	100±0
	APPLIVER 10 nM	99±17	99±3	118±37
	APPLIVER 50 nM	90±16	82±1	105±21

ACTEOS 100 nM	93±12	82±3	96±20
ACTEOS 10000 nM	82±7	*69±7	*71±6

The cell viability was determined by MTT assay. Values presented are the mean ± SD of three biological replicates. * 80%–60% cell viability = weak cytotoxic.

2.2 Effects of APPLIVER and ACTEOS on fat accumulation

The content of intracellular lipid droplets was determined by Nile Red staining through flow cytometry. As shown in figure 8a, FFA induces a 203 ± 35% ($p < 0.001$) increase in fat accumulation *vs* vehicle-treated cells in Huh7 monoculture, similar to our previous data [80]. The co-treatment with both compounds did not alter the intracellular fat content. Likewise, the addition of both compounds in the absence of FFA did not induce steatosis (Figure 8b).

We then assessed the effect of the compounds on the intracellular fat content of the SCC system at a longer exposure time (96h). 96h FFA exposure induces a 214 ± 11% ($p < 0.01$) increase of intracellular fat *vs* vehicle-control and as for the 24h, the intracellular fat accumulation was not changed by either of the two compounds (Figure 9a). The addition of both compounds in the absence of FFA did not induce steatosis on SCC (Figure 9b).

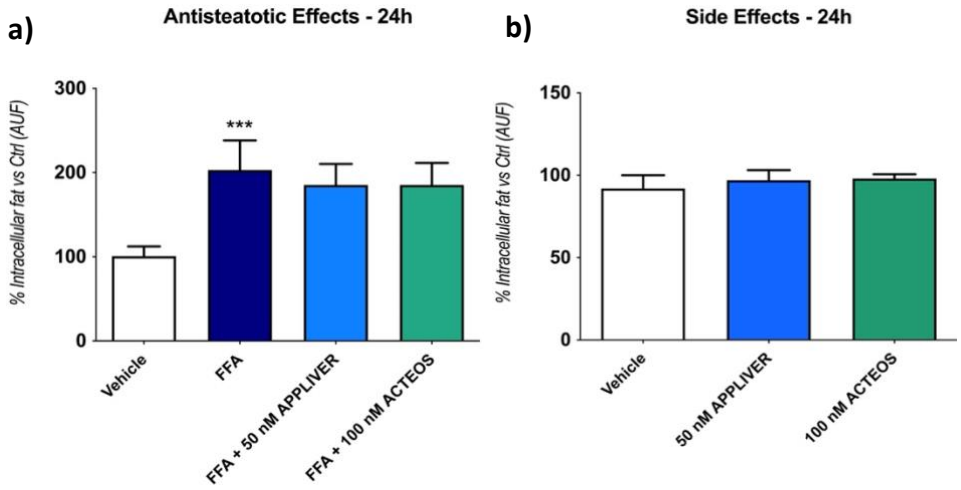

Figure 8. Assessment of the effect of APPLIVER and ACTEOS as antisteatotic (a) and its side effects (b) after 24h on hepatocytes. Values presented are the mean ± SD of three biological replicates. ** $p < 0.01$ vs Vehicle, *** $p < 0.001$ *vs* Vehicle. Abbreviations: AUF, arbitrary unit of fluorescence; FFA, free fatty acids.

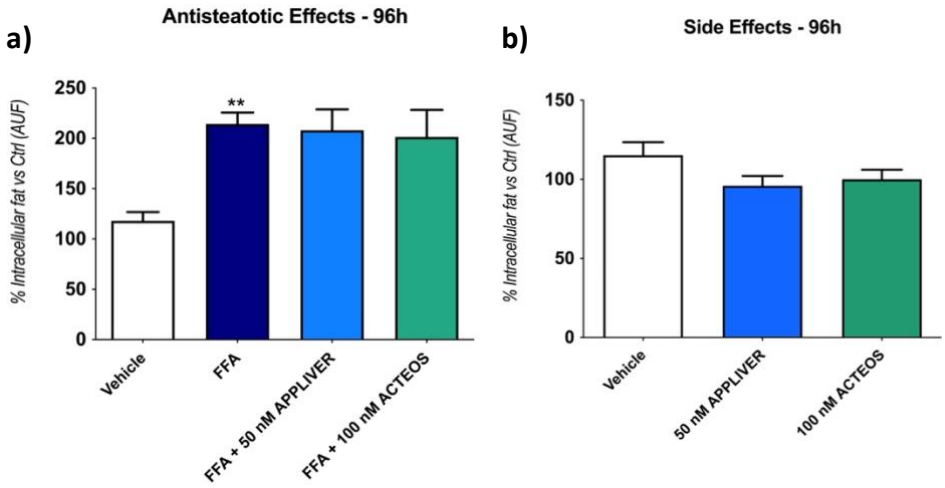

Figure 9. Assessment of the effect of APPLIVER and ACTEOS as antisteatotic (a) and its side effects (b) after 96h on SCC. Values presented are the mean ± SD of three biological replicates. ** $p < 0.01$ *vs* Vehicle, *** $p < 0.001$ *vs* Vehicle. Abbreviations: AUF, arbitrary unit of fluorescence; FFA, free fatty acids.

2.3 Effects of APPLIVER and ACTEOS on the inflammatory response

To assess the anti-inflammatory effect of APPLIVER and ACTEOS, we determined the gene expression of the pro-inflammatory cytokines IL-6, IL-8, and TNF-α. FFA induced an upregulation of the inflammatory mediators, but only IL-8 and TNF-α were statistically significant (Figure 10). Both APPLIVER and ACTEOS induced a significant ($p < 0.05$) downregulation of the TNF-α gene expression. Moreover, neither of the compounds in the absence of FFA changed the expression of the cytokines (Figure 11).

The effect of the compounds on TNF-α release in the cell culture supernatant was determined by ELISA (Figure 12) after 1h of treatment since it has been reported the peak concentrations of TNF-α in the cell supernatant usually occur at 1-2h [82–84]. In line with the gene expression results, APPLIVER and ACTEOS significantly reduced the release of TNF-α. The treatment of either APPLIVER or ACTEOS in the absence of FFA did not induce TNF-α release in the cell culture supernatant (Figure 13).

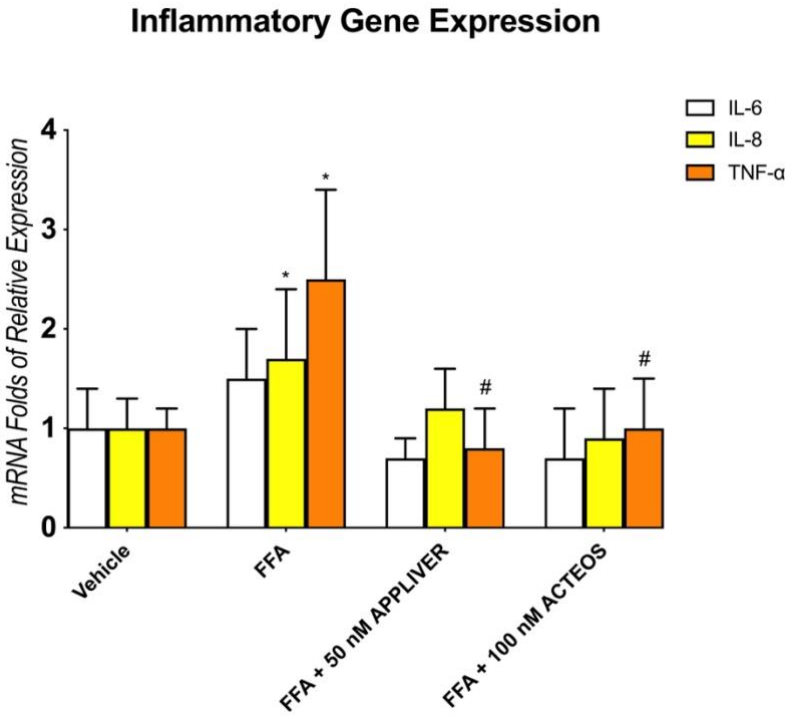

Figure 10. Assessment of anti-inflammatory properties of APPLIVER and ACTEOS on inflammatory cytokines mRNA expression. Gene expression analysis of pro-inflammatory cytokines (folds of mRNA expression *vs* vehicle). Values presented are the mean ± SD of three biological replicates. *p < 0.05 *vs* Vehicle, # p < 0.05 *vs* FFA.

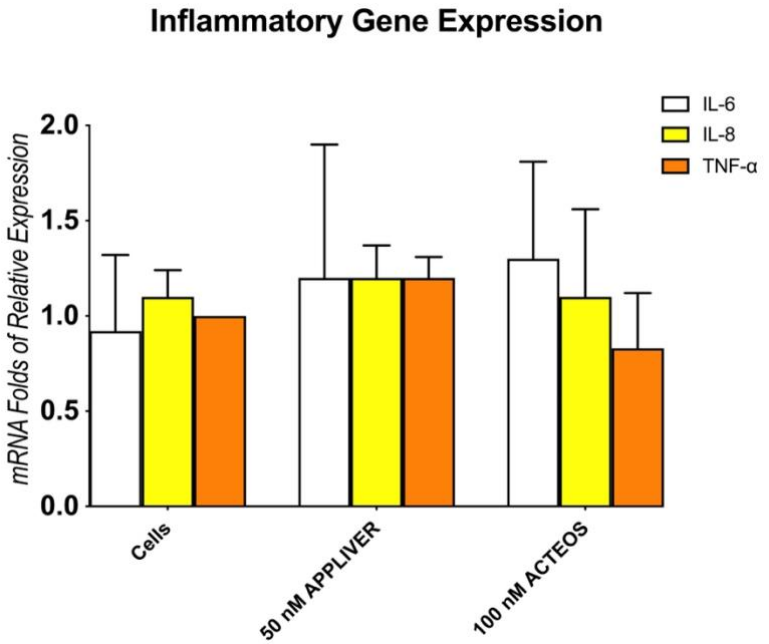

Figure 11. Assessment of anti-inflammatory properties of APPLIVER and ACTEOS without FFA on inflammatory cytokines mRNA expression. Gene expression analysis of pro-inflammatory cytokines (folds of mRNA expression *vs* cells without treatment). Values presented are the mean ± SD of three biological replicates. No significant results *vs* cells. Abbreviations: FFA, free fatty acids; IL-6, interleukin-6; IL-8, interleukin-8; TNF-α, tumor necrosis – alpha.

7/19/2023 1:17:00 PM

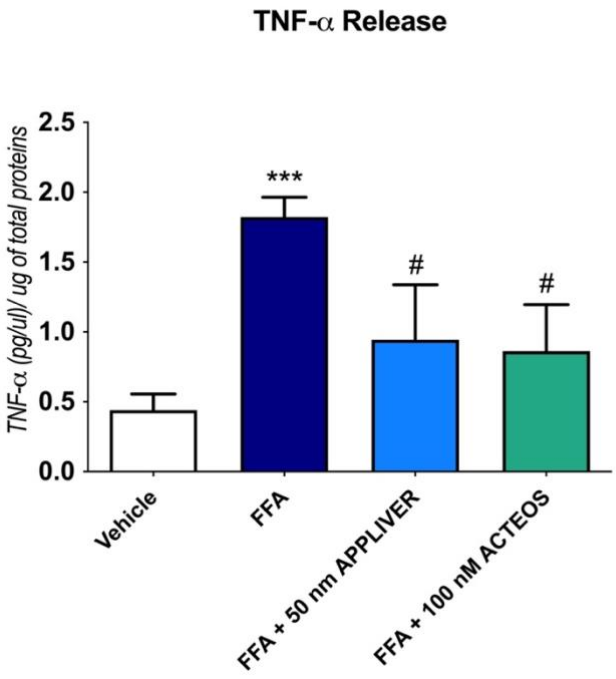

Figure 12. Quantification of TNF-α release in cell culture supernatant ((pg/µl)/ µg of total proteins) upon treatment of either APPLIVER or ACTEOS ± FFA after 1h. Values presented are the mean ± SD of three biological replicates. *** $p < 0.001$ *vs* Vehicle, # $p < 0.05$ *vs* FFA. Abbreviations: FFA, free fatty acids; TNF-α, tumor necrosis – alpha.

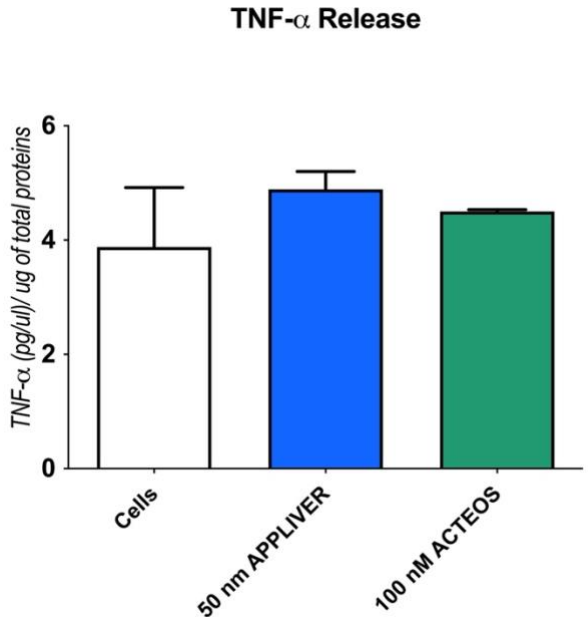

Figure 13. Quantification of TNF-α release in cell culture supernatant ((pg/µl)/ µg of total proteins) upon treatment of either APPLIVER or ACTEOS without FFA after 1h. Values presented are the mean ± SD of three biological replicates. No significant results *vs* cells. Abbreviations: FFA, free fatty acids; TNF-α, tumor necrosis – alpha.

2.4 Effects of APPLIVER and ACTEOS on the production reactive oxygen species

The antioxidant properties of APPLIVER and ACTEOS alone or in combination with FFA were evaluated on Huh7 monoculture after 1h of treatment. The exposure to FFA induces a 40% ($p < 0.001$) increase in ROS generation *vs* the vehicle-treated control, similar to hydrogen peroxide, the positive control (Figure 14). In the presence of FFA, APPLIVER reduced ROS generation though the difference was not statistically significant, while ACTEOS significantly ($p < 0.05$) reduced ROS production. The exposure to APPLIVER and ACTEOS in the absence of FFA did not induce any change in the cellular redox state (Figure 15).

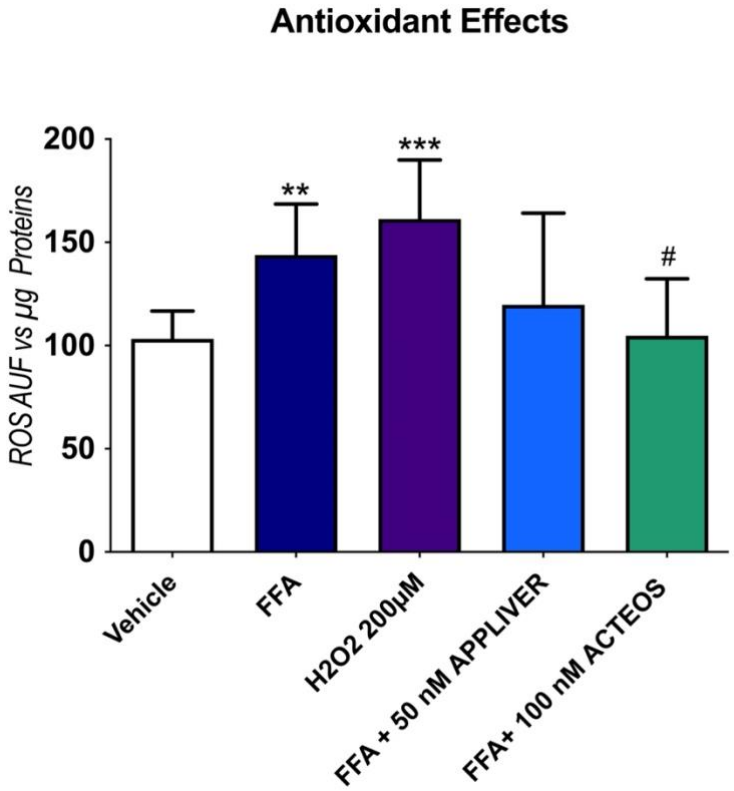

Figure 14. Assessment of antioxidant properties of APPLIVER and ACTEOS induced by FFA. Fluorescence was normalized by the total proteins present in the cell lysates (µg) assessed using fluorescamine assay. Values presented are the mean ± SD of three biological replicates. ** $p < 0.01$ *vs* Vehicle, *** $p < 0.001$ *vs* Vehicle, # $p < 0.05$ vs FFA. Abbreviations: AUF, arbitrary unit of fluorescence; FFA, free fatty acids; H_2O_2, hydrogen peroxide.

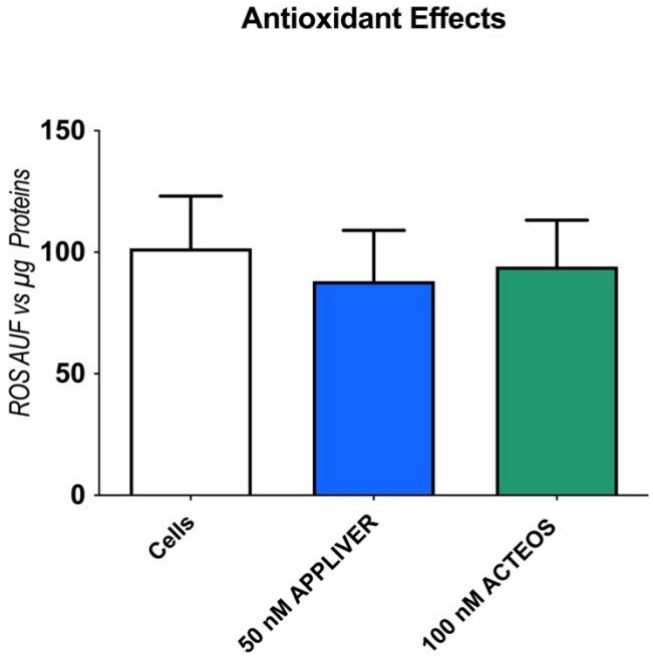

Figure 15. Assessment of antioxidant properties of APPLIVER and ACTEOS without FFA. Fluorescence was normalized by the total proteins present in the cell lysates (µg) assessed using fluorescamine assay. Values presented are the mean ± SD of three biological replicates. No significant results *vs* cells without treatment. Abbreviations: AUF, arbitrary unit of fluorescence; FFA, free fatty acids; H_2O_2, hydrogen peroxide.

2.5 Effects of APPLIVER and ACTEOS on collagen (COL1A1) production of SCC

The production of fibrillar type 1 collagen is associated with ECM remodeling and liver fibrosis. We evaluated the effects of APPLIVER and ACTEOS in the expression of collagen type I alpha 1 chain (COL1A1). The gene expression of *COL1A1* was increased in SCC after 96h and even more after 144H of FFA exposure (Figure 16). APPLIVER showed a not significant reduction in COL1A1 expression both at 96h and 144h, while ACTEOS significantly ($p < 0.05$) reduced the expression by 50% *vs* FFA at 96h; this effect was not observed at 144h.

At protein level (Figure 17), treatment with either APPLIVER or ACTEOS showed a 60% reduction of collagen at 96h *vs* FFA ($p < 0.05$). This effect was present also at the longest time tested (144h). Exposure to APPLIVER and ACTEOS only, in the absence of FFA did not affect the gene expression and extracellular collagen deposition at both time points (Figures 18 and 19).

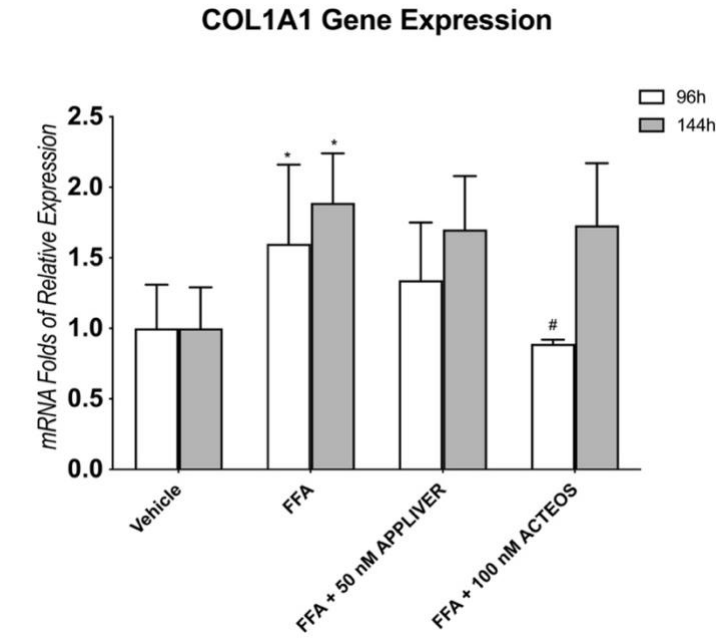

Figure 16. Gene expression of COL1A1 upon exposure to FFA and APPLIVER and ACTEOS after 96h and 144h. Values presented are the mean ± SD of three biological replicates. * $p < 0.05$ *vs* Vehicle, # $p < 0.05$ *vs* FFA. Abbreviations: COL1A1, collagen type I alpha 1 chain; FFA, free fatty acids.

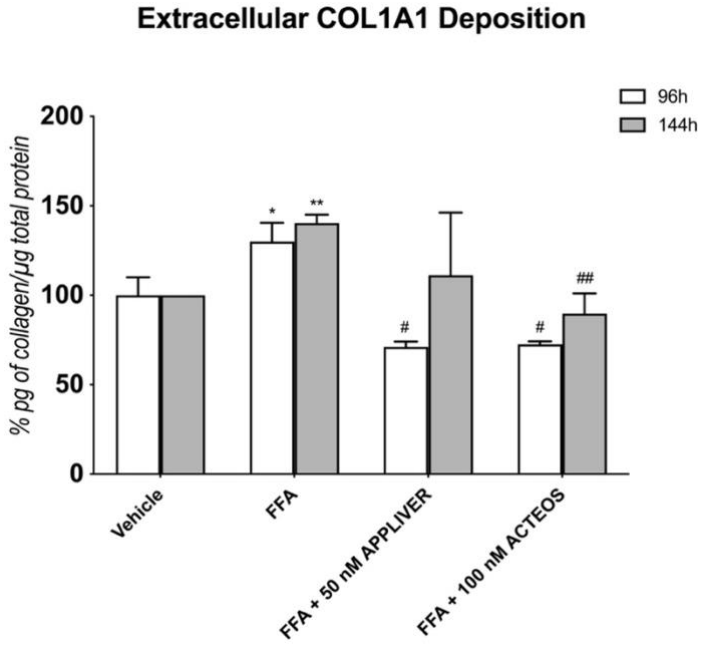

Figure 17. Quantification of extracellular COL1A1 deposition (% pg of collagen/µg total protein) using ELISA upon treatment of either APPLIVER or ACTEOS ± FFA after 96h and 144h. COL1A1 deposition was normalized to the total proteins in the cell lysate and reported as percentage *vs* Vehicle. Values presented are the mean ± SD of three biological replicates. * $p < 0.05$ vs Vehicle, # $p < 0.05$ *vs* FFA, ## $p < 0.01$ *vs* FFA. Abbreviations: COL1A1, collagen type I alpha 1 chain; FFA, free fatty acids.

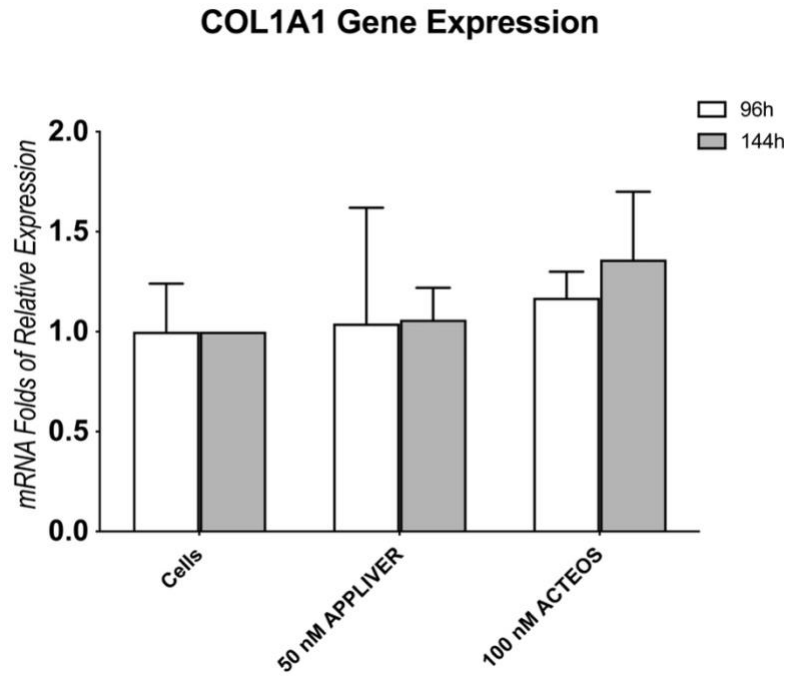

Figure 18. Gene expression of COL1A1 upon exposure to APPLIVER and ACTEOS after 96h and 144h without FFA. Values presented are the mean ± SD of three biological replicates. No significant results *vs* cells without treatment. Abbreviations: COL1A1, collagen type I alpha 1 chain; FFA, free fatty acids.

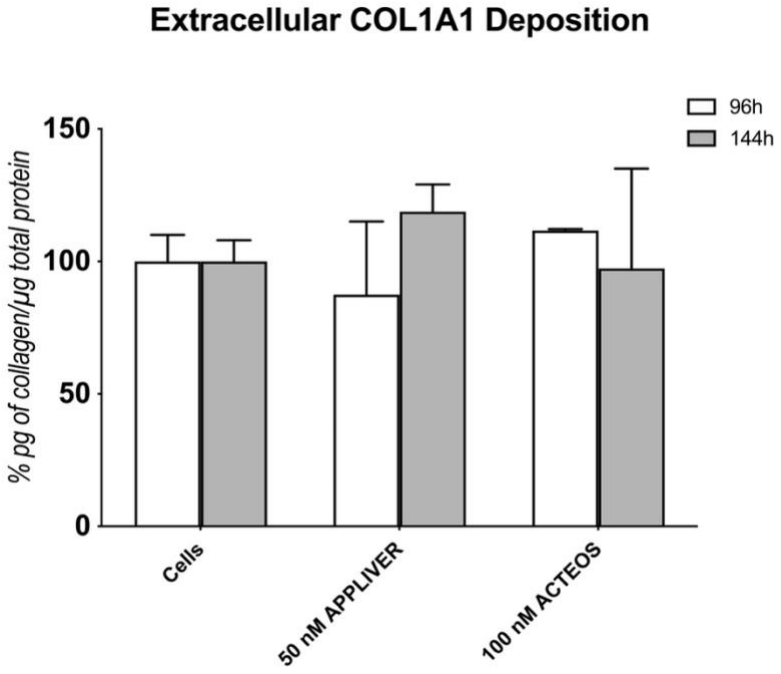

Figure 19. Quantification of extracellular COL1A1 deposition (% pg of collagen/µg total protein) using ELISA upon treatment of either APPLIVER or ACTEOS without FFA after 96h and 144h. COL1A1 deposition was normalized to the total proteins in the cell lysate and reported as percentage *vs* Vehicle. Values presented are the mean ± SD of three biological replicates. No significant results *vs* cells without treatment. Abbreviations: COL1A1, collagen type I alpha 1 chain; FFA, free fatty acids.

3. Discussion

APPLIVER and ACTEOS are two biotechnological compounds obtained by an innovative biotechnological platform of plant cell culture [85]. Triterpenic acid, the main component of APPLIVER is isolated from various plants such as *Vochysia divergens, Potentilla chinensis, Cydonia oblonga,* and *Malus domestica* [86,87]. Mounting evidence suggests that TA exerts several biological activities including anticancer, anti-inflammatory, antidiabetic, and antihepatotoxic properties [74,88–90]. Acteoside, also known as verbascoside, is the major component of ACTEOS. Acteoside is a phenylethanoid glycoside ingredient that can be found in more than 200 plant species, including *Plantago* and *Lippia* species [91]. As for TA, acteoside has been reported to exert various pharmacological activities such as antioxidant, antimicrobial, anti-inflammatory, neuroprotective, anticancer, and hepatoprotective effects [92,93].

Both compounds showed hepatoprotective effects in chemically-induced liver damage in mice by lowering transaminase levels and improving total bilirubin levels [76]. Additionally, both compounds were found to reduce histological alterations in liver tissues [76,87]. However, only few evidence is found in the literature when it comes to their effects on MASLD/MASH-related pathophysiological mechanisms such as steatosis, oxidative stress, inflammation, and fibrosis. The marginal data regarding the molecular mechanisms hamper drug development, particularly in the context of MASLD/MASH.

In this study, we assessed the effects of the compounds in counteracting the cellular events following lipid accumulation in both hepatocytes and simultaneous co-culture (hepatocytes-HSCs). Several models of MASH propose that the FFA accumulation in hepatocytes results in hepatocyte injury, inflammation, and oxidative stress [78,79]. In particular, persistent inflammation in hepatocytes may trigger the activation of HSCs, which in turn are responsible for the production and deposition of the extracellular matrix such as collagen, which is a hallmark of MASH [94,95].

We developed an *in vitro* model of MASH where the exposure of hepatocytes to high concentrations of FFA promotes inflammation, oxidative stress, and fibrogenic response, similar to those observed in patients with MASH [80]. Moreover, our group also developed an *in vitro* model that reproduces the initial events involved in fibrosis with overexpression of alpha-smooth muscle actin (α-SMA), accumulation of extracellular collagen, modulation of metalloproteinases (MMPs) and tissue inhibitor of metalloproteinases (TIMP) [96].

FFA overload in hepatocytes results in inflammation. Although resident liver macrophages (Kupffer cells) are important drivers of hepatic inflammation, hepatocytes *per se* have a role in initiating the inflammatory response [80,96,97]. Cytokines are crucial players in inflammatory-associated disorders like MASLD and are considered potential therapeutic targets. In the present study, we observed that APPLIVER and ACTEOS showed a significant reduction of TNF-

α at both gene and protein levels. TNF-α plays a pivotal role in the multiple steps process of MASH development by inducing key enzymes of lipid metabolism, inflammatory cytokines, and fibrosis-associated proteins [97]. Hence, the attenuation of TNF-α action in the liver may help prevent or delay the development of MASH associated with metabolic syndrome. Although not directly on MASH model, the role of TA in attenuating the levels of proinflammatory cytokines has been demonstrated in chemical-induced inflammation in mice. In lipopolysaccharide (LPS)-induced neuroinflammation in mice, TA downregulated the expression of TNF-α and IL-1β by inhibiting nuclear factor-kappa B (NF-κB) and activating liver X receptor alpha (LXRα) receptors [89]. This was confirmed by the observation that TA decreased the serum IL-1β, IL-6, and TNF-α levels in acetaminophen-induced liver damage in mice by inhibiting the NF-κB and mitogen-activated protein (MAP) kinases activities [98].

Several reports pointed out that excess FFA can also directly trigger mitochondrial dysfunction leading to reactive oxygen species (ROS) production, another key hallmark of MASH [39,43,99]. ROS production has also been linked to hepatic inflammation by increasing the secretion of TNF-α from hepatocytes and Kupffer cells, thus upregulating the synthesis of inflammatory cytokines [95]. We, therefore, assessed the role of APPLIVER and ACTEOS in attenuating the production of ROS in FFA-overloaded hepatocytes. In line with our previous results, FFA excess enhanced the production of ROS, similar to a level induced by hydrogen peroxide (positive control). Cotreatment of APPLIVER resulted in an apparent but not significant antioxidant effect while ACTEOS showed a significant reduction in ROS generation. A similar observation was reported in oxidative stress-induced HepG2 and SH-SY5Y cell lines, implying the role of acteoside as a hepatoprotective and neuroprotective agent, respectively [93].

As mentioned earlier, the severity of hepatic fibrosis is the primary predictor of liver-related morbidity and mortality in MASLD patients [19]. The role of HSCs in liver fibrogenesis is well established and occurs through the activation and alteration of genes involved in the turnover of extracellular matrix components [70]. We showed that excess FFA in hepatocytes activates the HSCs, indicating that cell-to-cell proximity between the two cell types is necessary for the initiation of the fibrotic process and overproduction of collagen type I [71]. ACTEOS was able to reduce both the gene expression and protein levels of COL1A1 in our SCC model of MASH. Acteoside was shown as a potential renal and prostate fibrosis antagonist by inhibiting the TGF-β1/Smads signaling pathway in some studies [100,101].

APPLIVER at 96h showed a non-significant reduction in *COL1A1* gene expression while the level of the collagen protein was significantly reduced. This discrepancy may be due to the differences in the transcription and translation rates of COL1A1 gene and protein, as well as differences in their half-lives in achieving steady-state levels [102]. A recent study showed that TA inhibited

platelet-derived growth factor-BB-stimulated HSC activation, as evidenced by the inhibition of cell proliferation, migration, and colony formation, as well as the decreased expression of TGF-β and α-SMA through blocking the PI3K/Akt/mTOR and NF-κB signaling pathways [103]. The same study also revealed that TA decreased the expression of collagen type I and III alleviating the excessive deposition of ECM.

Overall, the present study showed that the *in vitro* model provides a promising tool for investigating the efficacy of new candidate drugs, particularly on pathophysiological mechanisms involved in MASH. The use of human cell lines in both monoculture and simultaneous co-culture setups facilitates standardized protocol and reproducible studies. However, caution is needed to export *in vitro* data to far more complex animal and human subjects. Nevertheless, the data obtained herein support the beneficial effects of APPLIVER and ACTEOS in the *in vitro* MASH environment.

In summary, our results revealed that APPLIVER and ACTEOS are promising therapeutic compounds in counteracting the pathophysiological mechanisms caused by excess of FFA in the hepatocytes. ACTEOS provided solid results by reducing both the inflammation and the oxidative stress and, most importantly, attenuating collagen production elicited by the excess of FFA in the SCC model. In the absence of FFA, the use of APPLIVER or ACTEOS alone did not induce any cellular alteration of the processes under study, suggesting the safety of this compound in the absence of steatosis. The beneficial effects observed can be attributed to triterpenic acid and acteoside since they are the main components of APPLIVER and ACTEOS, respectively, but the contribution of other components present in the extracts cannot be excluded. Taken together, the use of the data obtained herein using the *in vitro* MASH model remains to be explored before its use in the clinical MASLD/MASH setting.

4. Materials and Methods

4.1 Compounds and Chemicals

APPLIVER is a new commercialized biotechnological compound (MRM01ECL, *Cydonia oblonga* extract, ABRESEARCH SRL, Brendola, Italy). It is an extract from the plant cell suspension culture of *Cydonia oblonga's* fruit (quince). This extract was obtained by an alcoholic extraction of freeze-dried cells, containing 10.8% of euscaphic acid, expressed as triterpenic acid (MW: 488.7 g/mol). The solubility of the extract is 25 mg on 0.5 mL of DMSO. From 2 g of APPLIVER, 5.4 mg were weighed to prepare a 50 mg/mL stock solution in DMSO.

ACTEOS is a commercialized biotechnological compound (LCK03ECL, *Lippia Citriodora* extract, ABRESEARCH SRL, Brendola, Italy). It is an extract from plant cell suspension culture of *Lippia citriodora* (or *Aloysia citriodora*) belonging to Verbenaceae family, containing 71.2% of phenylpropanoid expressed as acteoside (MW: 4624.59 g/mol). The solubility of the extract is 25 mg on 0.3 mL of 60/40% water/ethanol. From 2 g of ACTEOS, 59.3 mg were

weighed to prepare an 83.3 mg/mL stock solution in 60/40% water/ethanol. For each experiment, dilutions of the stock solutions in cell culture media were freshly prepared every time.

Dulbecco's modified Eagle's high glucose medium (DMEM-HG), L-glutamine, penicillin/streptomycin, and fetal bovine serum were purchased from Euroclone (Milan, Italy). 3-(4,5-dimethylthiazol-2-yl)-2,5-diphenyltetrazolium bromide (MTT), bicinchoninic acid solution-kit (B9643); bovine albumin Cohn V fraction (A4503); dimethyl sulfoxide (DMSO), hydrogen peroxide (H1009), Nile Red (N3013), oleic acid (C18:1), palmitic acid (C16:0), phosphate-buffered saline (PBS) and Tri-Reagent (T9424) were obtained from Sigma Chemical (St. Louis, MO, USA). AlphaLISA cell lysis buffer and Alpha Immunoassay buffer were from PerkinElmer (Boston, MA, USA). iScript™ cDNA Synthesis kit (170-8890) and iQ SYBR Green Supermix (170-8860) were purchased from Bio-Rad Laboratories (Hercules, CA, USA). 2',7'-dichlorodihydrofluorescein diacetate (H_2DCFDA) (D399) was obtained from Molecular Probes (Milan, Italy).

4.2 Cell Culture

Hepatic stellate cell line, LX2 was kindly provided by S.L. Friedman (Mount Sinai School of Medicine, New York, NY, USA) while hepatoma-derived cell line, Huh7 (JHSRRB, Cat#JCRB0403) was obtained from the Japanese Health Science Research Resource Bank (Osaka, Japan). LX2 cells express α-SMA under all culture conditions and therefore must be regarded as at least partially activated. Despite this, LX-2 cells can be quiesced by growth in matrigel or low serum [104,105]. Therefore, LX2 cells were maintained in DMEM High Glucose (HG) supplemented with 100 U/mL penicillin/streptomycin, 2 mM L-glutamine, and 1% v/v fetal bovine serum at 37°C in 5% CO2 air humidified atmosphere.

The simultaneous co-culture was prepared in a cell ratio of 5:1 (hepatocytes:HSCs), resembling the *in vivo* ratio of parenchymal to non-parenchymal cells in the liver [106]. For each experiment, SCC was maintained in DMEM-HG supplemented with 100 U/mL penicillin/streptomycin, 2 mM L-glutamine, and 1% v/v fetal bovine serum. LX2 cells were maintained all throughout in 1% FBS while Huh7 cells were first adapted to 1% FBS medium by reducing gradually the medium serum concentration two weeks before the experiment. For the induction of MASH, SCC, and monoculture were exposed to 1200 μM of free fatty acids (FFA) (oleic:palmitic ratio 2:1 μmol/μmol) as previously described by our group [71,79]. Media containing FFA and APPLIVER and ACTEOS were refreshed every 2 days until they reach the experimental time point. Effects of APPLIVER and ACTEOS were evaluated also in the absence of FFA to assess possible side effects. For each culture setup (monoculture or SCC), cells exposed to the vehicle were used as a control. The maximal concentration of vehicle (DMSO) was 0.22% v/v. SCC total cell densities for each time point were 20,000 cells/cm^2, 10,000 cells/cm^2, and 5000 cells/cm^2 at 24h, 96h, and 144 h, respectively. Summary of the experimental setup, conditions, and experimental checkpoints are described in figure 20 below.

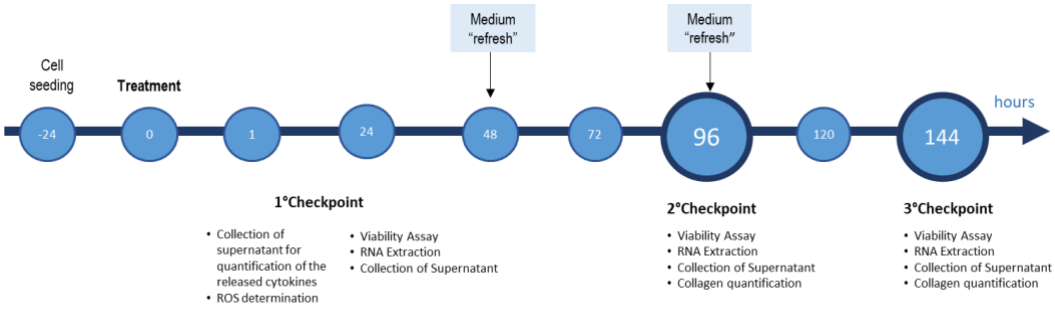

Figure 20. Scheme of the culture proceedings and the experimental checkpoints with the relative determinations.

4.3 Experimental Dose Determination and Cell Viability Assay

The cytotoxic effect of FFA (1200 μM), APPLIVER, and ACTEOS alone or in combination was assessed by MTT colorimetric assay at 24, 96, and 144 hours. Monoculture and SCC were plated at a cell density as described before [96] and treated accordingly with increasing concentrations of APPLIVER and ACTEOS. Likewise, cells were also exposed to control medium with increasing concentrations of APPLIVER and ACTEOS only to assess their intrinsic toxicity in the system without FFA. After each experimental time, the medium was removed and cells were incubated for 1 hour with MTT at the concentration of 0.5 mg/ml. Afterward, the culture medium was removed, and formazan crystals were dissolved in 200 μl of DMSO. 100 μl from each well was transferred to a microtiter plate and optical density (OD) was determined at 562 nm wavelength on an Enspire® Multimode Plate Reader (PerkinElmer, Waltham, MA USA).

To identify the experimental concentration for each compound, we followed the recommendation of ISO 10993-5 (*in vitro* cytotoxicity test on extracts) [81]. A reduction in cell viability of more than 20% was considered as the exclusion criterion. The cutoff concentration meeting this requirement was selected as the experimental concentration for each compound.

4.4 Fluorimetric determination of intracellular fat content - Nile red staining

Intracellular fat content was determined by flow cytometry using Nile Red staining, a vital lipophilic dye used to label fat accumulation in the cytosol [80]. After 24h and 96h of FFA exposure, adherent monolayer cells were washed twice with PBS and detached by trypsinization. After 5 minutes of centrifugation at 1500 rpm, the cell pellet was resuspended in 3 mL of PBS and incubated with 0.75 μg/mL Nile red dye for 15 min at room temperature. Nile Red intracellular fluorescence was detected using a Becton Dickinson FACSCalibur System on the FL2 emission channel through a 585 ± 21 nm bandpass filter, following excitation with an argon-ion laser source at 488 nm. Data were collected in 10,000 cells and analyzed using Cellquest software from BD Biosciences (San Jose, CA, USA).

4.5 RNA Extraction, cDNA Synthesis, and Gene Expression Analysis by qRT-PCR

Total RNA was extracted from culture harvest using Tri-reagent kit (SIGMA) according to the manufacturer's instructions. The total RNA concentration was then quantified spectrophotometrically at 260 nm in a Beckman CoulterDU®730 spectrophotometer (Fullerton, CA, USA) while purity was evaluated by measuring the A260/A280 ratio. Total RNA (1 μg) was reverse transcribed using the High Capacity cDNA Reverse Transcription Kit (Applied Biosystems, Waltham, MA, USA) according to the manufacturer's protocol in a Thermal Cycler (GeneAmp PCR System 2400, PerkinElmer, Boston, MA, USA). Quantitative PCR was performed in i-Cycler IQ (Bio-Rad, Hercules, CA USA). All primer pairs were designed using the software Beacon Designer 8.12 (PREMIER Biosoft International Palo Alto, CA, USA) and were synthesized by Sigma Genosys Ltd. (London Road, UK). Primer sequences are specified in table 2. 18S and HPRT were used as reference genes. PCR amplification was performed in 20 μL reaction volume containing 25 ng of cDNA, 1X iQ SYBR Green Supermix, and 250 nM gene-specific sense and antisense primers and 100 nM primers for 18S. The data were analyzed using Bio-Rad iQ5 software (version 3.1).

Table 2. Primer sequences used for the *in vitro* experiments.

Gene Name	Accession Number	Forward	Reverse
IL-8	NM_000584	GACATACTCCAAACCTTTCCAC	CTTCTCCACAACCCTCTGC
IL-6	NM_000600	ACAGATTTGAGAGTAGTGAGGAAC	GGCTGGCATTTGTGGTTGG
TNF-α	NM_000594	GTGAGGAGGACGAACATC	GAGCCAGAAGAGGTTGAG
COL1A1	NM_000088	CGGAGGAGAGTCAGGAAG	ACACAAGGAACAGAACAGTC
18S	NR_003286.2	TAACCCGTTGAACCCCATT	CCATCCAATCGGTAGTAGCG
HPRT	NM_000194.	ACATCTGGAGTCCTATTGACATCG	CCGCCCAAAGGGAACTGATAG

4.6 Intracellular ROS Generation by H_2DCFDA

Intracellular Reactive Oxygen Species (ROS) generation was measured using the cell-permeable fluorogenic substrate H_2DCFDA. This non-fluorescent probe is easily taken up by cells and, after intracellular cleavage of the acetyl groups, is trapped and may be oxidized to the fluorescent compound 2',7'-dichlorofluorescein (DCF; the monitored fluorophore) by intracellular ROS. Huh7 cells were exposed for 1 hour with APPLIVER and ACTEOS, FFA co-treated with APPLIVER and ACTEOS, hydrogen peroxide as the positive control, and vehicle control. Then cells were washed with PBS and incubated for 30 min with FBS free culture medium supplemented with 25 mM HEPES/ 20 μM H_2DCFDA at 37°C. Afterward, cellular fluorescence was quantified by scanning the signal of the attached cells in each well with an Enspire® Multimode Plate Reader (PerkinElmer) at excitation wavelength 505 nm and emission 525 nm.

Fluorescence was normalized by the total proteins present in the cell lysates (μg) assessed using fluorescamine for each sample.

4.7 Quantification of COL1A1 Deposition (AlphaLISA quantification)

The amount of collagen present in the SCC system was quantified by AlphaLISA (PerkinElmer AL371), according to the manufacturer's protocol. Briefly, after 96 and 144 hours of treatment, cells were washed with PBS and lysed with AlphaLISA lysis buffer. Cell lysates were diluted 1:10 in AlphaLISA Immunoassay Buffer, and 2 μL of samples were incubated for 30 min at 23°C with 4 μL of 5X AlphaLISA Anti-hCOL1A1 acceptor beads. Subsequently, 4 μl of 5X Biotinylated Anti-hCOL1A1 antibody was added and incubated for 60 min. Then 10 μl of 2X SA-Donor Beads were added to each sample and incubated for another 30 min in the dark. The signal reading was performed using an EnVision-Alpha Reader at 615 nm. Collagen concentration was calculated by extrapolation of the data in a standard curve constructed with known concentrations of collagen.

4.8 Normalization vs μg of total proteins

To obtain more accurate data and to exclude misleading results due to eventual differences in the number of attached cells, data from collagen quantification, ROS assay, and AlphaLISA assay were normalized by μg of total proteins in each well. AlphaLISA lysis buffer interfered with the normal techniques for protein quantification (BCA, Bradford, 280nm absorbance), thus the total protein concentration was calculated fluorometrically (ex: 390nm – em: 460nm) by fluorescamine reaction. Total proteins were quantified by fluorescamine, a nonfluorescent molecule that reacts readily with primary amines in amino acids and peptides to form stable, highly fluorescent compounds. Ten microliters of fluorescamine at 4 mg/mL in DMSO were mixed with 40 μL of cell lysate diluted 1:2 v/v. Fluorescence was read at 460 nm (excitation wavelength of 390 nm) in an EnSpire® Multimode Plate Reader (PerkinElmer, Waltham, MA USA). Total protein was calculated using a BSA standard curve dilution.

4.9 TNF-α ELISA and Bicinchoninic acid (BCA) Assay

The TNF-α release in cell culture supernatant was quantified by Human TNF alpha SimpleStep ELISA® Kit (ABCAM, AB181421), according to the manufacturer's protocol. Briefly, after 1 hour of treatment, cell culture supernatants were collected. 50 μL of samples or standard were loaded to appropriate wells. After which, 50 μL of the antibody cocktail were added to each well. Plate was incubated for 1 hour at room temperature on a plate shaker set to 400 rpm. Plate was then washed 3 times with 50 μL 1X Wash Buffer PT in each well. Then, 100 μL of TMB development solution to each well were added and incubated for 10 minutes in the dark on a plate shaker set to 400 rpm. Finally, 100 μL of stop solution in each well were added the absorbance was read at 450

nm. TNF-α (pg/μL) concentration was calculated by extrapolation of the data in a standard curve constructed with known concentrations of TNF-α.

To obtain more accurate data and to exclude misleading results due to eventual differences in the amount of proteins released in the supernatant, data from TNF-α ELISA were normalized by μg of total proteins in each well. Total protein was calculated by Bicinchoninic acid (BCA) Assay using a BSA standard curve dilution.

4.10 Statistical Analysis

All values are presented as mean ± standard deviation (S.D.) from three biological replicates. Statistical analysis was performed by one-way ANOVA (with post hoc test) or student's t-test, whenever applicable using GraphPad Prism, version 5.0 (GraphPad Software, CA, USA) (v5). Statistical significance was determined at $p < 0.05$.

Author Contributions: Conceptualization, N.S., N. R. and C.T.; methodology, N.S and N.R..; investigation, N. R. and C.T.; resources, A. S. and C.B.; data curation, N.S and N.R writing—original draft preparation, N.S., N. R., C.T., A.S. and C.B.; writing—review and editing, N.S., N. R., C.T., A.S. and C.; funding acquisition, A. S. and C.B. All authors have read and agreed to the published version of the manuscript.

Funding: This research was funded by ABRESEARCH SRL, via dell'Impresa, 1, 36040 Brendola (VI), Italy.

Acknowledgments: The present study has been supported by a grant from ABR (ABRESEARCH SRL, Brendola Italy). NS is funded by the Department of Science and Technology - Philippine Council for Health Research and Development (DOST-PCHRD), Philippines. NR is partially supported by Fondazione Cassa di Risparmio di Trieste (CRTrieste) and by Fondazione Italiana Fegato – ONLUS.

CHAPTER 4

PROJECT 2 (DIAGNOSIS)

Ficolin-2 plasma levels assess liver fibrosis in metabolic-associated fatty liver disease

Abstract

Fibrosis is the strongest predictor for disease-specific mortality in metabolic dysfunction-associated steatotic liver disease (MASLD), but the need for liver biopsy limits its diagnosis. We assessed the performance of plasma ficolin-2 (FCN-2) as a biomarker of fibrosis identified by an *in silico* discovery strategy. 235 morbidly obese (MO) subjects with biopsy-proven MASLD stratified by fibrosis stage (F0, n = 44; F1, n = 134; F2, n = 46; F3, n = 11) and 40 cirrhotic patients were enrolled. The cohort was subdivided into discovery (n = 76) and validation groups (n = 159). The plasma level of FCN-2 and other candidate markers was determined. FCN-2 inversely correlated with the stage of liver fibrosis (ϱ = -0.49, $p < 0.001$); independently of steatosis (p = 0.90), inflammation (p = 0.57), and ballooning (p = 0.59). In the global cohort, FCN-2 level decreased significantly in a stepwise fashion from F0/F1 (median 4753 ng/mL) to F2-F3 (2760 ng/mL) and in cirrhotic subjects (1418 ng/mL). The diagnostic performance of FCN-2 in detecting F≥2 was higher than other indexes (APRI, FIB-4) (AUROC 0.82, 0.68, and 0.6, respectively). The accuracy improved when combined with APRI score and HDL values (FCNscore, AUROC 0.85). Overall, FCN-2 plasma level can accurately discriminate liver fibrosis status (minimal *vs.* moderate/advanced), thereby significantly improving the fibrosis diagnostic algorithms.

Publications:

- Giraudi PJ, **Salvoza N**, Bonazza D, Saitta C, Lombardo D, Casagranda B, de Manzini N, Pollicino T, Raimondo G, Tiribelli C, Palmisano S, Rosso N. Ficolin-2 Plasma Levels Assess Liver Fibrosis in Non-Alcoholic Fatty Liver Disease. International Journal of Molecular Sciences. 2022; 23(5):2813. https://doi.org/10.3390/ijms23052813**.**

Poster Presentation:

- "The International Liver Congress 2022" by The European Association for the Study of the Liver (EASL). London, United Kingdom. June 22-26, 2022.

1. Introduction

Liver biopsy, the gold standard for MASLD diagnosis, was established almost a century ago [107]. Despite the invasiveness, costs, and sampling error limitations, there are still no reliable non-invasive diagnostic tests for fibrosis in MASLD. Two pathways have been exploited in approaching alternatives to the gold standard: blood-based non-invasive indirect tests have been combined in indexes such as the fibrosis-4 (FIB-4) score [108], the AST to platelet ratio index (APRI), or individual markers indirect tests such as the type III collagen neo-epitopes (PRO-C3) [109].

Imaging technologies (magnetic resonance elastography, shear wave elastography, or acoustic radial force imaging) have been used for the non-invasive diagnosis of MASLD/MASH and fibrosis. However, none of these modalities satisfies the desired clinical accuracy and practicability [110].

Interestingly, in the big-data era, new approaches contribute to the discovery of promising biomarkers. The fast development of omics technologies has enormously favored biomedical sciences. Specifically, the improvements in data acquisition and analysis through high-throughput technologies (such as microarrays and RNA-seq) have the power to evolve biomedical science from a static to a more dynamic form [111]. Thus, the availability of harmonized datasets in many public repositories allows *in silico* strategies to develop biomarker discovery pipelines.

Using enrichment analysis of phosphoproteomic datasets, Page S *et al.* proposed C-C motif chemokine (CCL2) and tumor necrosis factor ligand superfamily member 6 (sFasL) as biomarkers in MASLD pathogenesis [112]. Through a transcriptomic study, Hotta K. e*t al.* [113] described a core gene networks associated with MASLD progression. By transcriptomic meta-analysis, Ryaboshapkina M. *et al.* identified several genes involved in MASLD progression and biomarkers for disease stratification [114].

In the present study, we assessed the performance of Ficolin-2 protein (FCN-2) as a putative novel biomarker of liver fibrosis and tested its utility combined with a blood-based score test. We also described the *in silico* strategy used to identify FCN-2 and other protein candidates that are potentially functional in fibrosis diagnosis.

2. Results

2.1. Identification by the in silico funnel strategy of candidate biomarkers for liver fibrosis

We used a systematic discovery strategy in which the human proteome (originated from ~20,000 protein-coding genes [115]) was visualized at the top of a giant funnel. Several *in silico* filters were cross-placed at different heights (Figure 21a). Proteins moving down in the funnel reach a thicker grade of selectivity and specificity. In the approach, the *in silico* filters were represented by Venn diagrams used to apply selection criteria at the bio-datasets, consequently obtaining the most selective sub-bio-datasets (Figure 21b). The full description of the *in silico* strategy performed by Giraudi, PJ is presented in the supplementary materials of our published paper [67]. By using the described strategy, we identified some proteins as candidate biomarkers for liver fibrosis. Those markers fulfilled the following desired characteristics: 1) candidates must participate in the acquisition of myofibroblast phenotype; 2) be expressed in liver tissue; 3) the expression must be modified during fibrosis; and 4) must be secreted and measurable in plasma. From this analysis, 35 proteins were identified as putative candidates, excluding collagen proteins or other extracellular matrix components, since they might be stabilized in the surrounding area of liver cells without the release into the bloodstream. Thus, we obtained 29 candidate biomarkers (Table 3). Five randomly selected proteins of the total candidates were evaluated in this study.

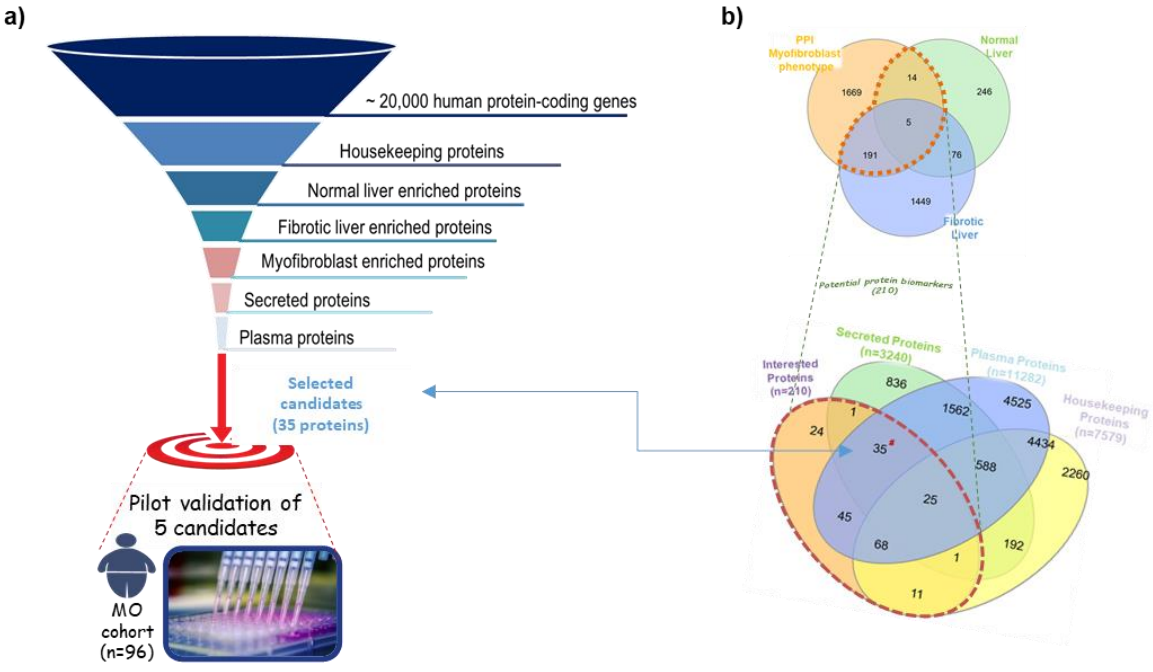

Figure 21. Summary of the *in silico* biomarker discovery strategy used in the study. (a) Layout of the *in silico* funnel strategy. **(b)** Venn diagrams illustrating the different datasets used to identify candidates satisfying our selection criteria.

Table 3. List of the candidate biomarkers individuated by the *in silico* funnel discovery strategy.

UniprotKb ID	Protein name	Subcellular Location	Selection Criteria
Q15485	Ficolin-2	Secreted	Fibrotic liver + PPI myofibroblasts + normal liver
P24593	Insulin-like growth factor-binding protein 5	Secreted	PPI myofibroblasts + fibrotic liver
Q12805	EGF-containing fibulin-like extracellular matrix protein 1	Extracellular space	
P27918	Properdin	Secreted	
O75636	Ficolin-3	Secreted	
Q8NEA6	Zinc finger protein GLIS3	Nucleous, predicted secreted	
O95897	Noelin-2	Secreted	
P13726	Keratin, type I cytoskeletal 10	Extracellular region	
Q13332	Receptor-type tyrosine-protein phosphatase S	Cell membrane, secreted	
Q9H6X2	Anthrax toxin receptor 1	Cell membrane, secreted	
Q00796	Sorbitol dehydrogenase	Mitochondrion	
P35555	Fibrillin 1	Secreted, extracellular matrix	
Q9Y6N6	Laminin subunit gamma-3	Extracellular matrix, secreted	
P09341	Growth-regulated alpha protein	Secreted	
P24592	Insulin-like growth factor-binding protein 6	Secreted	
P00749	Urokinase-type plasminogen activator	Secreted	
Q9UKQ2	Disintegrin and metalloproteinase domain-containing protein 28	Secreted	
P13612	Integrin alpha-4	Membrane, secreted	
P21246	Pleiotrophin	Secreted	
Q9UM22	Mammalian ependymin-related protein 1	Secreted	
P05156	Complement factor I	Extracellular space	PPI myofibroblast + normal liver
P03950	Angiogenin	Nucleous, secreted	
P19652	Alpha-1-acid glycoprotein 2	Secreted	
P04114	Apolipoprotein B-100	Secreted	
P00747	Plasminogen	Secreted	
Q14624	Inter-alpha-trypsin inhibitor heavy chain H4	Secreted	
P02749	Beta-2-glycoprotein 1	Secreted	
P09237	Matrilysin	Secreted	
P81172	Hepcidin	Secreted	

2.2. *Demographics and biochemical data, and association with liver fibrosis*

Table 4 summarizes the clinico-demographic details of the patients included in the discovery, validation, and combined MO cohorts. Since the primary endpoint of this study was to predict fibrosis, we stratified the cohorts accordingly to the fibrosis stage (F0-F1 *vs* F2-F3-F4). We used the discovery cohort to qualify the candidates and the validation cohort for their verification, testing the reproducibility of the diagnostic performances of the best candidate.

Table 4. Clinical characteristics of all morbidly obese patients.

Variable	Combined cohort (n = 235)	Discovery cohort (n = 76)	Validation cohort (n = 159)	*p* value
Age (years)	45.0 ± 10.0	44.5 ± 10.6	45.3 ± 9.8	0.95
Sex (female)	159 (67%)	52 (68%)	107 (67%)	0.98
BMI (Kg/m^2)	43.9 ± 5.8	43.9 ± 6.4	43.9 ± 5.5	0.96
Fasting glucose (mg/dL)	112.6 ± 30.0	118.2 ± 33.4	110 ± 28.0	0.27
T2DM (yes)	61 (26%)	19 (25%)	42 (26%)	0.97
AST (U/L)	25.9 ± 14.0	26.8 ± 15.2	25.8 ± 14.0	0.93
ALT (U/L)	32.4 ± 24.6	34.9 ± 29.6	31.2 ± 22.0	0.79
GGT (U/L)	39.7 ± 39.2	39.1 ± 34.6	40.0 ± 41.3	0.81
Albumin (g/dL)	4.2 ± 0.3	4.2 ± 0.3	4.1 ± 0.3	0.06
Platelets ($X10^9/L$)	251.0 ± 68.0	253.0 ± 71.0	246.0 ± 63.0	0.68
Total Cholesterol (mg/dL)	205.0 ± 41.0	200.0 ± 49.0	207 ± 37.5	0.45
HDL cholesterol(mg/dL)	47.3 ± 10.7	48.1 ± 10.0	45.7 ± 12.0	0.08
Triglycerides (mg/dL)	144.0 ± 77.0	140.0 ± 67.3	151.5 ± 93.2	0.70
Steatosis grade (0/1/2/3)	53/79/61/42	12/22/27/15	41/57/34/27	0.02*
Lobular inflammation (0/1/2/3)	76/134/25/0	23/39/14/0	53/95/11/0	0.18
Ballooning (0/1/2)	124/68/43	31/28/17	93/40/26	0.16
Fibrosis stage (0/1/2/3-4)	45/132/46/12	18/24/28/6	27/108/18/6	<0.0001***
AST/ALT	0.92 ± 0.31	0.93 ± 0.30	0.90 ± 0.32	0.67
APRI	0.32 ± 0.57	0.32 ± 0.68	0.30 ± 0.24	0.98
FIB4	0.94 ± 0.68	0.95 ± 0.79	0.93 ± 0.61	0.88
FORNS	3.57 ± 1.8	3.55 ± 1.73	3.56 ± 1.80	0.95
NFS	-0.93 ± 1.36	-0.88 ± 1.35	-0.70 ± 1.38	0.57

Data are shown as mean ± SD for continuous variables, number (%) for binary variables, and frequency for categorical variables. ANOVA was used to test for significant differences within continuous variables that were normally distributed while Kruskal-Wallis with Dunn post-test when not normally distributed. Chi-Square test was used for categorical variables. ***significant at $p < 0.001$, **significant at $p < 0.01$, and *significant at $p < 0.05$. Abbreviations: BMI, body mass index; ALT, alanine aminotransferase; AST, aspartate aminotransferase; GGT, gamma-glutamyl transferase; T2DM, type 2 diabetes mellitus; HDL, high density cholesterol; APRI, AST to platelet ratio index; FIB4, fibrosis-4; FORNS, Forns index; NFS, NAFLD fibrosis score.

In table 5, the clinico-demographic characteristics of the discovery cohort are presented. Significant differences between both fibrotic groups were observed in sex (30% female higher in the F0-F1 group) and blood parameters. AST and GGT levels were higher in the moderate/advanced fibrosis group (32 ± 18 IU/L vs. 23 ± 12 IU/L, p = 0.02, and 49 ± 41 IU/L vs. 32 ± 27 IU/L, p = 0.04, respectively) while blood platelets were reduced (220 ± 57 x103/μL vs. 266 ± 60 x103/μL, p = 0.002). The differences were also reflected by the blood-based indexes, such as FIB-4

(1.27 ± 1.1 F2/F3-F4 vs. 0.72 ± 0.3 F0-F1, p = 0.007), FORNS (4.2 ± 1.9 F2/F3-F4 vs. 3.0 ± 1.4 F0-F1, p = 0.003) and NFS (-0.06 ± 1.3 F2/F3-F4 vs. -1.2 ± 1.2 F0-F1, p = 0.0003).

Table 5. Demographic and clinical characteristics of the discovery cohort.

MO discovery cohort			
Variable	**F0-F1 (minimal fibrosis) n = 42**	**F2-F3 (moderate/advanced fibrosis) n = 34**	***p* value**
Age (years)	45.0 ± 10.0	44.5 ± 10.6	0.27
Sex (female)	35 (81%)	17 (51%)	0.005**
BMI (kg/m^2)	42.8 ± 10.4	45.4 ± 7.1	0.09
Fasting glucose (mg/dL)	115.1 ± 33.5	122.2 ± 33.4	0.37
T2DM (yes)	8 (19%)	11 (33%)	0.16
AST (UI/L)	23.1 ± 11.7	32.0 ± 18.0	0.02*
ALT (UI/L)	32.6 ± 29.5	38.0 ± 29.9	0.44
GGT (UI/L)	31.8 ± 27.5	48.6 ± 40.6	0.04
Albumin (g/dL)	4.1 ± 0.3	4.2 ± 0.4	0.09
Platelets (X10^9/L)	266 ± 60	220 ± 57	0.002**
Total Cholesterol (mg/dL)	201.7 ± 47.3	198.5 ± 52.0	0.78
HDL Cholesterol (mg/dL)	47.4 ± 13.3	43.6 ± 10.0	0.18
Triglycerides (mg/dL)	150.8 ± 108	152.4 ± 70.0	0.94
Steatosis grade (0, 1, 2, 3)	6/15/14/7	6/7/13/8	0.55
Lobular Inflammation (0, 1, 2, 3)	17/19/6/0	6/20/8/0	0.09
Ballooning (0, 1, 2)	17/16/9	14/12/8	0.91
Fibrosis stage (0, 1, 2, 3, 4)	18/24/0/0/0	0/0/28/5/1	<0.0001***
AST/ALT	0.87 ± 0.33	0.94 ± 0.32	0.33
APRI	0.22 ± 0.12	0.41 ± 0.35	0.002**
FIB-4	0.72 ± 0.30	1.27 ± 1.09	0.007**
FORNS	3.0 ± 1.4	4.24 ± 1.9	0.003**
NFS	-1.2 ± 1.2	-0.06 ± 1.3	0.0003***

Data are shown as mean ± SD for continuous variables, number (%) for binary variables, and frequency for categorical variables. ANOVA was used to test for significant differences within continuous variables that were normally distributed while Kruskal-Wallis with Dunn post-test when not normally distributed. Chi-Square test was used for categorical variables. ***significant at p < 0.001, **significant at p < 0.01, and *significant at p < 0.05. Abbreviations: BMI, body mass index; ALT, alanine aminotransferase; AST, aspartate aminotransferase; GGT, gamma-glutamyl transferase; T2DM, type 2 diabetes mellitus; HDL, high density cholesterol; APRI, AST to platelet ratio index; FIB4, fibrosis-4; FORNS, Forns index; NFS, NAFLD fibrosis score; NA, not available.

The clinico-demographic characteristics of the validation and cirrhotic cohorts are reported in table 6. MO and cirrhotic cohorts showed significant differences in several parameters, particularly GGT, platelets, total cholesterol, and triglycerides, among others in the blood-based indexes (APRI, FIB-4, NFS).

Table 6. Clinical characteristics of the validation cohorts.

	MO Validation cohort (n = 159)		Cirrhotic cohort (n = 40)	*p* value	
Variable	**F0-F1, n=135**	**F2-F3, n=24**	**Positive controls**	**F2-F3 vs F0-F1**	**Cirrhotic vs F0-F1, F2-F3**
Age (years)	45 ± 10	47 ± 10	68 ± 12	0.3	<0.001, <0.001
Sex (female)	95 (70%)	11 (46%)	16 (40%)	0.02	<0.001, 0.80
BMI (kg/m²)	44 ± 5	44 ± 6	27 ± 3	0.98	<0.001, <0.001
Fasting glucose (mg/dL)	108 ± 27	121 ± 32	122 ± 44	0.14	0.02, 0.72
T2DM (yes)	33 (24%)	9 (37%)	20 (50%)	0.12	0.003, 0.78
AST (UI/L)	24 ± 12	34 ± 17	28 ± 13	0.01	0.02, 0.32
ALT (UI/L)	30 ± 21	40 ± 24	24 ± 10	0.04	0.39, 0.02
GGT (UI/L)	36 ± 39	61 ± 48	48 ± 33	0.01	0.02, 0.60
Albumin (g/dL)	4.2 ± 0.3	4.2 ± 0.3	3.9 ± 0.5	0.32	<0.001, 0.002
Platelets (X10⁹/L)	259 ± 71	217 ± 57	101 ± 60	0.007	<0.001, <0.001
Total Cholesterol (mg/dL)	209 ± 36	193 ± 36	149 ± 37	0.06	<0.001, 0.002
HDL cholesterol (mg/dL)	49 ± 10	44 ± 10	50 ± 14	0.03	0.6, 0.07
Triglycerides (mg/dL)	138 ± 66	153 ± 73	104 ± 33	0.28	0.004, 0.004
Steatosis grade (0. 1. 2. 3)	34/55/24/2 2	7/2/10/5	NA	0.008	NA
Lobular Inflammation (0. 1. 2. 3)	47/82/6/0	6/13/5/0	NA	0.014	NA
Ballooning (0. 1. 2)	80/34/21	13/6/5	NA	0.62	NA
Fibrosis stage (0. 1. 2. 3. 4)	27/108/0/0	0/0/18/6	0/0/0/0/40	<0.001	NA
AST/ALT	0.9 ± 0.3	0.9 ± 0.3	1.3 ± 0.5	0.6	<0.001, 0.005
APRI	0.3 ± 0.7	0.4 ± 0.3	0.9 ± 0.8	0.002	<0.001, <0.001
FIB-4	0.8 ± 0.3	1.4 ± 1.2	5.1 ± 3.3	0.006	<0.001, <0.001
NFS	.-0.8 ± 1.3	.-0.1 ± 1.4	0.7 ± 1.4	0.01	<0.001, 0.01

Morbidly obese (MO) and Cirrhotic validation cohorts. Data are shown as mean ± SD for continuous variables, number (%) for binary variables, and frequency for categorical variables. ANOVA was used to test for significant differences within continuous variables that were normally distributed while Kruskal-Wallis with Dunn post-test when not normally distributed. Chi-Square test was used for categorical variables. significant at $p < 0.05$. Abbreviations: BMI, body mass index; ALT, alanine aminotransferase; AST, aspartate aminotransferase; GGT, gamma-glutamyl transferase; T2DM, type 2 diabetes mellitus; HDL, high density cholesterol; APRI, AST to platelet ratio index; FIB4, fibrosis-4; FORNS, Forns index; NFS, NAFLD fibrosis score.

2.3. FCN-2 plasma levels correlate with the fibrosis stage

The plasma levels of the five candidates were assessed in all MO discovery samples (n = 76). No significant differences were found in the four candidates (Figure 22) while FCN-2 levels significantly decreased when liver fibrosis progresses from minimal to moderate/advanced stage (Figure 23a). FCN-2 was able to distinguish F0/F1 from F2/F3/F4 with level decreasing from 4313 ng/mL (interquartile range: 3295 - 5849) to 2676 ng/mL (1983 - 3482), independently of gender and steatosis grade (Figures 23b and 23c).

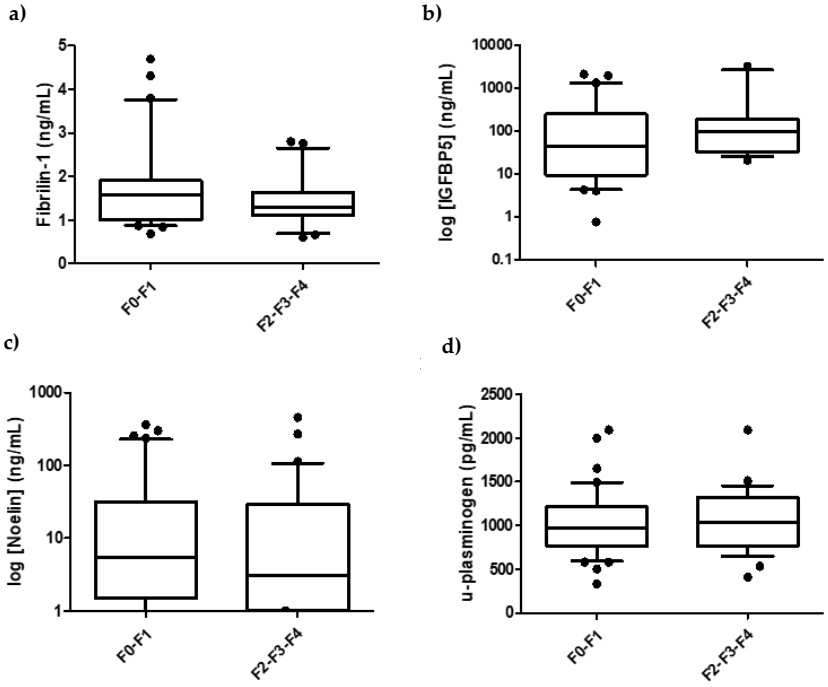

Figure 22. Plasma abundances of 4 candidates in the MO discovery cohort stratified by fibrosis stage.
a) Fibrillin **b)** IGFB5 **c)** Noelin-2 **d)** U-plasminogen

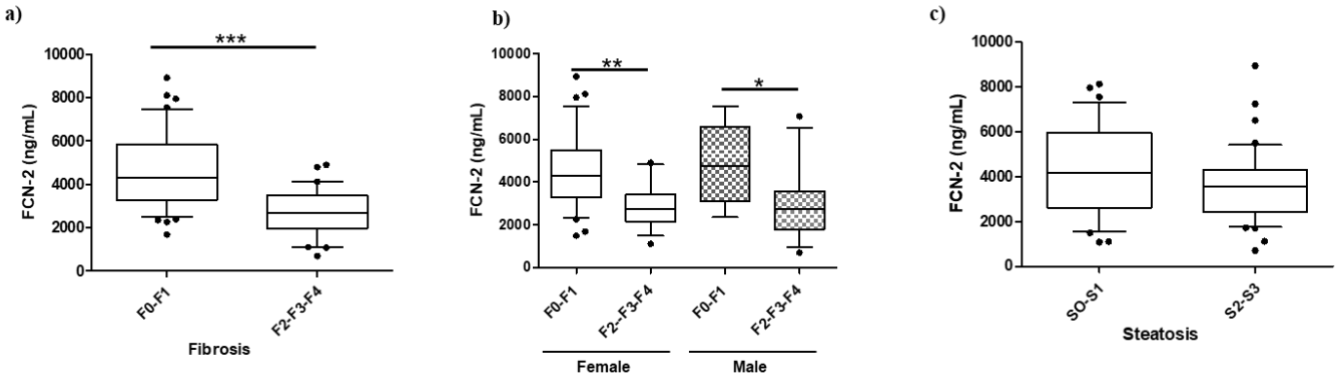

Figure 23. Boxplot for FCN-2 measurements in the morbidly obese discovery cohort. (a) Plasma abundances of FCN-2 determined by ELISA in MO subjects stratified by fibrosis' stage, **(b)** MO stratified by gender and fibrosis' stage, and **(c)** MO stratified by steatosis' grade. ***significant at $p < 0.001$, **significant at $p < 0.01$, and *significant at $p < 0.05$.

Having shown an association between the plasma level of FCN-2 and the stage of fibrosis, we investigated the relationships with other biochemical and histological parameters. FCN-2 plasma level had a significant positive correlation with platelets ($\varrho = 0.37$, $p = 0.001$) and negative correlation with fibrosis stage ($\varrho = -0.49$, $p < 0.001$), FIB-4 ($\varrho = -0.32$, $p = 0.006$) and NFS ($\varrho = -0.30$, $p = 0.01$) (Table 7). The correlations indicate that changes in FCN-2 level reflect liver fibrosis but not steatosis, inflammation, and ballooning, as observed when the cohort was stratified by MASLD stages or the grade of the different histological characteristics (Figures 24-25).

Table 7. Correlations between blood parameters and fibrosis in the discovery cohort.

XY, n=76	X = [FCN-2]		X = Fibrosis Kleiner score	
Parameter (Y)	**Rho**	***p* value**	**Rho**	***p* value**
BMI	-0.071	0.54	0.25	0.03
Triglycerides	0.23	0.05	0.23	0.06
Total Cholesterol	0.064	0.68	-0.1	0.39
Glc	0.024	0.83	0.2	0.09
AST	-0.056	0.62	0.32	0.006
ALT	0.035	0.77	0.22	0.06
GGT	0.026	0.82	0.39	0.004
Platelets	0.37	0.001	-0.33	0.004
INR	-0.3	0.009	0.33	0.004
Albumin	-0.047	0.68	0.17	0.14
AST/ALT ratio	-0.12	0.3	0.08	0.5
Steatosis score	-0.014	0.901	0.13	0.25
Lob. Inflammation score	-0.06	0.575	0.33	0.004
Portal Inflammation score	-0.028	0.811	0.25	0.03
Ballooning score	-0.062	0.593	0.11	0.34
Fibrosis score	-0.49	<0.001	-	-
APRI	-0.15	0.19	0.37	<0.001
FIB-4	-0.32	0.006	0.4	<0.001
FORNS	-0.22	0.06	0.36	0.002
NFS	-0.3	0.01	0.45	<0.001

Histological scores were according to Kleiner-Brunt classification. Pearson's or Spearman's correlation coefficient (Rho) measure the strength and direction of association between the two variables under study. ***significant at $p < 0.001$, **significant at $p < 0.01$, and *significant at $p < 0.05$. Abbreviations: BMI, body mass index; ALT, alanine aminotransferase; AST, aspartate aminotransferase; GGT, gamma-glutamyl transferase; T2DM, type 2 diabetes mellitus; HDL, high-density cholesterol; APRI, AST to platelet ratio index; FIB4, fibrosis-4; FORNS, Forns index; NFS, NAFLD fibrosis score.

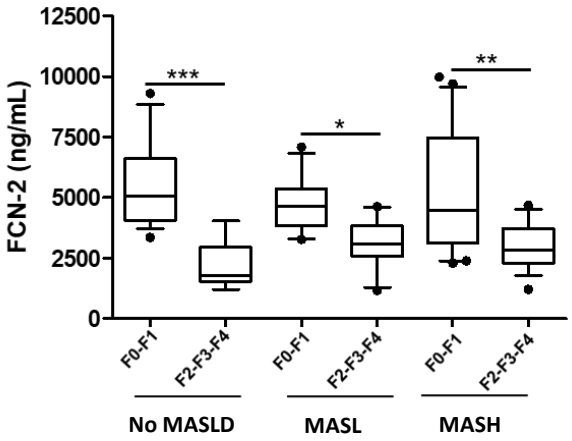

Figure 24. Bloxpot of FCN-2 plasma levels in the MO discovery cohort stratified by liver histology. Plasma samples from 76 MO patients were stratified by fibrosis and MASLD stage. NO MASLD (F0-F1, n=6; F2-F3-F4, n = 6); MASL (F0-F1, n = 13; F2-F3-F4, n = 11) and MASH (F0-F1, n = 23; F2-F3-F4, n = 17). ***significant at $p < 0.001$, **significant at $p < 0.01$, and *significant at $p < 0.05$.

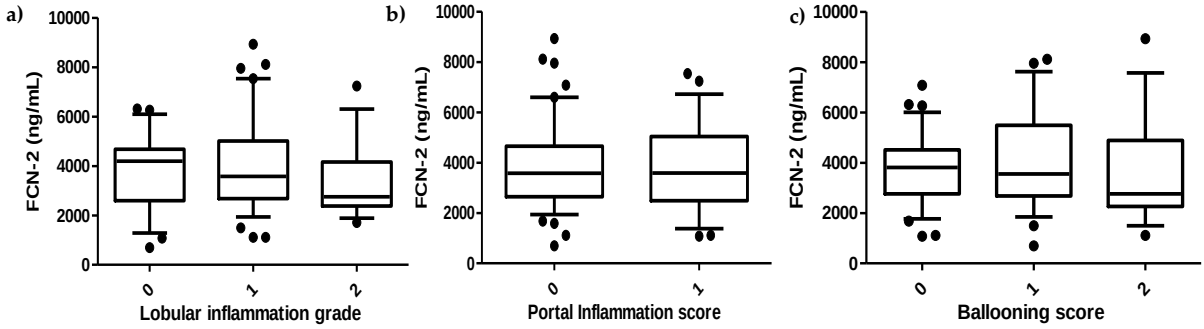

Figure 25. FCN-2 plasma level in the MO cohort stratified by liver histology. (a) lobular inflammation, **(b)** portal inflammation, and **(c)** ballooning. Histological scores were based on Kleiner-Brunt classification.

2.3. Diagnosis of liver fibrosis using FCN plasma level

In the discovery cohort (n = 76), an optimal FCN-2 cut-off level for the detection of moderate-advanced fibrosis was determined. FCN-2 of ≤ 3650 ng/mL had an AUROC of 0.79 for moderate-advanced fibrosis detection (sensitivity 85%, specificity 71%). This was replicated in the validation cohort (n = 159, AUROC = 0.80, sensitivity 71%, specificity 84%) and also in the overall combined cohort (n = 235, AUROC = 0.82, sensitivity 79%, specificity 81%) (Figure 23a-c). The FCN-2 plasma concentration in all analyzed samples stratified by liver injury is shown in Figure 26d.

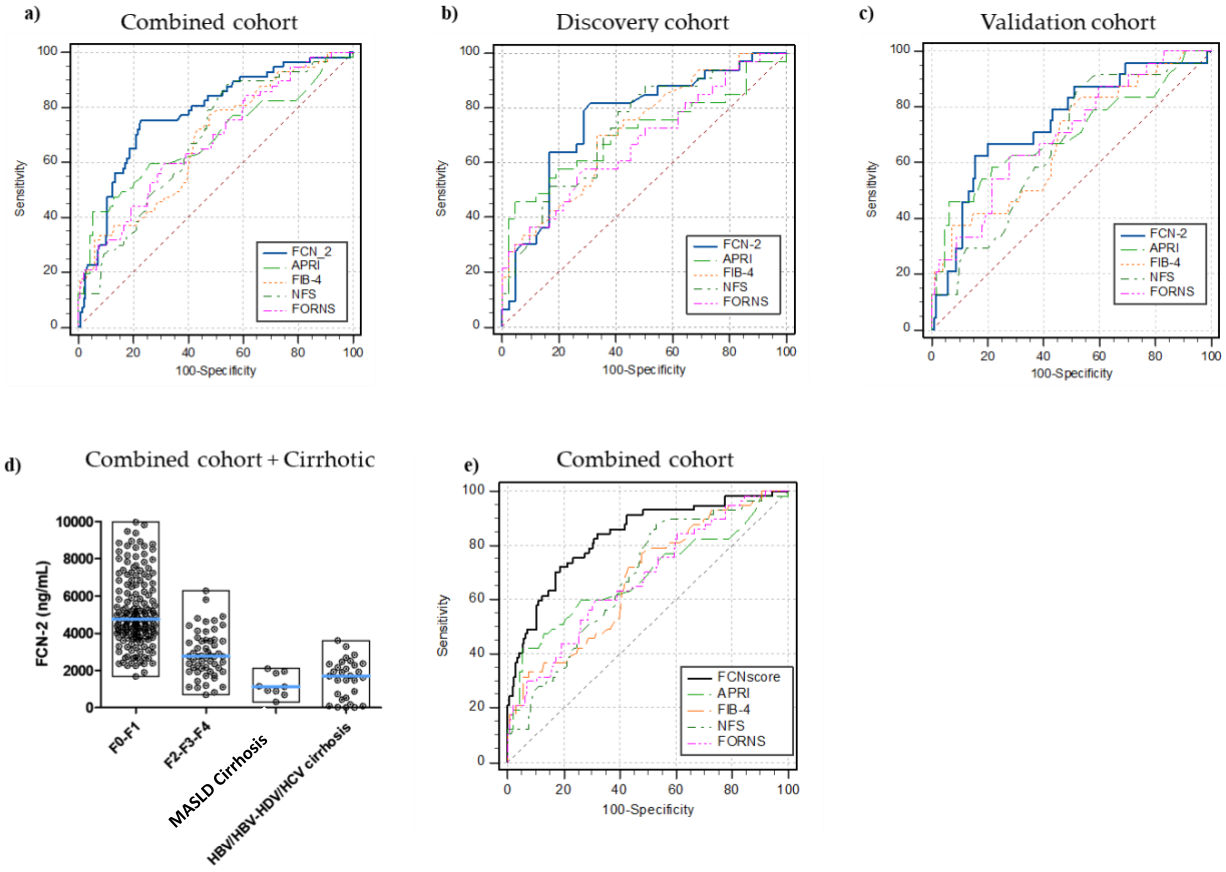

Figure 26. Receiver operating characteristics (ROC) curves for diagnosis of significant fibrosis. FCN-2 *vs* blood-based tests (APRI, FIB-4, NFS, FORNS) AUROCs in **(a)** Combined cohort (n = 235, disease prevalence 24%), **(b)** Discovery MO cohort (n = 76, disease prevalence 43%), **(c)** Validation MO cohort (n = 159, disease

prevalence 15%), **(d)** Full picture for FCN-2 plasma levels in all samples included in the study**, (e)** FCNscore (FCN-2 levels, APRI and HDL combined in a diagnostic model) vs common blood-based tests (FIB-4, NFS, APRI, FORNS) AUROCs in the combined cohort. Significant fibrosis (F2, F3, and F4 stages).

Next, we compared the diagnostic performance of FCN-2 in detecting fibrosis with those from APRI, FIB-4, FORNS, and NFS indexes. FCN-2 marker has the best diagnostic accuracy for significant fibrosis diagnosis in the discovery, validation, and combined cohorts. A comparison of AUROCs using DeLong's method demonstrated that FCN-2 was superior to APRI ($p < 0.013$), FIB-4 ($p < 0.002$), FORNS ($p < 0.005$) and NFS ($p < 0.005$) in the combined cohort. AUROCs, sensitivity, specificity, PPVs, NPVs, and significant comparisons for optimal cut-off values in the three cohorts are summarized in table 8.

Several blood parameters or their combination in diagnostic scores displayed differences with the fibrosis stage. Using the data from the discovery cohort, logistic regression analysis was done to determine the appropriate variables to be included in the regression model, thus, improving the diagnostic performance. AUROC of the combined model designed as FCNscore (FCN-2, APRI, and HDL) was 0.85 (95% confidence interval: 0.75 to 0.92) for the diagnosis of significant fibrosis (cut-off value > 0.35, specificity 86% and sensitivity 75%, Figure 26e) in the discovery cohort. In the validation and combined cohorts, AUROCs were 0.83 and 0.85, respectively. AUROC comparison analysis also demonstrated that FCNscore applied to the combined cohort was superior to all the included simple non-invasive scores: APRI, FIB-4, FORNS, and NFS, with accuracies of 0.68 ($p = 0.0001$), 0.67 ($p < 0.0001$), 0.68 ($p = 0.0001$) and 0.68 ($p = 0.0002$), respectively (Table 9). Using the FCNscore model in combined cohort, the optimal threshold correctly staged 189 out of the 235 patients (80%), as compared to 179 patients (76%) with APRI, to 142 patients (60%) with FIB-4, to 148 (63%) with FORNS and 136 (58%) with NFS. Considering the negative predictive value (NPV) for each model, out of the 178 patients with non-significant fibrosis, 148 (83%) were staged correctly using FCNscore, and 152 (85%), 100 (56%), 114 (64%) and 91 (51%) using APRI, FIB-4, FORNS, and NFS, respectively (Table 10).

Table 8. Comparison of the performance of each test for the diagnosis of significant fibrosis in the MO cohorts.

Discovery MO cohort (n = 76, prevalence 44%)						
Biomarker/Test	**AUROC (95% CI)**	**Sens (%)**	**Spec (%)**	**PPV**	**NPV**	***p* value**
FCN-2 ≤ 3650	0.79 (0.68-0.88)	85	71	70	86	-
APRI > 0. 35	0.71 (0.59-0.81)	45	95	88	69	0.27
FIB-4 > 0.78	0.71 (0.60-0.81)	70	67	62	74	0.28
FORNS > 3.72	0.67 (0.55-0-78)	57	71	61	68	0.13
NFS > -0.96	0.73 (0.61-0.82)	79	59	60	78	0.40
Validation MO cohort (n = 159, prevalence 15%)						
FCN-2 ≤ 3650	0.80 (0.73-0.86)	71	84	44	94	-

APRI > 0. 35	0.70 (0.62-0.77)	50	80	36	90	0.23
FIB-4 > 0.78	0.68 (0.66-0.75)	75	54	22	92	0.09
FORNS > 3.72	0.70 (0.62-0.77)	62	71	28	91	0.16
NFS > -0.96	0.66 (0.57-0.73)	71	51	21	90	0.05
Combined MO cohort (n = 235, prevalence 24%)						
FCN-2 ≤ 3650	0.82 (0.76-0.87)	79	81	58	92	-
APRI > 0. 35	0.68 (0.62-0.74)	47	87	55	83	0.013
FIB-4 > 0.78	0.67 (0.61-0.73)	72	57	36	86	0.002
FORNS > 3.72	0.68 (0.61-0.73)	59	68	38	84	0.005
NFS > -0.96	0.68 (0.61-0.74)	79	53	36	88	0.005

AUROC. Sens. sensitivity; Spec. specificity; PPV. positive predictive value; NPV. negative predictive value. Cut-off according to Youden index J.

Table 9. Diagnostic accuracies for FCNscore and blood-based indexes in the combined MO cohort.

Combined MO Cohort (n = 235, prevalence 25%)						
Biomarker/Test	**AUROC (95% CI)**	**Sens (%)**	**Spec (%)**	**PPV**	**NPV**	***p* value**
FCNscore > 0.35	0.85 (0.79-0.89)	72	84	60	90	-
FCN-2 ≤ 3650	0.82 (0.76-0.87)	79	81	58	92	0.14
APRI > 0. 35	0.68 (0.62-0.74)	47	87	55	83	0.0001
FIB-4 > 0.78	0.67 (0.61-0.73)	72	57	36	86	<0.0001
FORNS > 3.72	0.68 (0.61-0.73)	59	68	38	83	0.0001
NFS > -0.96	0.68 (0.61-0.74)	79	53	36	88	0.0002

Pairwise comparison of AUROCs was according to DeLong's method, considering significant $p < 0.05$ (FCNscore *vs* other models or markers).

Table 10. Classification of subjects in the combined cohort according to moderate/advanced fibrosis (prevalence 25%, n = 235).

	F0-F1, n = 178 ("rule out" significant fibrosis)		**F2-F3-F4, n = 57 ("rule in" significant fibrosis)**		**Total, N = 235**	
	Correctly identified	Incorrectly identified	Correctly identified	Incorrectly identified	Well-classified	Misclassified
Parameter/model	n/N (%)	n/N (%)	n/N (%)	n/N (%)	n/N (%)	n/N (%)
FCNscore (>0.344)	148/178 (83%)	30/178 (17%)	41/57 (72%)	16/57 (28%)	189/235 (80%)	46/235 (20%)
FCN-2 (<3650)	144/178 (81%)	34/178 (19%)	45/57 (79%)	12/57 (21%)	189/235 (80%)	46/235 (20%)
APRI (>0.35)	152/178 (85%)	26/178 (15%)	27/57 (47%)	30/57 (53%)	179/235 (76%)	43/235 (24%)
FIB-4 (>0.78)	100/178 (56%)	78/178 (44%)	42/57 (74%)	15/57 (26%)	142/235 (60%)	93/235 (40%)
FORNS (>3.72)	114/178 (64%)	64/178 (46%)	34/57 (60%)	23/57 (40%)	148/235 (63%)	82/235 (35%)
NFS (>-0.96)	91/178 (51%)	87/178 (49%)	45/57 (79%)	12/57 (21%)	136/235 (58%)	99/235 (42%)

3. Discussion

MASLD affects a quarter of the global population, and its prevalence increases in parallel with the increasing prevalence of obesity, MetS, and T2DM [116,117]. In the obese population, MASLD prevalence varies from 60 to 95% [118]. Notably, MASH and fibrosis have been reported with prevalence ranges of 18 - 60% and 6 - 90% in severely obese subjects, respectively [119–121]. Not all MASLD patients, including those with MASH develop liver fibrosis. However, it is crucial to assess fibrosis severity since it is one of the strongest predictors of liver-related complications and mortality [122].

The gold standard for diagnosing MASLD and fibrosis stages is histological analysis. Considering the well-known limitations of liver biopsy (invasiveness, observer variability, sampling errors, among others), the development of alternatives is challenging in clinical management. In the present study, we assessed the plasma FCN-2 levels in a well-histologically characterized MASLD obese cohort and evaluated its potential use for fibrosis diagnosis.

FCN-2 is among the 29 candidate biomarkers identified by a systematic *in silico* strategy. These candidates fulfill the desired selection criteria as relevant in the fibrotic process, secreted, and traceable in plasma. Specifically, 19 are differentially expressed in fibrotic liver and part of the myofibroblast phenotype acquisition PPI network (MyoPheNet); and 9 are enriched proteins with elevated expression in healthy liver and MyoPheNet components. FCN-2 is the only candidate to accomplish the three main selection criteria. It was part of the MyoPheNet, showed reduced expression with fibrosis, and was expressed in healthy liver.

The main finding of this study is that FCN-2 plasma level was strongly associated with the fibrosis stage assessed by histological analysis. Besides fibrosis, no association between histology and FCN-2 levels was shown, or if MO cohort was stratified into No MASLD, MASL, and MASH. We found a reduction of FCN-2 level in MO subjects with significant fibrosis (≥2), further reduced in cirrhosis, regardless of fibrosis etiology. To our knowledge, this is the first study reporting the potential use of plasma FCN-2 as a marker of fibrosis in morbidly obese patients. Our data agree with those reported by Dai where FCN-2 and CPB2 proteins were shown as biomarkers of liver fibrosis through serum proteomics analysis and quantified using ELISA, in a cohort of 46 CHB subjects [123]. Furthermore, Chen observed that intrahepatic expression and serum levels of FCN-2 were much lower in HCC and cirrhosis than in healthy controls [124]. On the contrary, Liu reported an increase in serum FCN-2 associated with the severity of fibrosis and the activity of HCV infection [125].

FCN-2 is a serum protein expressed by hepatocytes and secreted into the circulation [126]. The serum/plasma median concentration in healthy people is approximately 5000 ng/mL; values below 1000 ng/mL have not been found in healthy adults. FCN2 plays a significant role in the host's innate immunity. It appears to bind in human DNA and attaches to apoptotic/necrotic cells, thereby

promoting their removal [127]. Relative FCN-2 deficiencies have been found to be associated with prematurity, low birth weight, and infections in neonates [128].

The plasma level of FCN-2 showed good discriminative power in categorizing hepatic fibrosis. The AUROC for diagnosis of significant fibrosis was 0.82 (F ≥ 2) and was superior to any other indexes tested (FIB-4, FORNS, and NFS). Moreover, the plasma FCN-2, when combined with APRI and HDL in FCN score, yields an excellent discriminative power with AUC of 0.85 and identified correctly 80% of patients included in the study.

The limitations of the study include a relatively small cohort size and a low number of subjects with advanced fibrosis or cirrhosis. Nevertheless, our data strongly suggest that FCN-2 is a potential fibrosis biomarker and should be included in future non-invasive indexes of hepatic fibrosis. Our observation needs to be validated in large independent cohorts such as the RESOLVE-IT [129] or the European NAFLD registry longitudinal cohort [130], in which candidates like PRO-C3, YKL-40, A2M have been recently tested [109,125].

In conclusion, we developed an *in silico* strategy to detect putative proteins as biomarkers for fibrosis and demonstrated that FCN-2 either alone or in combination with APRI and HDL, is a good non-invasive diagnostic index for significant fibrosis.

4. Materials and Methods

4.1 Study design and participants

The assessment of our candidate biomarkers was performed retrospectively in a cohort of morbidly obese (MO) subjects enrolled in a bariatric surgery program. The liver biopsy was performed at the time of the surgical procedure. All subjects gave their written consent to participate in the study. Sensitive data were protected through anonymization. The local Ethical Committee has approved the study under protocol N. 22979 (Comitato Etico Regionale Unico, FVG, SSN, Italy). Enrolled subjects were ≥18 years, with a body mass index (BMI) > 40 kg/m^2 (or > 35 kg/m^2 if obesity-related comorbidities were already present), with acceptable operative risks, failure of nonsurgical treatments, and declared compliance to follow lifelong medical surveillance. Subjects were excluded if they had coexistent chronic liver disease, including suspected/confirmed hepatocellular carcinoma, alcoholic liver disease (>25 g/day alcohol consumption), known HBV, HCV, HIV positivity, and therapy with drugs that could affect the liver.

Blood samples from subjects with cirrhosis attributable to either MASLD (n = 10) as well as chronic viral infection (HBV, HDV, and HCV) (n = 30) were collected and considered positive controls of advanced fibrosis (F4).

4.2 Clinical assessment

Anthropometric parameters including age, gender, body weight and height, BMI calculation, and waist circumference were recorded in the baseline visit. After overnight fasting, blood samples were collected before surgery to determine glucose, liver biochemistry (AST, ALT, GGT), albumin, platelets, lipid profile (TG, T-Chol, HDL), and others. Diabetes was diagnosed according to the ESC-EASD guidelines [131]. Blood-based tests of liver fibrosis such as FIB-4, APRI, FORNS, and NFS were calculated as described [132].

4.3 Liver biopsy, histopathology, diagnosis of fibrosis and cirrhosis

Liver specimens collected during the surgical procedure (wedge biopsy) were histologically analyzed by an expert pathologist blinded to all clinical data. Steatosis was graded according to the amount of fat (as lipid droplets in hepatocytes) on hematoxylin and eosin staining. Biopsies showing no or minimal (<5%) steatosis and absent injury or fibrosis were considered normal. The samples showing more than 5% steatosis were labeled as MASLD. The histological diagnosis of MASH and fibrosis was made according to Kleiner-Brunt criteria [51]. In most cases, cirrhosis in positive controls was diagnosed by ultrasound and three via needle biopsy.

4.4 Plasma Ficolin-2 and other candidates' assessment

Plasma levels of five of the total thirty-five candidates were measured by ELISA commercial kits: Fibrillin 1 (RayBio® Human FBN1 ELISA Kit, E-EL-H2266, Elabscience), Insulin-like growth factor-binding protein 5 (RayBio® Human IGFBP-5 ELISA Kit, ELH-IGFBP5, RayBiotech), Noelin-2 (RayBio® Human Olfactomedin 2, ELH-OLFM2, RayBiotech), Urokinase-type plasminogen activator (Human U-Plasminogen Activator Simple Step ELISA® Kit, ab226904, Abcam), and Ficolin-2 (RayBio® Human Ficolin-2 ELISA Kit, RayBiotech).

4.5 Statistical analysis

The MO cohort (n = 235) was divided into two subsequent cohorts: the discovery MO cohort including 76 MO subjects in which the prevalence of fibrosis was adjusted to 44% (enrichment of the moderate/advanced fibrosis proportion) and the validation MO cohort in which 159 MO subjects were included, maintaining the fibrosis prevalence (15%) close to those of the global MO population (24%). In both MO discovery and validation cohorts, the subjects were stratified according to fibrosis stage (F0-F1, minimal fibrosis; F2-F3-F4, moderate/advanced fibrosis) to assess the best candidate based on diagnostic performance analysis (accuracy and determination of optimal cut-off values). Continuous variables were expressed as mean ± standard deviation and categorical as numbers or percentages. Categorical variables were analyzed using chi-square tests with correction, when appropriate. Independent t-test and

ANOVA were used for normally distributed continuous variables. Non-parametric tests (Mann–Whitney, and Kruskal–Wallis) were applied for ordinal or continuous variables that failed to pass D'Agostino & Pearson omnibus normality test. Correlation analyses were performed using Pearson or Spearman's correlation coefficients to estimate the association of plasma levels and several factors of interest. Statistical analysis was performed using GraphPad Prism version 5.01 software. Logistic regression analysis was used to identify independent factors associated with fibrosis. The predictive model was built, including the four best-associated variables (independent factors) selected after using the hierarchical forward selection algorithm in the subset selection test modality performed in NCSS statistical software (version12.0.16). The diagnostic performance of the selected candidate FCN-2 was assessed by receiver operating characteristic (ROC) curves. The area under the ROC (AUROC) using DeLong method was used to compare the accuracy among the different fibrosis diagnostic tests. The sensitivity, specificity, positive predictive values (PPVs), and negative predictive values (NPVs) for relevant cut-offs (according to Youden's index) were also calculated using MedCalc statistical software version16.4.3.

Author Contributions: Enrollment and clinical assessment of the patients' cohort: SP, CS, DL, BC, NdM, TP, GR. Performed bariatric surgery, blood samples and liver biopsy collection: SP, NdM, CS, DL, TP, GR. Conceive and designed the experiments: PJG, NS, NR. Conceived and perform the *in silico* discovery strategy: PJG. Performed experiments: PJG, NS, NR. Analyzed and interpreted the experimental data: PJG, NR, NS, CT. Clinical data and histological analysis: DB, PJG, NR, SP, GR, CT. Contributed reagents/materials/analysis tools: NR, SP, NM, GR, CT. Wrote the paper: PJG, NR, CT. All authors approved the final manuscript.

Funding: This study was supported by Fondazione Italiana Fegato. PJG was sponsored by Fondazione Umberto Veronesi (Postdoctoral Grants 2017, 2020, 2021). Dr. Rosso reports grants from Fondazione Cassa di Risparmio di Trieste (CRTrieste) ProFeGra Project. Dr. Salvoza is funded by the Department of Science and Technology - Philippine Council for Health Research and Development (DOST-PCHRD), Philippines.

Institutional Review Board Statement: The study was conducted according to the guidelines of the Declaration of Helsinki, and approved by the Institutional Review Board (or Ethics Committee) of Fondazione Italiana Fegato.

Informed Consent Statement: The study was approved by the local ethics committees under protocol N. 22979 (Comitato Etico Regionale Unico, FVG, SSN, Italy) and performed in accordance with the current version of the Helsinki Declaration. All patients signed an informed consent form prior to study inclusion.

CHAPTER 5

PROJECT 3 (PATHOPHYSIOLOGY)

The potential role of Omentin-1 in Obesity-Related Metabolic dysfunction-associated steatotic liver disease (MASLD): Evidence from translational studies

Abstract

Obesity, characterized by excessive visceral adipose tissue (VAT) is tightly associated with MASLD. The pathogenesis of MASLD is complex, but recent studies reveal that the adipose tissue–liver axis plays a key role in MASLD development. We investigated the potential role of omentin-1, a novel adipokine expressed by VAT, in obesity-related MASLD pathogenesis. *In silico* analysis of differentially expressed genes in VAT from obese patients with and without MASH showed that omentin-1 might play a significant role. For *in vivo* clinical validation, omentin-1 VAT and plasma levels were measured in lean controls and obese patients with biopsy-proven MASLD. The expression of omentin-1 in the VAT of juvenile mice MASLD model was also assessed. For *in vitro* and *ex vivo* studies, we assessed the effects of omentin-1 in the MASLD-related mechanisms such as steatosis, inflammation, ER stress, and oxidative stress. Finally, the effects of D-glucose and insulin on VAT omentin-1 were also analyzed *ex vivo*. The obese groups showed significantly lower VAT mRNA expression and protein expression, as well as plasma levels of omentin-1 as compared to the lean group. Interestingly, within the MASH group, fibrosis does not affect omentin-1 expression. Likewise, VAT of mice fed with high-fat diet, showing histological signs of MASH showed decreased omentin-1 mRNA and protein levels as compared to their control diet counterpart. *In vitro*, the addition of omentin-1 on fat-laden (FFA) human hepatocytes showed no effect in steatosis but significantly decreased TNF-α levels, ER stress, and oxidative stress. The same results were obtained using *ex vivo* VAT explants from obese patients upon omentin-1 supplementation. In addition, omentin-1 reduced nuclear factor kappa B (*NF-κB*) mRNA expression in both *in vitro* and *ex vivo* studies. In VAT explants, D-glucose and insulin significantly reduced omentin-1 mRNA expression and protein levels. Taken together, our findings suggest that reduced levels of omentin-1 contribute to MASLD development. Omentin-1 supplementation reduces inflammation, ER stress, and oxidative stress probably via inhibiting the NF-κB pathway and might also play a role in the regulation of

glucose and insulin metabolism. Further studies are needed for omentin-1 to be considered as a possible therapeutic target and/or biomarker.

Publications:

- **Salvoza N,** Giraudi PJ, Gazzin S, Bonazza D, de Manzini N, Zanconari F, Palmisano S, Tiribelli C, Rosso N. The potential role of Omentin-1 in Obesity-Related Metabolic dysfunction-associated steatotic liver disease (MASLD): Evidence from translational studies (*manuscript submitted*).

Poster Presentation:

- "The International Liver Congress 2023" by The European Association for the Study of the Liver (EASL). Vienna, Austria. June 21-24, 2022.

1. Introduction

The prevalence of obesity is rapidly increasing; hence, it is now considered a global pandemic [133]. The WHO 2016 report revealed more than 1.9 billion overweight adults, of which, 650 million were obese [14]. In Europe alone, overweight and obesity affect almost 60% of adults, according to WHO 2022 European Obesity Report [13]. The numbers are also alarming in children and adolescents, mainly due to more sedentary lifestyles and the consumption of less healthy diets [14].

Obesity, characterized by excessive visceral adipose tissue (VAT) is linked to noncommunicable diseases such as type 2 diabetes (T2DM), metabolic syndrome, cardiovascular diseases, and metabolic associated fatty liver disease (MASLD) [12,13,34]. MASLD, where the majority is obese, has become the most common cause of chronic liver disease worldwide and is expected to be the leading cause of liver transplantation in the coming years [12].

VAT has been found to play a pivotal role in MASLD development independent of generalized obesity [48]. VAT harbors adipocytes along with a wide range of other cells, including macrophages, mast cells, fibroblasts, and stromal vascular cells. Aside from its role in lipid metabolism, VAT also performs various additional functions, including hormone synthesis, adipokines production, and immunological modulation [134]. Over 600 bioactive cytokines have been identified, including a group known as adipokines, also referred to as adipocytokines. Adipocytokines act systemically in an endocrine manner and locally in an autocrine and paracrine manner. In the context of the adipose tissue-liver axis, adipocytokines are involved in regulating glucose and lipid metabolism, inflammation, and immunity [26]. VAT dysfunction, including the dysregulation of adipocytokines has been implicated in the pathogenesis of metabolic disorders such as obesity, T2DM, and MASLD [134,135]. Understanding the role of adipocytokines in the adipose tissue-liver axis can lead to the development of novel therapeutic strategies for treating metabolic disorders.

Omentin-1 (also known as intelectin-1, intestinal lactoferrin receptor, endothelial lectin HL-1, or galactofuranose-binding lectin), a novel adipocytokine, is a peptide of 313 amino acids containing a secretory signal sequence and a fibrinogen-related domain [136]. Omentin-2, a homolog with 83% amino acid identity with omentin-1 is found in the same chromosomal region [137,138]. Several reports indicated that omentin-1 and -2 are highly expressed in VAT, but omentin-1 was shown to be the major circulating isoform in human plasma [138]. Further, omentin-1 protein was found to be secreted into the culture medium of VAT, but not subcutaneous adipose tissue (SAT) [136]. Within VAT, stromal vascular cells, but not adipocytes, are mainly involved in omentin-1 production [136].

Plasma omentin-1 level decreases in overweight and obese humans, while it increases after obese patients lose weight or after taking antidiabetic drugs [139,140]. Regarding its biological activity, omentin-1 enhances insulin-stimulated glucose uptake via Akt activation in human adipocytes, suggesting its role in T2DM susceptibility [136]. Aside from insulin action, it has also been reported that omentin-1 ameliorates macrophage activation via inhibiting the nuclear factor kappa B (NF-κB) pathway in obese mice, suggesting its role as an anti-inflammatory cytokine [141]. Both insulin resistance and inflammation are associated with MASLD. These two molecular mechanisms, along with steatosis, oxidative stress, endoplasmic reticulum (ER) stress, and fibrosis, are key pathologic drivers in MASLD development. In the context of MASLD, minimal published studies investigate the role of omentin-1. One study showed that VAT omentin expression, but not serum level, was lower in MASH versus simple steatosis patients [142]. However, no studies are available demonstrating its beneficial effects in MASLD-related pathophysiological mechanisms.

In this study, we conducted a simple *in silico* analysis identifying omentin-1 and investigated its role in MASLD for the first time, using different translational approaches. We simultaneously determined the expression of omentin-1 in VAT at both mRNA and protein levels in MASLD patients and mice fed with high-fat diet. Furthermore, we present novel data regarding the plasma levels of omentin-1 in obese subjects with different stages of MASLD. Successively, to elucidate its role in the liver and VAT, we evaluated its beneficial effects in the MASLD-related pathophysiological mechanisms such as steatosis, inflammation, oxidative stress, and ER stress.

2. Results

2.1 In silico analysis

2.1.1 Electronic literature search

We performed an electronic literature search about VAT transcriptomics experimental data of MASLD using PubMed database. The literature review was conducted following the guidelines of the Preferred Reporting Items for Systematic Reviews and Meta-analysis (PRISMA) [143]. The following query terms were used: transcriptomics/gene expression/microarray data in NAFLD adipose tissue. "NAFLD" MeSH term was used instead of "MASLD," because the latter was coined only in 2023 [11], and most of the available research articles used "NAFLD."

When the analysis was performed, limited information on transcriptomics data was available in NAFLD, particularly about expression profiles in VAT. As reported in materials and methods, the work of du Plessis *et al.* was selected due to its similarity with our morbidly obese cohort's patient selection and the availability of transcriptomic data in VAT [68]. The gene expression dataset GSE58979 was downloaded from Gene Expression Omnibus [144], which included 9 obese VAT samples and 7 MASH VAT samples.

2.1.2 *Identification of Differentially Expressed Genes (DEGs) in MASH development*

In this study, the public dataset (GSE5897) of du Plessis *et al.* was re-analyzed using GEO2R, the interactive web tool of the GEO platform that compares two or more groups of samples in a GEO Series, identifying those differentially expressed across the experimental condition [145]. According to the threshold we set (p-value < 0.05 and $\log_2$ fold change |1|), 110 upregulated and 35 downregulated genes were found between obese and obese MASH groups (Figure 27).

To focus the study on the most important protein-coding genes involved in MASLD, we used a simple systematic discovery strategy. Briefly, we collected data of the human proteome (and their corresponding UniProtKB identifiers [146]) from Human Protein Atlas [147] and filtered them by applying several *in silico* sieves to select the proteins with the desired characteristics (Figure 28a). Proteins moving down in the funnel reach a thicker grade of selectivity and specificity. In the approach, the *in silico* filters were represented by Venn diagrams used to apply selection criteria at the bio-datasets, consequently obtaining the most relevant proteins (Figure 28b). Our selection criteria include visceral adipose tissue-enriched proteins, secreted proteins, experimental evidence in plasma or blood, and not included as part of the housekeeping proteome. From this analysis, we obtained 8 relevant protein-coding genes. We finally selected omentin-1 as the most pertinent gene for our subsequent analysis as it is the only adipocytokine on the list.

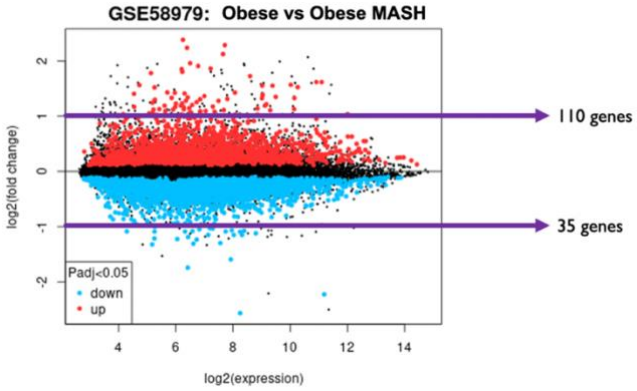

Figure 27. A mean difference (MD) plot displays $\log_2$ fold change versus $\log_2$ expression using limma. Upon setting the threshold for the DEGs at corrected p-value < 0.05 and $\log_2$ fold change (FC) of |1|, 110 upregulated and 35 downregulated genes were identified.

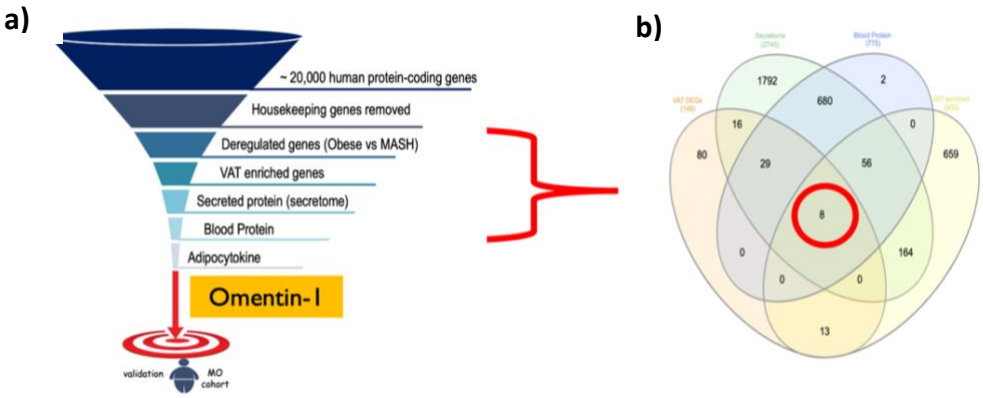

Figure 28. Summary of the simple in silico protein discovery strategy used in the study. (a) Layout of the *in silico* funnel strategy and the criteria used. **(b)** Venn diagrams illustrating the different datasets used to identify candidates satisfying our selection criteria. Abbreviations: MO, morbidly obese.

2.2 In vivo clinical validation

2.2.1 Baseline clinical and laboratory characteristics of morbidly obese patients

The morbidly obese (MO) cohort was stratified according to the criteria described in the methods section: obese (Ob) group = 19; obese MASH (Ob-M) group = 20; and obese MASH with fibrosis (Ob-MF) group = 16. The baseline clinical and laboratory characteristics of MO patients (n = 55) included in the study are shown in table 11.

In all MO groups, female is the most prominent sex as compared to male. Compared with the Ob group, Ob-M and Ob-MF groups have significantly higher fasting glucose, AST, ALT, GGT, total cholesterol, triglycerides, and transferrin levels (all p values < 0.05). As expected, the Ob-MF with fibrosis group had significantly lower platelets level as compared to the two other groups (p = 0.03). Moreover, AST/ALT ratio showed was significantly higher in the obese group as compared to Ob-M and Ob-MF groups (p < 0.01).

Table 11. Clinical and laboratory characteristics of the study groups.

Variable	Obese (Ob) (n = 19)	Obese MASH (Ob-M) (n = 20)	Obese MASH with Fibrosis (Ob-MF) (n = 16)	*p* value
Age (years)	39.3 ± 8.65	46.8 ± 11.9	44.9 ± 11.3	0.08
Sex (female)	19 (100%)	16 (80%)	9 (56%)	0.006
BMI (kg/m^2)	41.0 ± 5.6	43.3 ± 4.9	46.4 ± 8.4	0.09
Fasting glucose (mg/dL)	99.5 ± 10.6	118.5 ± 37.0*	114.1 ± 25.6#	0.04
T2DM (yes)	3 (16%)	6 (30%)	4 (25%)	0.387
AST (U/L)	18.6 ± 5.12#	25.4 ± 10.5	33.3 ± 20.5#	0.02
ALT (U/L)	18.1 ± 8.7	35.2 ± 19.3**	44.7 ± 37.9##	<0.001
GGT (U/L)	21.0 ± 13.6	36.3 ± 24.0	45.9 ± 36.1##	0.005
ALP (U/L)	76.53 ± 34.4	78.4 ± 19.4	85.3 ± 19.8	0.15
Albumin (g/dL)	3.91 ± 0.76	4.16 ± 0.28	4.29 ± 0.38	0.08
Platelets ($X10^9/L$)	256.8 ± 92.7	284.7 ± 66.7	226.1 ± 44.6∞	0.03

Total Cholesterol (mg/dL)	174.2± 31.2	208.0 ± 37.9*	207.1 ± 49.0$^{\#}$	0.03
HDL cholesterol(mg/dL)	59.5 ± 50.9	45.6 ± 11.4	45.7 ± 12.0	0.26
Triglycerides (mg/dL)	105.2 ± 34.9	147.2 ± 58.4*	150.0 ± 74.3$^{\#}$	0.02
AST/ALT Ratio	1.12 ± 0.44	0.80 ± 0.21*	0.82 ± 0.20$^{\#}$	<0.01
Iron (mcg/dL)	66.6 ± 34.1	73.5 ± 31.9	66.5 ± 20.0	0.871
Transferrin (mg/dL)	260.0 ± 71.2	280.7 ± 44.0	306.9 ± 50.13$^{\#}$	0.05
Ferritin (ng/mL)	37.8 ± 23.6	69.6 ± 84.9	72.5 ± 62.3	0.39

Data are shown as mean ± SD for continuous variables, number (%) for binary variables, and frequency for categorical variables. ANOVA was used to test for significant differences within continuous variables that were normally distributed while Kruskal-Wallis with Dunn post-test when not normally distributed. Chi-Square test was used for categorical variables. **$p < 0.001$ *vs* Ob-M, *$p < 0.05$ *vs* Ob-M, $^{\#\#}p < 0.001$ *vs* Ob-MF, $^{\#}p < 0.05$ *vs* Ob-MF, $^{\infty}p < 0.05$ Ob-M *vs* Ob-MF. Abbreviations: BMI, body mass index; ALT, alanine aminotransferase; AST, aspartate aminotransferase; GGT, gamma-glutamyl transferase; T2DM, type 2 diabetes mellitus; HDL, high-density cholesterol.

2.2.2 Omentin-1 VAT mRNA and protein expression

Based on *in silico* analysis, omentin-1 expression is one of the downregulated genes in VAT of obese MASH. Considering this result, we evaluated the omentin-1 expression in adipose tissue biopsies collected from MO subjects and controls (five lean patients). It is noted that omentin-1 is mainly produced in VAT. To confirm this, we assessed its expression also on SAT, and as expected, mRNA expression was barely detectable in almost all samples (data not shown). Therefore, the subsequent analysis was focused only on VAT. Real-time PCR analysis (Figure 29a) revealed that there is a significant decrease in omentin-1 expression in all obese groups (all p values < 0.05) as compared to lean controls. Moreover, expression data demonstrated a further reduction ($p < 0.05$) in the Ob-M group. However, no significant difference was noted when comparing Ob-M group against Ob-MF group.

Further, the changes noted at the mRNA level were also reflected at the protein level (Figure 29b). Western blot analysis of total protein from representative VATs demonstrated that omentin-1 (normalized to α-tubulin) in all the obese groups have significantly higher protein expressions as compared to the lean group. Consistent with mRNA expression, omentin-1 protein expression is also significantly decreased in Ob-M and OB-MF groups compared to Ob group.

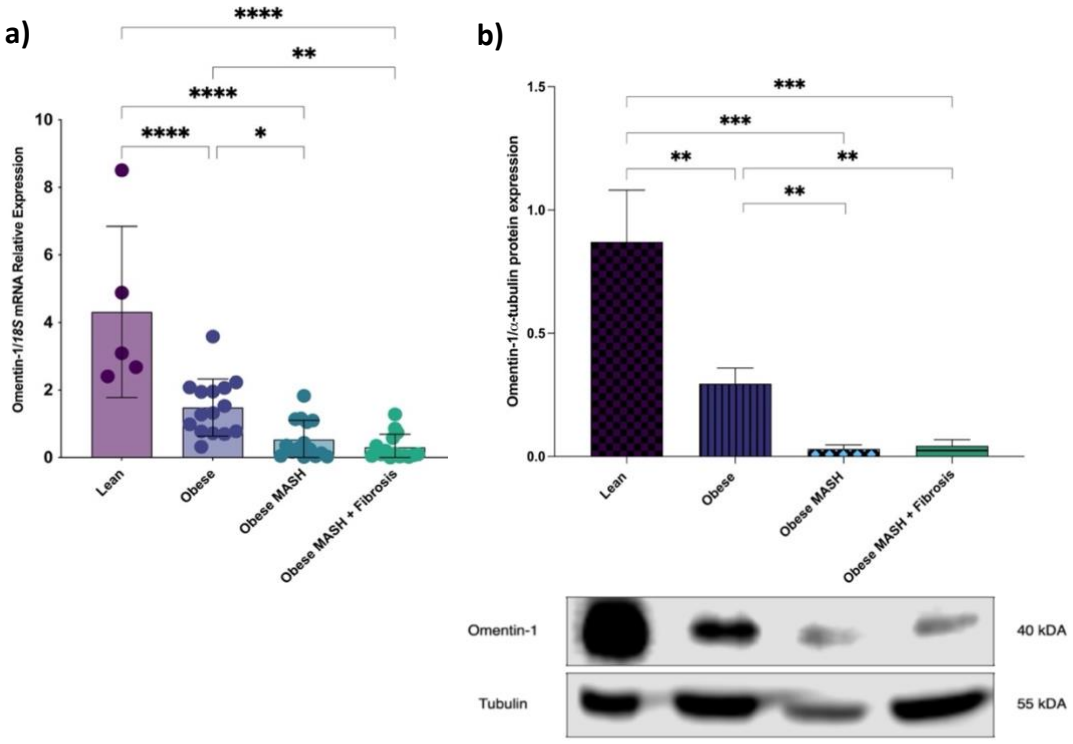

Figure 29. Human VAT omentin-1 (a) mRNA expression and (b) protein expression in obese groups and lean controls. Omentin-1 mRNA expression is significantly decreased in the VAT of all obese groups as compared to the lean controls. For mRNA expression, values presented are the mean ± SD of individual patients (N = 60). Representative blot and densitometric analysis of omentin-1 normalized to α-tubulin revealed that protein expression is also significantly decreased in the VAT of all obese groups as compared to the lean controls. For protein expression, data are mean ± SD of 3 representative patients per group. Group comparison by Kruskal-Wallis and post hoc Dunn's test. *p < 0.05, **p < 0.01, ***p < 0.001, ****p < 0.0001.

2.2.3 Omentin-1 plasma level

Plasma omentin-1 levels were measured in our well-characterized morbidly obese cohort (n = 55) and a reference lean group was included as a control (n = 17). As shown in figure 30, plasma omentin-1 levels were lower in all the 3 obese groups than in the lean control group (all p values are < 0.05). Subsequently, we observed that as the MASLD severity progresses, the plasma omentin-1 level also decreases. Interestingly, within the MASH group, the presence of fibrosis does not affect omentin-1 expression.

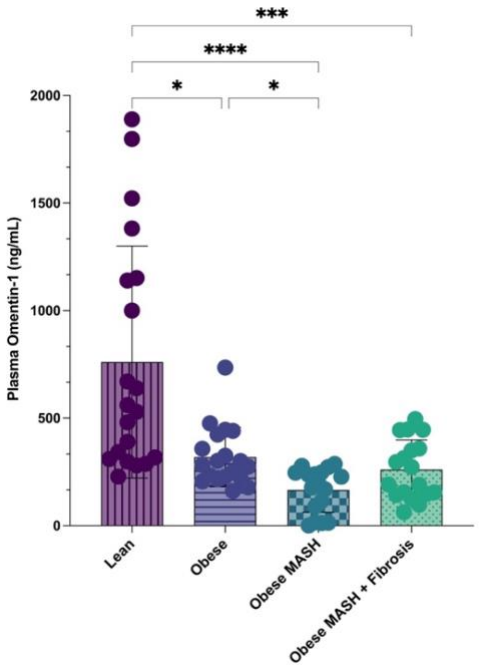

Figure 30. Human plasma omentin-1 levels in obese groups and lean controls. Omentin-1 plasma level is significantly decreased in all obese groups as compared to the lean controls. Values presented are the mean ± SD of individual patients (N = 72). Group comparison by Kruskal-Wallis and post hoc Dunn's test. *p < 0.05, **p < 0.01, ***p < 0.001, ****p < 0.0001.

2.2.4 Correlation between omentin-1 plasma level and patients' clinico-laboratory parameters

Having shown that the plasma level of omentin-1 in obese groups differ, we investigated the relationship of omentin-1 with their clinical and biochemical parameters (n = 55). Omentin-1 plasma level had a significant positive correlation with omentin-1 mRNA ($\varrho = 0.382$ $p = 0.013$) and a significant negative correlation with total cholesterol ($\varrho = -0.307$, $p < 0.022$), as shown in table 12. Interestingly, omentin-1 plasma level negatively correlates with ALT ($\varrho = -0.279$, $p < 0.039$) but not AST. Further, the AST/ALT ratio positively correlates with the omentin-1 plasma level ($\varrho = 0.285$, $p < 0.042$). Among the transaminases, ALT level exceeding those of AST is the usual observed biochemical pattern in hepatic steatosis due to MASLD [148].

Table 12. Correlation of clinical and laboratory parameters with plasma omentin-1 level.

Variable	rho	*p* value
Omentin-1 mRNA	0.382	0.013*
BMI (kg/m^2)	-0.230	0.093
Fasting Glucose (mg/dL)	0.026	0.851
AST (UI/L)	-0.206	0.136
ALT (UI/L)	-0.279	0.039*
AST/ALT Ratio	0.285	0.042*
GGT	-0.049	0.723
ALP (U/L)	-0.034	0.81
Triglycerides (mg/dL)	-0.212	0.119
Total Cholesterol (mg/dL)	-0.307	0.022*
HDL (mg/dL)	-0.029	0.836

Insulin (μU/mL)	-0.159	0.333
Platelet (x10^9 L)	-0.076	0.581

Pearson's or Spearman's correlation coefficient (Rho) measures the strength and direction of association between the two variables under study. *p < 0.05. Abbreviations: BMI, body mass index; ALT, alanine aminotransferase; AST, aspartate aminotransferase; GGT, gamma-glutamyl transferase; T2DM, type 2 diabetes mellitus; HDL, high-density cholesterol.

2.3 In vivo mice studies

2.3.1 Phenotypic and histological characterization of HFD mice

Human omentin-1 has been identified in this study to be associated with obesity and MASLD, a gene 80-85% homologous to mice omentin-1 [149]. To investigate the potential role of mouse omentin-1 during diet-induced obesity, we assigned C57Bl/6 littermates (N = 46) to receive either control or high-fat diet (HFD), supplemented with fructose/sucrose in drinking water, as described [63].

As shown in table 13 below, mice treated with HFD for 20 weeks developed obesity, dyslipidemia, glycemia, hyperinsulinemia, insulin resistance, and histological signs of MASH as compared to control diet mice. Moreover, obese mice exhibited a significant increase in AST and ALT levels versus control diet fed mice. In contrast, 3 weeks old mice on HFD only developed dyslipidemia with no significant histological changes as compared to their control diet counterpart.

Table 13. Anthropometric, biochemical, and histological characteristics of mice.

Variable	**3 weeks**			**20 weeks**		
	HFD (n = 8)	**CD (n = 7)**	***p* value**	**HFD (n = 18)**	**CD (n = 13)**	***p* value**
Sex (female)	4 (50%)	4 (57.1%)	0.782	11 (61.1%)	7 (53.8%)	0.686
Body Weight (g)	21.3 ± 2.61	18.9 ± 2.25	0.083	39.50 ± 7.38	28.06 ± 3.79	<0.001***
Body Length (cm)	8.65 ± 0.35	8.36 ± 0.42	0.160	9.27 ± 0.30	8.87 ± 0.32	<0.001***
BMI (kg/m^2)	28.38 ± 2.33	27.14 ± 2.61	0.351	45.82 ± 7.11	35.69 ± 3.40	<0.001***
Total Cholesterol (mg/dL)	141.50 ± 17.53	86.14 ± 10.75	<0.001***	168.22 ± 43.45	85.69 ± 11.71	<0.001***
HDL (mg/dL)	98.14 ± 13.93	59.43 ± 6.05	<0.001***	111.78 ± 25.19	63.69 ± 11.88	<0.001***
LDL (mg/dL)	82.03 ± 14.42	33.84 ± 9.48	<0.001***	110.02 ± 36.82	36.61 ± 10.05	<0.001***
Triglycerides (mg/dL)	110.00 ± 34.65	87.14 ± 24.31	0.089	74.33 ±22.47	69.54 ± 15.93	0.516
AST (U/L)	83.60 ± 40.15	73.60 ± 28.04	0.660	247.44 ± 181.57	69.44 ± 20.40	0.008**
ALT (U/L)	57.18 ± 33.68	40.20 ± 29.61	0.092	67.35 ± 31.64	46.08 ± 35.41	0.047*
Glucose (mg/dL)	329.25 ± 26.00	307.71 ± 34.04	0.188	321.94 ± 79.11	271.00 ± 35.00	0.039*
Insulin (μU/mL)	1.33 ± 0.71	0.96 ± 0.25	0.219	2.79 ± 1.88	1.22 ± 0.30	0.042*
HOMA-IR	1.08 ± 0.57	0.73 ± 0.22	0.162	2.38 ± 1.78	0.87 ± 0.28	0.010**
Steatosis grade (0/1/2/3)	75%/25%/ 0/0	100%/0/ 0/0	0.155	5.6%/66.7%/ 16.7%/11.1%	100%/0/0/0	<0.001***
Lobular inflammation (0/1/2/3)	62.5%/25%/ 12.5%/0	71.4%/28.6%/ 0/0	0.626	27.8%/27.8%/ 33.3%/11.1%	76.9%/23.1%/ 0/0	0.022*
Ballooning (No/Yes)	100%/0	100%/0	-	93.3%/6.7%	100%/0	-

Data are shown as mean ± SD for continuous variables, number (%) for binary variables, and frequency for categorical variables. T-test was used to test for significant differences with continuous variables. Chi-Square test was used for categorical variables. ***significant at p < 0.001, **significant at p < 0.01, and

*significant at $p < 0.05$. Abbreviations: BMI, body mass index; ALT, alanine aminotransferase; AST, aspartate aminotransferase; CD, control diet; HFD, high-fat diet; HDL, high-density cholesterol; HOMA-IR, homeostasis model assessment of insulin resistance; LDL, low-density cholesterol.

2.3.2 VAT omentin-1 expression in HFD mice

Real-time PCR showed decreased mRNA expression of omentin-1 in the VAT of HFD versus control diet mice (Figure 31). The difference is significant at 20 weeks of diet, where MASH histological signs are more prominent in HFD mice. Similarly, Western blot analysis from representative mice VAT also confirmed the decreased omentin-1 expression in HFD mice versus control (Figure 32).

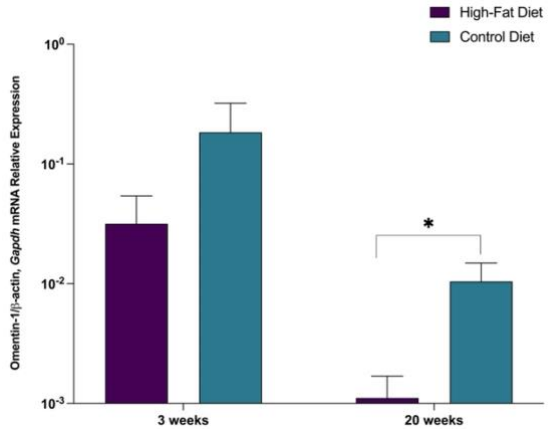

Figure 31. VAT omentin-1 mRNA expression in HFD mice and control diet mice. Quantitative RT-PCR analysis of omentin-1 mRNA in mice VAT fed with HFD showed significantly lower expression compared to mice fed with a control diet at 20 weeks. N = 46. * $p < 0.05$. Abbreviations: *Gapdh,* glyceraldehyde 3-phosphate dehydrogenase.

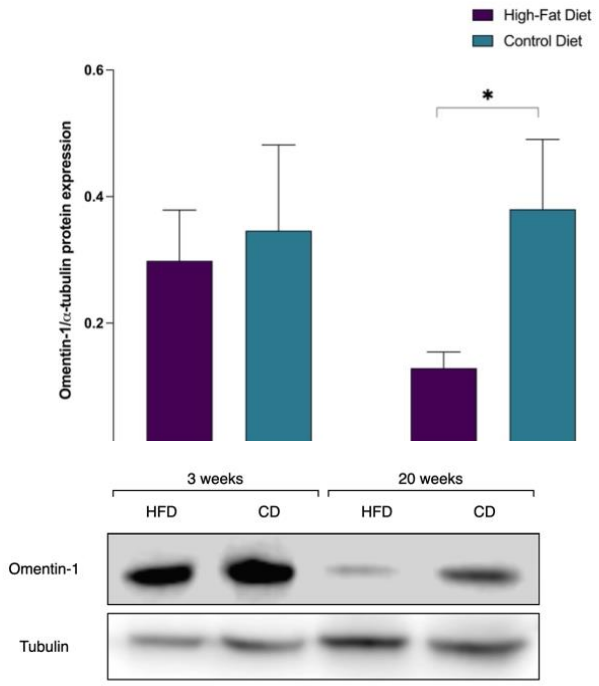

Figure 32. VAT omentin-1 protein expression in HFD mice and control diet mice. Representative blot and densitometric analysis of omentin-1 normalized to α-tubulin revealed that protein expression is

significantly decreased in the VAT of HFD mice as compared to control mice at 20 weeks. Values presented are the mean ± SD with 3-5 mice per group. *p < 0.05. Abbreviations: CD, control diet; HFD, high-fat diet.

2.4 In vitro studies

2.4.1 In vitro determination of omentin-1 experimental concentration

Since there are no available studies regarding the effect on cell viability of omentin-1 in Huh7 in the presence or absence of FFA, a cell viability test (MTT assay) was performed. MTT assay was also used to determine the effective treatment concentration of omentin-1 needed for the next experiments. Briefly, Huh7 cells were exposed to 1200 μM FFA in the presence of increasing concentrations of omentin-1 (150ng/mL, 300ng/mL, and 600ng/mL) for 24 hours. Cells were also exposed only to omentin-1 to assess its toxicity without FFA.

As reported in figure 33, no significant cytotoxicity was observed at all concentrations in Huh7 with or without FFA. We then selected 300 ng/mL as our concentration of interest for subsequent analysis. Other *in vitro* studies have also utilized a test concentration of 300 ng/mL for omentin-1, which corresponds to the approximate plasma level found in healthy lean individuals [134,141,150–152].

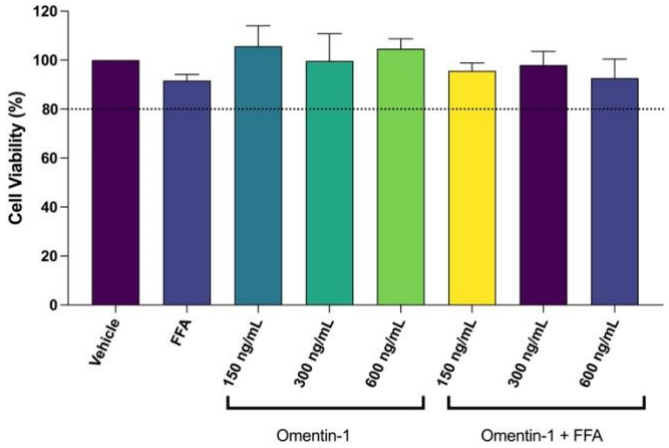

Figure 33. Cell viability of omentin-1 in Huh7 cells with or without FFA. The cell viability was determined by MTT assay with increasing concentrations of omentin-1 (150 ng/mL, 300 ng/mL, and 600 ng/mL) after 24 hours of treatment. Values presented are the mean ± SD of three biological replicates. Abbreviation: FFA, free fatty acids.

2.4.2 Effects of omentin-1 on hepatocyte fat accumulation

The content of intracellular fat was determined by Nile red staining. Exposure of hepatocytes to 1200 μM FFA for 24 h induced fat accumulation, confirming our previous results [80,153]. Flow cytometry analysis showed a shift in the median of the fluorescence peak as compared to vehicle control, indicative of intracellular fat deposition. After the co-treatment with omentin-1, no significant change was observed in the value of fluorescence (Figure 34). Therefore, co-treatment with omentin-1 did not alter the intracellular fat content. Likewise, the addition of omentin-1 in the absence of FFA did not induce steatosis (data not shown).

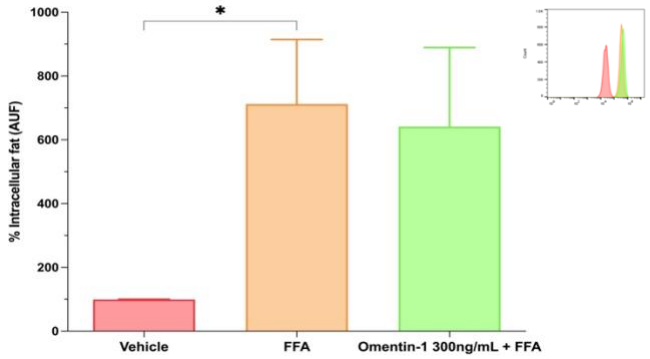

Figure 34. *In vitro* effects of omentin-1 on hepatocyte fat accumulation. Values presented are the mean ± SD of three biological replicates. Abbreviations: AUF, arbitrary unit of fluorescence; FFA, free fatty acids.

2.4.3 Effects of omentin-1 on TNF-α response in hepatocyte

To assess the anti-inflammatory effect of omentin-1, we determined the gene expression of the pro-inflammatory cytokine TNF-α. FFA significantly induced an upregulation of *TNF-α* ($p < 0.001$) *vs* vehicle-treated cells, as shown in figure 35a. Most importantly, the co-treatment of FFA with omentin-1 decreased the mRNA expression of *TNF-α* whose levels are comparable to those observed in the vehicle control. The effect of omentin-1 on the TNF-α release in the cell culture supernatant was also determined by ELISA (Figure 35b) after 1h of treatment. Consistent with the gene expression results, omentin-1 significantly reduced the release of TNF-α. Moreover, omentin-1 treatment did not induce TNF-α gene expression and release in the cell culture supernatant (data not shown).

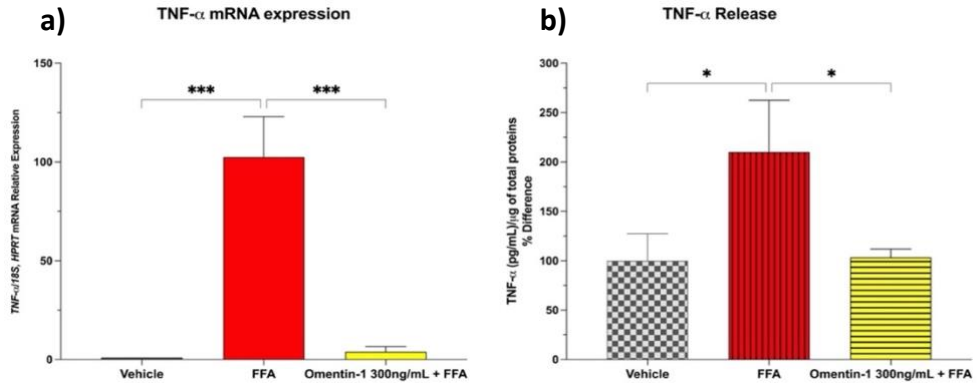

Figure 35. Effect of omentin-1 and FFA co-treatment on the (a) mRNA expression and (b) supernatant release of TNF-α in Huh7 cells with FFA. Values presented are the mean ± SD of three biological replicates. *$p < 0.05$, ***$p < 0.001$. Abbreviations: FFA, free fatty acids; *HPRT,* hypoxanthine-guanine phosphoribosyltransferase.

2.4.4 Effects of omentin-1 on NF-κB response in hepatocyte

The NF-κB family of inducible transcription factors is activated in response to TNF-α cytokine action. The activation of the NF-κB pathway regulates a variety of biological processes, such as inflammation, cell survival, proliferation, and differentiation [154]. Therefore, we determined the gene expression of NF-κB protein p65 in our *in vitro* model of steatosis. Huh7 cells treated with FFA

showed a significant increase in NF-κB mRNA expression versus vehicle control (Figure 36). Upon co-treatment with omentin-1, there is a significant reduction of *NF-κB* expression, suggesting that its anti-inflammatory effect may act via NF-κB pathway.

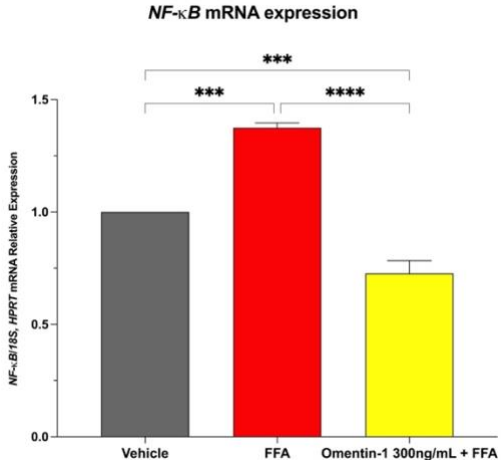

Figure 36. Effect of omentin-1 treatment on the *NF-κB* mRNA expression in Huh7 cells with FFA. Values presented are the mean ± SD of three biological replicates. ***p < 0.001, ****p < 0.001. Abbreviations: FFA, free fatty acids; *HPRT*, hypoxanthine-guanine phosphoribosyltransferase.

2.4.5 Effects of omentin-1 on ER stress in hepatocyte

Primary human hepatocytes loaded with free fatty acids showed the unfolded protein response (UPR) or endoplasmic reticulum (ER) stress [155]. To explore the involvement of omentin-1 in Huh7 ER stress induced by fat overload, we analyzed the expression levels of two ER stress markers (*BiP* and *CHOP* gene markers). The mRNA expression levels of both *BiP* and *CHOP* showed a nonsignificant increase upon treatment of FFA (Figure 37a). Moreover, both markers showed a nonsignificant decrease upon co-treatment with omentin-1 (Figure 37b).

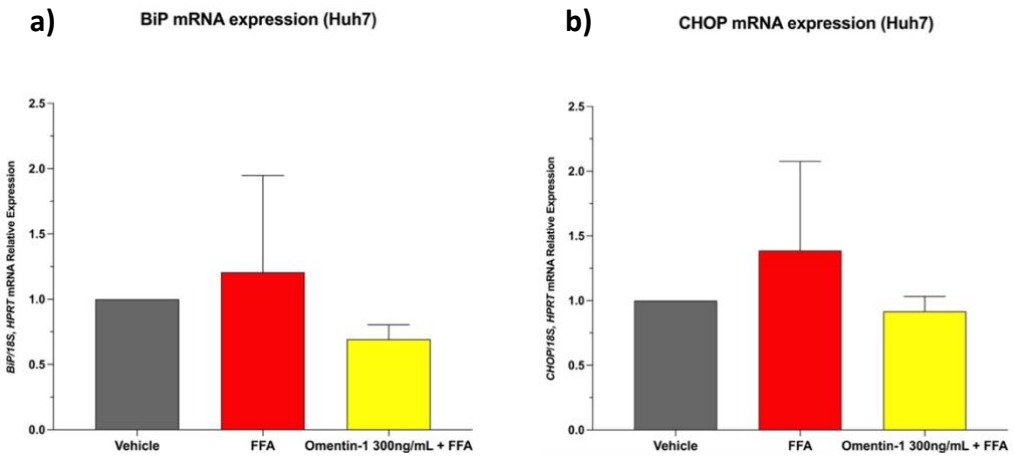

Figure 37. Effect of omentin-1 treatment on ER stress markers (a) *BiP* and (b) *CHOP* in Huh7 cells with FFA. Values presented are the mean ± SD of three biological replicates. Abbreviations: *BiP*, binding of immunoglobulin protein; *CHOP*, CCAAT/enhancer-binding protein homologous protein; FFA, free fatty acids; *HPRT*, hypoxanthine-guanine phosphoribosyltransferase.

2.4.6 Effects of omentin-1 treatment on the production of reactive oxygen species in hepatocytes

The antioxidant role of omentin-1 was evaluated on fat-laden Huh7 cells using glutathione content assay (Figure 38). Reduced glutathione (GSH) is one of the most important scavengers of reactive oxygen species, and its ratio with oxidized glutathione (GSSG) is used as a marker of oxidative stress. The GSH and GSH:GSSG ratio showed reduced levels upon FFA treatment and a significant increase upon co-treatment with omentin-1 (Figure 38a-38b). The exposure to FFA significantly increased the GSSG content ($p < 0.05$) *vs* the vehicle-treated control (Figure 38c), indicating a more consistent oxidative stress state.

Another important antioxidant defense system is the superoxide dismutase (SOD) enzyme activity. Total SOD activity (from cytosol and mitochondria) was measured in cell lysates. From the results, FFA treatment showed increased SOD total activity, probably a compensatory mechanism from oxidative stress. Interestingly, the SOD activity is further enhanced upon co-treatment with omentin-1 (Figure 38d).

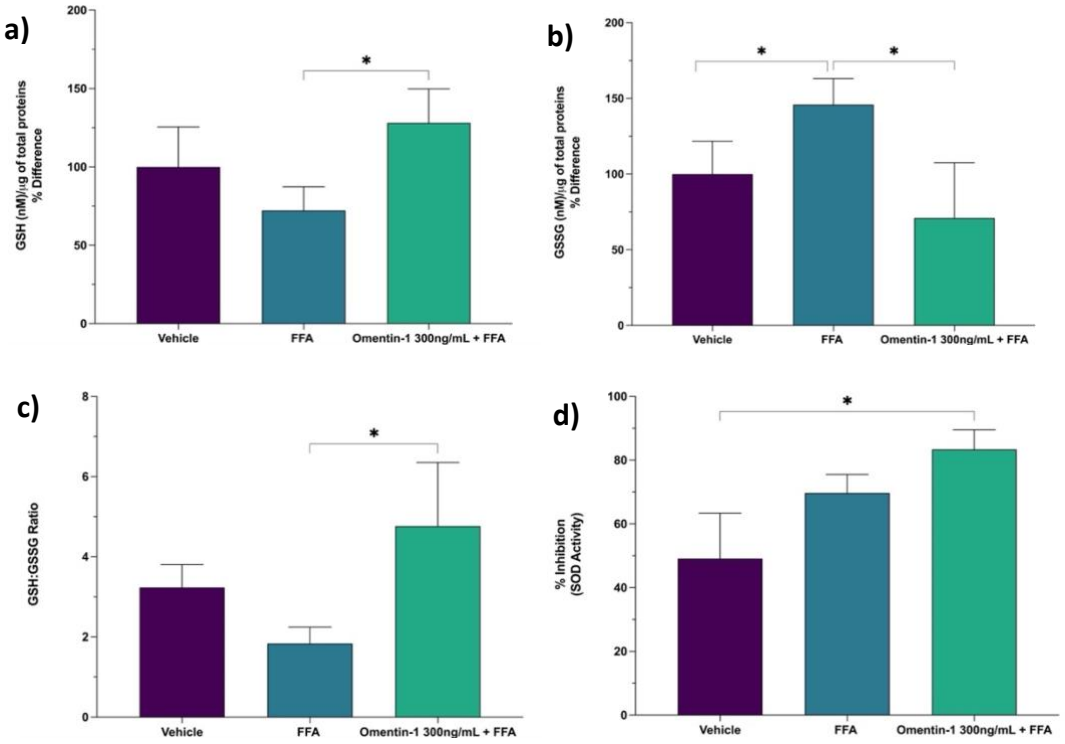

Figure 38. Effects of omentin-1 treatment on (a) GSH, (b) GSSG, (c) GSH:GSSG ratio, and (d) SOD activity in Huh7 with FFA. GSH and GSSG contents were normalized by the total proteins present in the cell lysates (μg) assessed using BCA. Values presented are the mean ± SD of three biological replicates. *p < 0.05. Abbreviations: BCA, bicinchoninic assay; FFA, free fatty acids; GSH, reduced glutathione; GSSG, oxidized glutathione; SOD, superoxide dismutase.

2.5 Ex-vivo VAT explant studies

2.5.1 Ex vivo effects of omentin-1 in TNF-α expression

Aside from secreting adipocytokines, VAT is innervated with inflammatory and immune cells, thus a major source of several inflammatory mediators. We explore the anti-inflammatory role of omentin-1 in the VAT of obese patients (a chronic state of systemic inflammation). The addition of recombinant omentin-1 in VAT explants of obese patients significantly reduced the basal *TNF-α* mRNA expression (Figure 39a). The observation was further reflected in the medium TNF-α release (Figure 39b).

Moreover, we also determined the gene expression of NF-κB protein p65 in VAT explants of obese patients, since NF- κB is a major inducible transcription factor involved in inflammation. VAT treated with omentin-1 showed a significant decrease in *NF-κB* mRNA expression versus control (Figure 39c). This confirms our *in vitro* results suggesting that the anti-inflammatory effect of omentin-1 may act via NF-κB pathway.

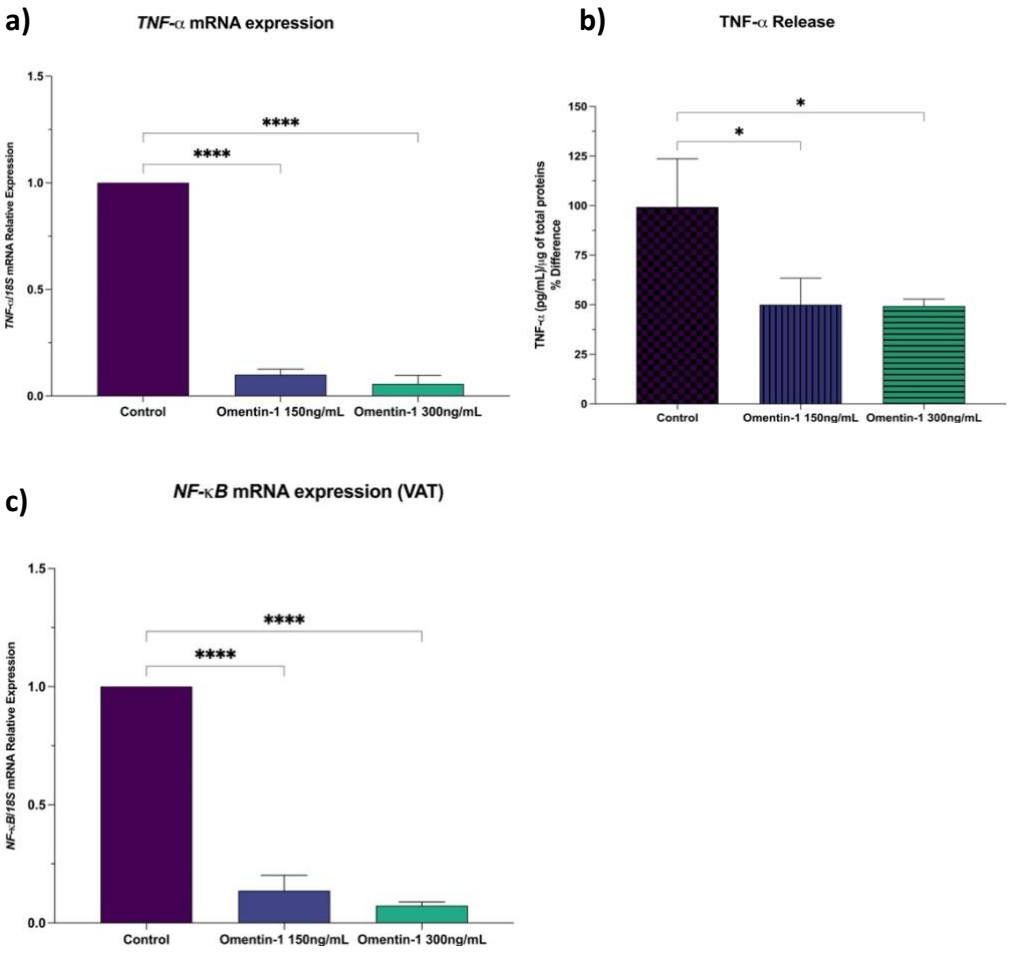

Figure 39. Effect of omentin-1 treatment on the (a) mRNA expression and (b) supernatant release of TNF-α, and (c) *NF-κB* mRNA expression in VAT explants. TNF-α supernatant release was normalized by the total proteins present in the culture medium (µg) assessed using BCA. Values presented are the mean ± SD of three patients. *p < 0.05, ****p < 0.0001. Abbreviations: BCA, bicinchoninic assay; FFA, free fatty acids; GSH, reduced glutathione; GSSG, oxidized glutathione.

2.5.2 Ex vivo effects of omentin-1 on ER stress

To examine the involvement of omentin-1 in VAT ER stress of obese patients, we analyzed the expression levels of *BiP* and *CHOP*. The mRNA expression level of *BiP* is significantly reduced upon treatment of omentin-1 as compared to the control (Figure 40a). Moreover, CHOP mRNA expression is dose-dependently reduced by omentin-1 as compared to the control (Figure 40b).

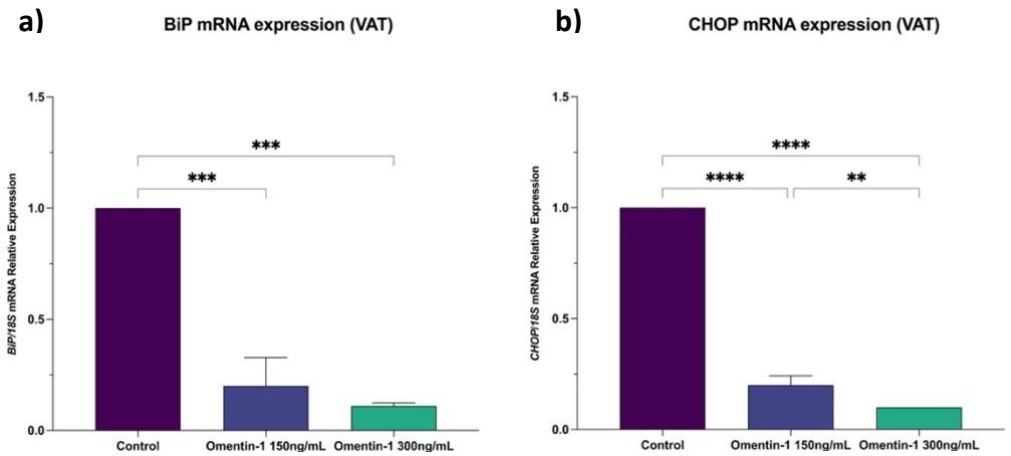

Figure 40. Effect of omentin-1 treatment on the mRNA expression of (a) *BiP* and (b) *CHOP* ER stress markers in *ex vivo* VAT explants. Values presented are the mean ± SD of three patients. ** $p < 0.01$, *** $p < 0.001$, **** $p < 0.0001$. Abbreviations: *BiP*, binding of immunoglobulin protein; *CHOP*, CCAAT/enhancer-binding protein homologous protein.

2.5.2 Effects of omentin-1 treatment on the production of reactive oxygen species in VAT

We evaluated the antioxidant role of omentin-1 in VAT of obese patients using glutathione content assay. The reduced glutathione (GSH) and GSH:GSSG ratio significantly increases upon the addition of omentin-1 300 ng/mL but not omentin-1 150ng/mL (Figures 41a, 41b). On the other hand, the oxidized glutathione (GSSG) almost dose-dependently decreased upon supplementation of omentin-1 (Figure 41c).

Another important antioxidant defense system is the SOD enzyme activity. VAT lysates containing total SOD activity from cytosol and mitochondria were used for the assay. From the results, omentin-1 supplementation significantly enhanced the SOD activity in both concentrations (Figure 41d).

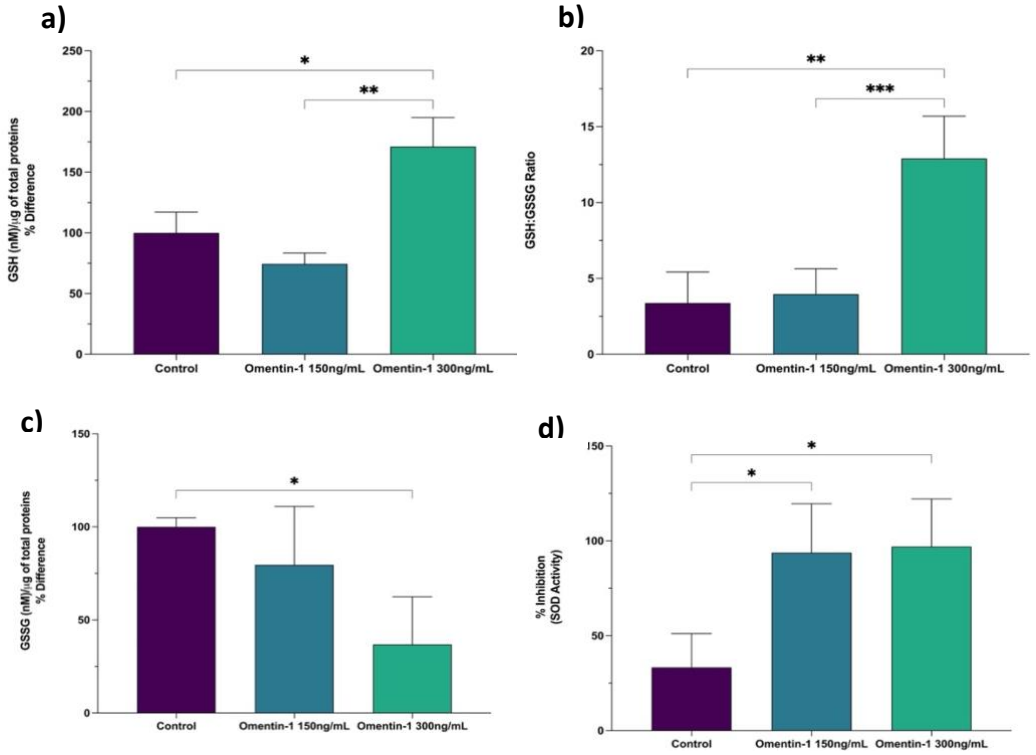

Figure 41. Effects of omentin-1 treatment on (a) GSH, (b) GSSG, (c) GSH:GSSG ratio, and (d) SOD activity in VAT of obese patients. GSH and GSSG contents were normalized by the total proteins present in the tissue lysates (µg) assessed using BCA. Values presented are the mean ± SD of 3-4 patients. * $p < 0.05$, **$p < 0.01$, ***$p < 0.001$. Abbreviations: BCA, bicinchoninic assay; FFA, free fatty acids; GSH, reduced glutathione; GSSG, oxidized glutathione; SOD, superoxide dismutase.

2.5.2 Effects of D-glucose and insulin on omentin-1 levels

Studies revealed that omentin-1 enhances insulin-stimulated glucose uptake *in vitro* in both omental and subcutaneous adipocytes and its serum levels are reduced in patients with T2DM and glucose intolerance [136,140]. We, therefore, hypothesized that omentin-1 level might be affected by glucose and insulin modulation.

Using the VAT explants from obese patients, we added either insulin or glucose in the medium and determined the levels of omentin-1. Both glucose and insulin resulted in a significant and almost dose-dependent decrease in omentin-1 mRNA expression levels (Figures 42a, 42b). Likewise, omentin-1 protein levels were also reduced in VAT homogenates showing consistent results with that of mRNA expression (Figures 42c, 42d).

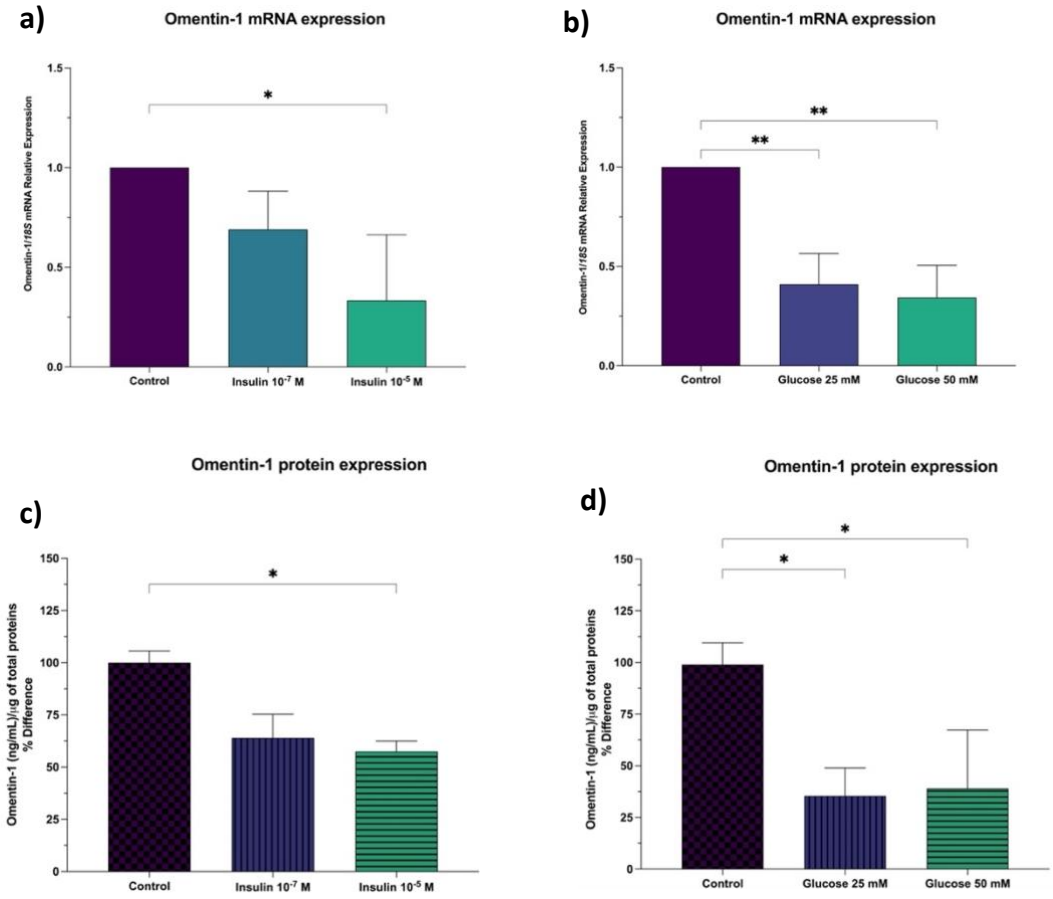

Figure 42. Effects of (a) insulin and (b) glucose on the mRNA expression of omentin-1 in VAT of obese patients; effects of (c) insulin and (d) glucose on the protein level of omentin-1 in VAT of obese patients. Omentin-1 protein level was normalized by the total proteins present in the tissue homogenates (μg) assessed using BCA. Values presented are the mean ± SD of 3-4 patients. * $p < 0.05$, **$p < 0.01$.

3. Discussion

Obesity is one of the most important risk factors for several noncommunicable diseases, including metabolic syndrome (MS), T2DM, cardiovascular diseases, and MASLD [12,13,34]. The increasing prevalence of MASLD is primarily related to the obesity pandemic, especially during childhood and adolescence [25]. Obesity, characterized by adipose tissue (AT) mass expansion, is seen in 51% of MASLD and 81% of MASH patients globally [12]. However, there are lean, or low AT mass patients that also develop MASLD, suggesting that AT function rather than AT mass/obesity could be the key driver of the disease [26,27]. Fat accumulation in the organs, especially the visceral tissue, leads to their dysfunction, promoting ectopic fat accumulation in the liver [156], inflammation [68,157,158], endoplasmic reticulum, and oxidative stress [39,43,159], impairment of glucose metabolism [40,156,158,160], among others. Aside from its role as the regulator of lipid flux to the liver, adipose tissue is also recognized as a major endocrine organ producing a large array of mediators, known as adipocytokines [26]. The role of adipocytokines in AT-liver crosstalk has become an important area of MASLD research because of the potential utility of those proteins/mediators, as diagnostic markers and or/ therapeutic targets —

since no reliable diagnostic marker and pharmacological treatment are currently approved for the disease.

Omentin-1 (also known as intelectin-1) is a novel adipocytokine that is mainly expressed in VAT and found to be related to obesity [138], T2DM[140], cancer [134,161], as well as cardiovascular diseases [140,162]. In our current study, we utilized a simple *in silico* analysis to identify omentin-1 as being differentially expressed between the VAT of obese versus obese MASH patients. For the first time, we also investigated its role in MASLD using a variety of translational approaches. We determined the expression of omentin-1 in VAT, simultaneously at both mRNA and protein levels in MASLD patients. Furthermore, we present novel data regarding the plasma levels of omentin-1 in different obese groups with MASLD. For its role in the liver and VAT, we describe original observations regarding its beneficial effects in the MASLD-related pathophysiological mechanisms.

Consistent with previous studies [136,163], we detected omentin-1 mRNA in VAT but not SAT. Both mRNA and protein levels of omentin-1 in VAT are lower in all obese groups than in lean controls. The expression is further decreased in obese groups with MASH (with or without fibrosis) *vs* the Ob group. Interestingly, no significant difference was noted in the Ob-M group compared to the Ob-MF group. Additionally, our *in vivo* mice results concur with our human validation results. According to reports, mice VAT does not express omentin-1 at a meaningful level compared to intestinal tissue [136,164]. Nonetheless, we are still able to demonstrate that HFD, which induced obesity and MASH histological features in mice, lowers VAT omentin-1 levels as compared to their control diet counterpart.

Omentin-1 is reported to be the major circulating form of omentin in human plasma [138]. Thus, we measured the plasma omentin-1 levels in our well-characterized morbidly obese cohort and additional lean group for comparison. Interestingly, the results of plasma omentin-1 levels as measured by ELISA are consistent with our VAT mRNA and protein data. As reviewed by Watanabe *et al.,* circulating blood levels of omentin-1 in healthy lean subjects vary from approximately 5 to 800 ng/mL, depending on the ELISA kit used [134]. The present study shows that the obese group without MASLD has a mean ± SD of 318.9 ± 138 ng/mL plasma omentin-1 level, coinciding with the data obtained by de Souza Batista *et al.* (310 ± 11 ng/mL in the overweight group) [138]. Successively, correlation analyses were performed to evaluate the relationship between biochemical parameters and plasma omentin-1 levels in morbidly obese patients. In our study, omentin-1 plasma levels were found to be positively correlated with AST/ALT ratio and negatively correlated with ALT level. These results indicate an association between liver damage and omentin-1 secreted by VAT, supporting the crosstalk theory between the two organs.

Taken together, our findings suggest that a reduced level of omentin-1 is associated with MASLD development, probably via adipose tissue–liver crosstalk. Furthermore, when considering only the obese groups in our study, it

is unlikely that BMI is solely responsible for their lower omentin-1 levels, since all patients had a BMI of > 35 kg/m^2. Therefore, we also hypothesized that the further decrease in omentin-1 level could be an additive effect of MASLD severity to obesity. As such, the severity of MASLD results from several pathophysiological mechanisms, such as oxidative stress and ER stress, inflammation, and glucose-insulin impairment. To answer our hypotheses, we employed *in vitro* and *ex vivo* studies to evaluate the role of omentin-1 in MASLD-related pathophysiological mechanisms.

MASLD pathogenesis is complex but the onset of the disease is still represented by the accumulation of fat in the liver [60,165]. Our group previously developed an *in vitro* model of MASH where the exposure of hepatocytes to high concentrations of FFA promotes steatosis, inflammation, oxidative stress, and fibrogenic response, similar to those observed in patients with MASLD [80]. Using this *in vitro* model to represent the pathologic events in the liver, we evaluated the beneficial effects of recombinant omentin-1. In parallel, we also studied its effects in *ex vivo* VAT explants obtained from obese patients with MASLD to determine its role in the actual diseased tissue setting.

TNF-α is primarily, but not exclusively, produced by immune cells since FFA overload and other insults to hepatocytes could also result in its secretion [80,166]. Moreover, adipose tissue is a major source of endogenous TNF-α production, and its expression in VAT is elevated in obese and/or MASLD patients [68,160,167]. The expression of TNF-α in steatotic hepatocytes and VAT supplemented with omentin-1 has not been examined to date. Here we have demonstrated that omentin-1 reduced the levels of TNF-α in both fat-laden hepatocytes and VAT explants from obese patients. TNF-α is a key mediator in the process of MASLD development by not only promoting inflammatory response, but also mediating insulin resistance, and inducing fibrosis-associated proteins [97]. Hence, the attenuation of TNF-α action may help prevent or delay the development of MASH. Previously, it has been demonstrated that omentin-1 plays an anti-inflammatory role by preventing the TNF-α-induced COX-2 expression in vascular endothelial cells by inhibiting the AMPK/eNOS/NO pathways [152]. In addition, another study showed that omentin-1 inhibits TNF-α-induced expression of adhesion molecules in endothelial cells by blocking ERK/NF-κB pathway [168]. NF-κB transcription factor regulates a cascade of inflammatory responses by TNF-α activation [154,169]. Based on this premise, we also investigated the role of omentin-1 in NF-κB expression. Indeed, we found that omentin-1 decreased the expression of NF-κB in both fat-laden hepatocytes and VAT explants, suggesting that the anti-inflammatory effect may act via inhibition of this pathway.

Obesity, a state of low-grade systemic inflammation, is associated with ROS overproduction and oxidative stress due to mitochondrial dysfunction [40]. As a result, inflammation and oxidative stress are involved in the induction of ER stress signaling pathways and subsequent UPR activation to restore ER

homeostasis [41]. This implies that oxidative stress, ER stress, and inflammatory pathways somewhat converge at different stages of obesity resulting in disease progression. Our group and other authors previously reported that fat-laden hepatocytes increase ROS production and ER stress [35,42,80,170]. Similarly, growing evidence suggests that excess energy substrate input associated with obesity enhanced ROS generation and ER stress by VAT [39,99,157]. Interestingly, we presented herein that adding omentin-1 mitigated both the oxidative stress and ER stress in our *in vitro* and *ex vivo* setups. Specifically, a significant decrease in oxidized glutathione (GSSG) levels and enhanced SOD enzyme activities were observed in fat-laden hepatocytes and VAT explants. In line with these observations, our results also showed that ER stress markers (*BiP* and *CHOP*) were also reduced by omentin-1 supplementation. Like omentin-1, vaspin, also exerts the same beneficial effects on ER stress–induced metabolic dysfunctions. However, unlike omentin-1, with no known receptor to date, vaspin binds to BiP, which is recruited from ER to the plasma membrane under ER stress [171]. Further investigations are needed to elucidate the role of omentin-1 in oxidative stress and ER stress, as well as to identify its specific receptor. Nonetheless, our findings suggest that oxidative stress and ER stress, as well as inflammation, all of which increase in parallel with metabolic dysfunctions, could be alleviated by omentin-1.

Metabolic disorders like obesity, diabetes, and polycystic ovarian syndrome are all characterized by insulin resistance and impairment of glucose metabolism. It has been shown that *in vitro* supplementation of recombinant omentin-1 enhances insulin-mediated glucose uptake by adipocytes via GLUT4 translocation and Akt phosphorylation [136,163]. Furthermore, as reported herein, omentin-1 decreases the ER stress marker BiP, which is also thought to maintain glucose uptake in glucose storage tissues [171]. Thus, given the role of omentin-1 in glucose homeostasis, we hypothesized that hyperinsulinemia and hyperglycemia decrease its expression. We found that upon increasing the concentration of insulin and glucose in the medium of VAT explants, the expression of omentin-1 is significantly decreased. This finding is in line with several studies showing that the reduced omentin-1 in adipose tissue may contribute to the development of insulin resistance and T2DM. However, it should be noted that our findings relate only to obese patients with MASLD without T2DM. Therefore, it would be of interest if we also determine the levels of omentin-1 in VAT of diabetic or lean patients.

Collectively, the present study provides evidence that reduced omentin-1 level is associated with obesity-related MASLD. Although the cause-and-effect relationship is still unclear, we are still able to show that omentin-1 is an adipocytokine that plays a significant role in the adipose tissue-liver crosstalk. As an endocrine factor, we report herein that VAT omentin-1 has a protective role against fat-loaded hepatocytes showing MASLD-related pathophysiological mechanisms (Figure 41). Locally, omentin-1 was able to regulate obese VAT mechanisms, especially insulin-glucose impairment. Further studies are

required to elucidate the biological activity of omentin-1 in obesity-related MASLD with a focus on specific receptor identification, which could then eventually facilitate new drug development.

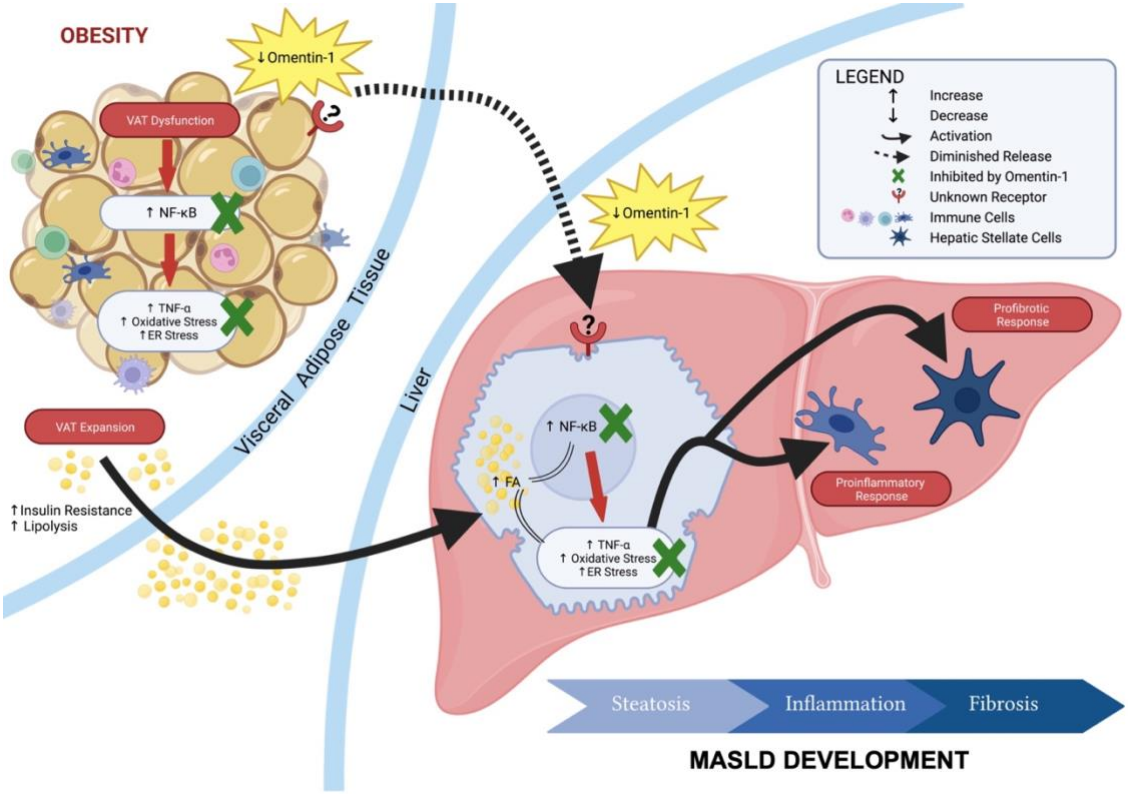

Figure 43. Schematic presentation of adipose tissue – liver crosstalk in obesity-related MASLD and how omentin-1 exerts its beneficial effects. Obesity leads to VAT expansion promoting lipolysis and excessive delivery of FA to the liver, which is further exacerbated by insulin resistance. Alongside VAT expansion, VAT dysfunction leads to increased inflammation, oxidative stress, and ER stress. In the liver, the presence of increased FA leads to lipotoxicity triggering the same cellular insults, which are all associated with NF-κB activation. Omentin-1, whose receptor is still unknown, exerts its beneficial effects by preventing NF-κB activation and thus, inflammation, oxidative stress, and ER stress in both steatotic hepatocytes and diseased VAT. By preventing these mechanisms, proinflammatory and profibrotic responses that contribute to MASLD development could also be halted.

4. Materials and Methods

4.1 In silico strategy

The literature review was conducted following the guidelines of the Preferred Reporting Items for Systematic Reviews and Meta-analysis (PRISMA) [143]. We electronically searched transcriptomics experimental datasets about NAFLD adipose tissue in PubMed database (query terms: transcriptomics/gene expression/microarray data in NAFLD adipose tissue). "NAFLD" mesh term was used instead of "MASLD," because the latter was coined only in 2023 [11] and most of the available data are still using "NAFLD."

The electronic search employed keywords with the use of Boolean operator "AND" as shown in figure 44. To narrow the search results for PubMed, the 5-year, full text, and associated dataset filters were used. During screening, we included all the studies performed on MO patients and those from animal

models were excluded. In addition, all datasets generated using microarrays or RNAseq technologies were considered.

At the time in which the analysis was performed, limited information on transcriptomics data was available in NAFLD, particularly using VAT. The paper of du Plesssis *et al.* was selected due to similarity to our morbidly obese cohort's patient selection and the availability of datasets in VAT [68]. The gene expression data set GSE58979 was downloaded from Gene Expression Omnibus [144], which included 9 obese VAT samples (group 1) and 7 NASH VAT samples (group 3). In du Plessis study, VAT samples were obtained percutaneously in a cohort study of morbidly obese patients undergoing bariatric surgery in several academic hospitals.

Liver histology assessment used in their study was according to the NASH–Clinical Research Network Scoring System criteria. Patients were divided into 4 distinct groups, as follows: obese (group 1): less than 5% steatosis, NAS of 0; NAFL (group 2): NAFLD without inflammation or NASH, NAS less than 4; NASH (group 3): NASH without significant fibrosis, NAS of 5 or greater and fibrosis score of 0–1; NASH with fibrosis (group 4): NASH with significant fibrosis (score, 2–3), but no cirrhosis.

The raw data of the mRNA expression profiles were downloaded and analyzed by GEO2R. GEO2R is an interactive web tool that allows users to compare two or more groups of samples in a GEO Series to identify genes that are differentially expressed across experimental conditions. The limma (Linear Models for Microarray Analysis) method was used to identify genes that are differentially expressed (DEG) among obese and NASH [145]. The significance of DEGs was calculated by the t-test and was represented by the p-value. The threshold for the DEGs was set as corrected p-value < 0.05 and $\log_2$ fold change (FC) of |1|.

In our systematic strategy, the identifiers (IDs) for protein-coding genes in the consulted data resources were standardized, through mapping to the UniProtKB identifiers on UniProt database and only those IDs were further used. Moreover, datasets of our interest (e.i. blood/plasma proteins) collected from Human Protein Atlas (HPA) were used as *in silico* sieve filters, [147].

Dataset comparison and sub-groups selection was performed by applying Venn diagrams using InteractiVenn web-based tool [172]. Venn diagrams were used as *in silico* filters to identify the interested proteins, those fulfilling the following desired criteria. They should be visceral adipose tissue-enriched, secreted proteins, experimental evidenced in plasma or blood, and not included as part of the housekeeping proteome.

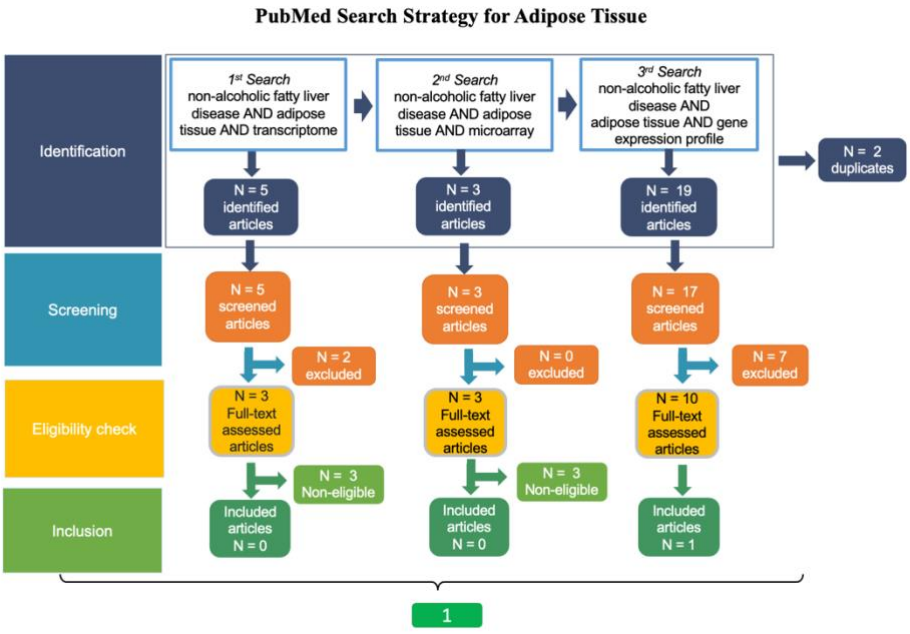

Figure 44. Flowchart of the results obtained using our electronic literature search strategy and implementing inclusion criteria for adipose tissue. PubMed database was used for the electronic literature search. Boolean operator "AND" and filters: 5-year, full text, and associated dataset filters were used. For the screening, animal studies and studies with no geodatasets were excluded.

4.2 Study Participants

The assessment of omentin-1 VAT mRNA and plasma level was performed retrospectively in a cohort of MO patients enrolled in a bariatric surgery program. All patients gave their written consent to participate in the study, and sensitive data were protected through anonymization. The study has been approved by the local Ethical Committee under protocol N. 22979 (Comitato Etico Regionale Unico, FVG, SSN, Italy). Patients enrolled were ≥18 years, with a body mass index (BMI) > 40 kg/m^2 or > 35 kg/m^2 if obesity-related comorbidities were already present, with acceptable operative risks, failure of nonsurgical treatments, and declared compliance to follow lifelong medical surveillance. Patients were excluded if they had coexistent chronic liver disease, including suspected/confirmed hepatocellular carcinoma, alcoholic liver disease (>25 g/day alcohol consumption), known HBV, HCV, HIV positivity, and therapy with drugs that could affect the liver.

In their baseline visit, anthropometric parameters including age, gender, body weight and height, BMI calculation, and waist circumference were recorded. After overnight fasting, blood samples were collected before surgery (wedge biopsy) for determination of glucose, liver biochemistry (AST, ALT, GGT), albumin, platelets, and lipid profile (TG, T-Chol, HDL), among others. VAT collection and liver biopsy were performed at the time of the surgical procedure. Liver histology was assessed by two independent pathologists according to Kleiner-Brunt criteria and NAS scoring through NASH–Clinical Research Network Scoring System criteria [51]. Patients were divided into 3 distinct groups, as follows: obese (group 1): less than 5% steatosis, NAS of 0; MASH (group 2): MASH without significant fibrosis, NAS of 3-6 and fibrosis

score of 0–1; MASH with fibrosis (group 3): MASH with significant fibrosis (score, 2–4).

In addition, a total of 17 lean controls with BMI of 18.5 – 24.9 kg/m^2 were included in the ELISA study. Plasma samples were collected from the lean controls after overnight fasting to assess the omentin-1 levels. For PCR and western blot, five lean VAT from our tissue biobank were used as controls.

4.3 Compounds and Chemicals

Reagent sources were as follows: recombinant human omentin-1 (Bio Vendor, Candler, NC, USA) and TNF-α (Sigma-Aldrich, MO, USA). Antibody sources were as follows: Omentin-1/Intelectin-1 (Santa Cruz Biotech, Santa Cruz, CA, USA), α-tubulin (Santa Cruz Biotech, Santa Cruz, CA, USA).

Dulbecco's modified Eagle's high glucose medium (DMEM-HG), Dulbecco's modified Eagle's low glucose medium (DMEM-LG), L-glutamine, penicillin/streptomycin, and fetal bovine serum were purchased from Euroclone (Milan, Italy). 3-(4,5-dimethylthiazol-2-yl)-2,5-diphenyltetrazolium bromide (MTT), bicinchoninic acid solution-kit (B9643); bovine albumin Cohn V fraction (A4503); dimethyl sulfoxide (DMSO), hydrogen peroxide (H1009), Nile Red (N3013), oleic acid (C18:1), palmitic acid (C16:0), phosphate-buffered saline (PBS) and Tri-Reagent (T9424) were obtained from Sigma Chemical (St. Louis, MO, USA). iScript™ cDNA Synthesis kit (170-8890) and iQ SYBR Green Supermix (170-8860) were purchased from Bio-Rad Laboratories (Hercules, CA, USA). 2',7'-dichlorodihydrofluorescein diacetate (H_2DCFDA) (D399) was obtained from Molecular Probes (Milan, Italy).

4.4 Cell Culture

Hepatoma derived cell line Huh7 (JHSRRB, Cat #JCRB0403) was obtained from the Health Science Research Resources Bank (Osaka, Japan). Cells were grown in DMEM-HG medium supplemented with 10% v/v fetal bovine serum, 2 mM L-Glutamine, 10,000 U/mL penicillin, and 10 mg/mL streptomycin at 37°C under 5% CO2, in a 95% humidified atmosphere. The cells were exposed for 24 h to 1200 μM of free fatty acids (FFA) (oleic:palmitic ratio 2:1 μmol/μmol) as previously described by our group [80]. Since albumin concentration is an important factor in determining the concentration of available FFA, the FFA were complexed with bovine serum albumin at a 4:1 molar ratio taking into consideration the albumin concentration already present in the medium due to the FBS supplementation.

4.5 Omentin-1 Experimental Dose Determination and Cell Viability Assay

The cytotoxic effect of FFA (1200 μM) and recombinant omentin-1, alone or in combination was assessed by MTT colorimetric assay after 24 hours. Huh7 monoculture was plated at a cell density as described before [96] and treated accordingly with increasing concentrations of omentin-1 (150ng/mL, 300ng/mL, and 600ng/mL). Likewise, cells were also exposed to control medium with increasing concentrations of omentin-1 only to assess their intrinsic toxicity in

the system without FFA. After 24 hours, the medium was removed, and cells were incubated for 1 hour with MTT at the concentration of 0.5 mg/mL. Afterward, the culture medium was removed, and formazan crystals were dissolved in 200 µl of DMSO. 150 µl from each well was transferred to a microtiter plate and optical density (OD) was determined at 562 nm wavelength on an Enspire® Multimode Plate Reader (PerkinElmer, Waltham, MA USA).

To identify the experimental concentration for each compound, we followed the recommendation of ISO 10993-5 (*in vitro* cytotoxicity test on extracts) [81]. A reduction in cell viability of more than 20% compared to the vehicle control was considered as the exclusion criterion. The cutoff concentration meeting this requirement was selected as the experimental concentration for omentin-1.

4.6 Ex vivo primary explant culture of VAT

VAT explants from morbidly obese patients (without T2DM) undergoing bariatric surgery were cultured using a protocol that was a modification of the methods described by Carswell *et al*., 2012 [173] & Tan *et al.,* 2008 [163]. Within 30 minutes after the surgery, tissue was minced into small pieces, approximately 5–10 mg per piece (~1–2 mm^3), using sterile sharp scissors. Then tissue fragments were poured through a 440 µM nylon mesh, affixed to a funnel, and placed on top of a 50 ml bottle to capture the waste. Two mL of PBS warmed at 37^0C was poured over the tissue on the funnel to remove broken cell debris and lipid. Several tubes of minced tissue were combined on the funnel and washed together. Visible blood clots and connective tissues were removed using sterile forceps and washed again with PBS if necessary. Tissue fragments were transferred into a pre-weighed sterile Petri dish using forceps/spoons and weighed. Since the tissue is not quite dry, the actual weight of the tissue is overestimated by about ~20%. Samples were then transferred into six-well plates (~100 mg/well) containing 3 mL of DMEM-LG supplemented with 1% FBS, 2 mM L-Glutamine, 100 IU/ml penicillin, 100 mg/ml streptomycin, 10^{-12} M of Humalog insulin, 1 µM dexamethasone, and 50 µg/ml gentamicin. VAT explants were cultured for 24 h with or without the addition of insulin (10^{-5} M, 10^{-7} M) or D-glucose (50 mmol/L, 25 mmol/L) in a 37°C incubator under an atmosphere of 5% CO2/95% air.

4.7 Animal Model (In Vivo)

C57Bl/6 mice pups were obtained from the local SPF animal facility of the University of Trieste. Immediately after weaning, animals were randomly group-housed in cages based on the final experimental protocol (Figure 45) in a temperature-controlled environment (22 °C ± 2 °C) and on a 12 h light/dark schedule, and fed ad-libitum with control diet (CD, 811900 Special Diets Services, England) or HFD diet (HFHC: D12331, Research Diets, New Brunswick, NJ, USA) plus 42 g/L fructose/sucrose in drinking water, as previously described [63]. Based on the knowledge of the model and the experimental goals, the diet was continued for 3 weeks and 20 weeks. Body weight was recorded at each experimental point just before sacrifice. After overnight fasting, blood was

collected under deep anesthesia (40μg/kg ketamine + 10 mg/kg xylazine, i.p.) by cardiac puncture, then the sacrifice was completed by decapitation. Liver and epididymal fat (a depot of VAT) were dissected for the histologic evaluation and experimental use, respectively. Whole blood was allowed to clot at room temperature (RT) for 20 min, followed by centrifugation at 3500× g for 5 min at RT to separate the serum. Hemolyzed samples, if present, were not used. All experimental protocols were approved by the local OPBA (Oorganismo Per il Benessere dell'Animale) of the University of Trieste and by the Competent National Authority (Ministero della Salute-Direzione Generale della Sanità Animale e dei Farmaci Veterinary. Approval 56/2022PR). All the procedures were performed according to the Italian Law (D.Lgs.26/2014) and European Community directive (2010/63/EU). A maximal effort to minimize the number of animals used and their sufferance was done (3R rule).

Blood tests and histology were performed as previously described [63]. Blood glucose level was assessed at every experimental checkpoint time. Enzymatic colorimetric kits (Roche Diagnostics GmbH; Mannheim, Germany) were used to measure these parameters in a Roche HITACHI Cobas e501 instrument (Roche Diagnostics GmbH; Mannheim, Germany) accordingly to manufacturer's instructions. Serum insulin content was quantified from the same blood sample, by AlphaLISA Insulin Kit (Perkin Elmer, Waltham, USA) following manufacturer's instructions. The homeostasis model assessment of insulin resistance HOMA-IR was calculated for each animal according to the following formula: blood glucose (mg/dL) x fasting insulin (μU/mL)/405.

At each checkpoint, the liver was harvested, and a portion of tissue immediately fixed in buffered formalin (formaldehyde 4%, NaH2PO4 4gr/L, Na2HPO4 6.5 gr/L: pH 6.8). Tissue sections were cut at a thickness of 3.5 μm and stained with Hematoxylin & Eosin (H&E) and Gömöri trichrome stain. Histology was read by a single independent pathologist, blinded to experimental design and treatment groups. Scores were attributed to steatosis (0–3), lobular inflammation (0–3), portal inflammation (0–1), and ballooning (0–2). Fibrosis was analyzed separately with a scale from 0 to 4.

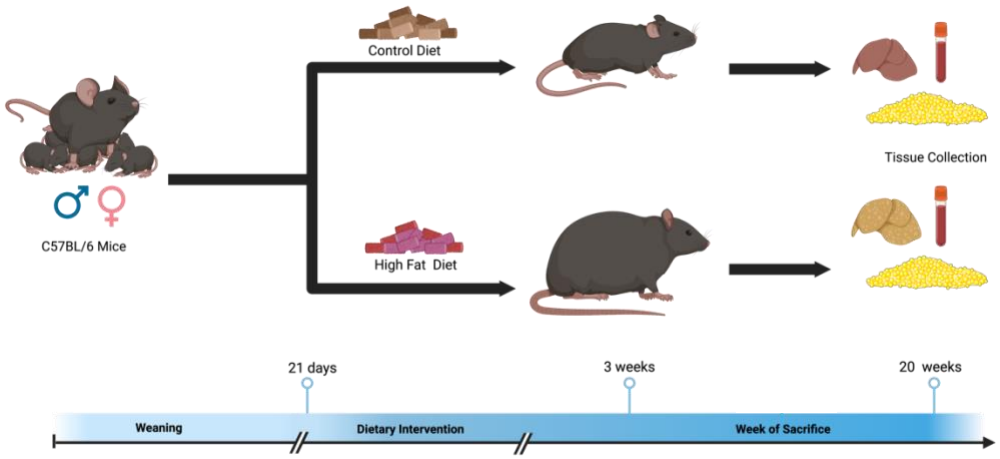

Figure 45. ***In vivo*** **mice experimental set-up.** The experimentation started at p21 (after weaning), animals were divided in control and high-fat diet. Two experimental checkpoints were established (3 weeks and 20 weeks of diet), in which portion of the animals was sacrificed.

4.8 Fluorometric determination of intracellular fat content - Nile red staining

Intracellular fat content *in vitro* was determined by flow cytometry using Nile red staining, a vital lipophilic dye used to label fat accumulation in the cytosol [80]. After 24h of FFA exposure, adherent monolayer cells were washed with PBS and detached by trypsinization. After 5 minutes of centrifugation at 1500 rpm, the cell pellet was resuspended in 3 mL of PBS and incubated with 0.75 μg/mL Nile red dye for 15 min at room temperature. Nile red intracellular fluorescence was detected using a Becton Dickinson FACSCalibur System on the FL2 emission channel through a 585 ± 21 nm bandpass filter, following excitation with an argon-ion laser source at 488 nm. Data were collected in 10,000 cells and analyzed using FlowJo (Tree Star Inc., Ashland, OR, USA) analysis software.

4.9 RNA Extraction, cDNA Synthesis, and Gene Expression Analysis by q-PCR

Total RNA was extracted from cell culture harvest and homogenized VAT using Tri-reagent kit (Sigma-Aldrich, MO, USA) according to the manufacturer's instructions. The total RNA concentration was then quantified spectrophotometrically at 260 nm in a UV-31 Scan spectrophotometer (Vetro Scientifica srl, Rome, Italy) while purity was evaluated by measuring the A260/A280 ratio. Isolated RNA was resuspended in RNAse free water and stored at −80 °C until analysis. Total RNA (1 μg) was reverse transcribed using the High Capacity cDNA Reverse Transcription Kit (Applied Biosystems, Waltham, MA, USA) according to the manufacturer's protocol in a Thermal Cycler (GeneAmp PCR System 2400, Perkin Elmer, Boston, MA, USA). Retrotranscription was performed using the following temperature protocol: 10 min at 25 °C (annealing), 120 min at 37 °C (cDNA synthesis), 5 min at 85 °C (enzyme denaturation).

Quantitative PCR was performed in CFX Connect Real-Time PCR Detection System (Bio-Rad, Hercules, CA USA). All primer pairs were designed using the NCBI tool Primer-BLAST and were synthesized by Metabion International AG

(Planegg, Germany) or Sigma Genosys Ltd. (London Road, UK). PCR amplification was performed in a specific reaction volume containing 25 ng of cDNA, 1X iQ SYBR Green Supermix, and specific sense and anti-sense primers. Primer sequences for both human and mouse genes are specified in table 14. Standard curves were prepared using a 'calibrator' cDNA for each target and reference gene. To verify the specificity of the amplification, a melt-curve analysis was performed immediately after the amplification protocol. The relative quantification was made using the Pfaffl modification of the ΔΔCt equation, considering the efficiencies of individual genes. The results were normalized *in vivo* (mice VAT) to β-actin and *Gapdh*, *ex vivo* (human VAT) to ribosomal subunit 18S, and *in vitro* (Huh7) to β-actin and ribosomal subunit 18S, as reference genes. The data were analyzed using CFX Manager™ software (Bio-Rad Laboratories Hercules, CA, USA).

Table 14. Primer sequences for the *in vitro, ex vivo*, and animal experiments.

Human Genes	Accession Number	Forward	Reverse	Length (bp)
BiP	NM_005347	GCACAGACAGAT TGACCTATT	GTAGCACAGGAGCACAGC	157
CHOP	NM_004083	CACTCTCCAGA TTCCAGTCAG	AGCCGTTCA TTCTCTTCAGC	182
HPRT	NM_000194.1	ACATCTGGAGTCCTATTGACATCG	CCGCCCAAAGGGAACTGATAG	193
ITLN1	NM_017625.3	GACGCCCAGAAAACAGCATC	CGTTGGCTGCTCTCTCGTTA	103
NF-κB	L19067.1	GAATGCTGTGCGGCTCTG	CACGATTGTCAAAGATGGGATG	101
TNF-α	NM_000594	GTGAGGAGGACGAACATC	GAGCCAGAAGAGGTTGAG	95
18S	NR_003286.2	TAACCCGTTGAACCCCATT	CCATCCAATCGGTAGTAGCG	150
Mouse Genes	**Accession Number**	**Forward**	**Reverse**	**Length (bp)**
β-Actin	NM_007393	CCTTCTTGGGTATGGAATCCTGTG	CAGCACTGTGTTGGCATAGAGG	104
Gapdh	NM_008084	CCAGTATGACTCCACTCACG	CTCGCTCCTGGAAGATGGTG	101
Itln1	NM_010584.3	ATCATGGTTGCTACCAGAGGTT	AAGAATTGCCCCACCTGTTG	70

4.10 Total Protein Extraction and Western Blot Analysis

For tissue homogenization, VAT was added to a 2-mL screw cap tube with 651 mg of 1.4 mm ceramic beads (OMNI, GA, USA). 500 µL of ice-cold 1X Cell lysis buffer (Cell Signaling Technology, Inc., MA, USA) with 1mM PMSF was added and processed on the Bead Ruptor 4 Bead Mill Homogenizer (OMNI, GA, USA) for two 30-second cycles at 5 m/s. For cell lysates, cells were scraped using 500 µL of ice-cold 1X Cell lysis buffer with 1mM PMSF. The homogenized samples were placed in an ice water bath afterwards. Lysates were centrifuged at 16000 g for 10 minutes at 4°C to collect the supernatants. Bicinchoninic acid (BCA), a copper-based colorimetric assay was used for total protein quantification of the VAT homogenates and cell lysates.

For mice and human VAT, 80 μg of protein was denatured in 1X sample buffer with beta-mercaptoethanol at 100^0C for 5 minutes. After denaturation, protein samples were subjected to sodium dodecyl sulfate-polyacrylamide gel electrophoresis (SDS-PAGE) in a 10% polyacrylamide gel. After electrophoresis, proteins were transferred to PDVF membranes, blotted for 1 h at 180V, blocked in 4% dry milk in PBS-Tween buffer, and incubated with specific primary antibodies for 2 nights at 4°C. The following primary antibodies were used: Omentin-1/Intelectin-1 1:100 (Santa Cruz Biotech, Santa Cruz, CA, USA) and the reference α-tubulin 1:2000 (Santa Cruz Biotech, Santa Cruz, CA, USA). Blots were incubated with anti-mouse IgG-HRP-conjugated secondary antibody (1:500 Omentin-1/Intelectin-1 and 1:2000 for α-tubulin) for 1 hour at room temperature. Protein bands were visualized using the ECL immunoblotting detection system (GE Healthcare, Buckinghamshire, UK) and developed on a C-DiGit ® Blot Scanner (LI-COR Biosciences, NE, USA). Results are expressed as the ratio of omentin-1 protein expression to that of a reference protein, α-tubulin. Relative densitometry analyses of the immunoblots were determined using IMAGE STUDIO software.

4.11 Glutathione Content Assay

The simultaneous assay for both GSH (reduced) and GSSG (oxidized) was done using the modified protocol of Mokrasch and Teschke, 1984 [174]. Stock standard solutions of GSH and GSSG (Sigma-Aldrich, MO, USA) were prepared in 10 mM solutions in 0.01 M HCO_2H. *o*-Pthaldehyde (Sigma-Aldrich, MO, USA) was prepared as 1mg/ml in methanol. For GSH and GSSG assay, 30 μL of VAT homogenates/cell lysates with 10 uL of 0.01 M HCO_2H or 40 μL of GSH/GSSG standards were mixed with 40 μL of buffered formaldehyde (1:4 (v/v) 37% formalin: 0.1 M Na_2HPO_4). After 1 to 5 minutes, for GSH assay, 0.4 mL of 0.1 M sodium phosphate: 5 mM EDTA (pH 8.0) was added to the mix. Meanwhile, for the GSSH assay, 0.4 mL 0.1 M NaOH was added to the mix. Afterward, 40 μL *o*-pthaldehyde was added to all wells. 250 μL of sample/standard solutions were then transferred into a 96-well fluorometric assay plate, in duplicates, for both GSH and GSSG assays. The plate was covered and left for 45 minutes at ambient temperature. Finally, the fluorescence was measured in the excitation wavelength 345 nm and the fluorescent wavelength 425 nm using an EnSpire® Multimode Plate Reader (PerkinElmer, Waltham, MA USA). The GSH and GSSG concentration of samples were calculated based on comparison to a standard curve generated from GSH and GSSG standards, respectively, and were normalized to total μg of proteins. GSH result was divided to GSSG result to obtain the GSH:GSSG ratio.

4.12 Superoxide Dismutase (SOD) Activity Assay

VAT homogenates/cell lysates containing total SOD activity from cytosol and mitochondria were used for the assay. Briefly, WST working solution (MAK379A) and enzyme working solution (MAK379B) were prepared according to the manufacturer's protocol (Sigma-Aldrich, MO, USA). The

sample/blank reaction mixes were then prepared in a 96-well plate according to the template included in the protocol. The samples were mixed well, and the plate was incubated at 37^0C for 20 minutes. Absorbance was read at 450 nm in an EnSpire® Multimode Plate Reader (PerkinElmer, Waltham, MA USA). Finally, the SOD activity (inhibition rate %) was calculated using the following formula: [[(A_{450} blank1 – A_{450} blank3) – (A_{450} sample – A_{450} blank2)] / (A_{450} blank1 – A_{450} blank3)] x 100.

4.13 Omentin-1 and TNF-α ELISA

The plasma level of omentin-1 in patients was measured using RayBio® Human/Mouse/Rat Omentin Enzyme Immunoassay Kit (RayBiotech, EIA-OME-1) according to the manufacturer's protocol. The design principle is competition-based ELISA. On the other hand, the omentin-1 level in VAT homogenates was measured using Human Omentin-1 ELISA Kit (BioVendor, RD191100200R) and the TNF-α levels of Huh7 and VAT supernatants were quantified by Human TNF alpha ELISA Kit (BioVendor, RAF128R). The design principle for both kits from Biovendor is sandwich ELISA. The levels of protein analytes from the samples were calculated based on comparison to a standard curve generated using their respective standards and were normalized to total μg of proteins.

4.14 Statistical Analysis

Unless indicated otherwise, all values are presented as means ± standard deviation (SD). The normal distribution of variables was evaluated by Kolmogorov–Smirnov test. Differences between two groups were assessed using the Mann-Whitney U test or student's t-test. Data involving more than two groups were assessed by One-way-ANOVA or Kruskal-Wallis test, followed by post-hoc analysis. Spearman rank correlation was used for the calculation of associations between variables. Specific analysis details are indicated in figure legends. Statistical significance was determined at $p < 0.05$. All figures and statistical analyses were generated using GraphPad Prism 9 and SPSS 29.

CHAPTER 6

CONCLUSION AND FUTURE PERSPECTIVES

Metabolic dysfunction-associated steatotic liver disease is a growing public emergency, affecting up to one-fourth of the global population. The pathogenesis of MASLD is complex, involving multiple molecular pathways and other non-hepatic players. For this reason, reliable biomarkers and effective drugs are still missing. To better understand the pathogenesis and to develop effective therapeutic strategies for MASLD, a translational approach is essential. Translational research aims to bridge the gap between basic science and clinical medicine by applying findings from preclinical studies to the development of diagnostic, preventive, and therapeutic approaches. Reverse translation is also critical in MASLD research because it facilitates the identification of relevant biomarkers, as well as the validation of therapeutic targets and efficacy in clinical trials. Therefore, in this Ph.D. research, translational research was utilized to fulfill the existing scientific gaps in terms of therapy, diagnosis, and pathophysiology of MASLD.

For the first part of this Ph.D. project, we evaluated the beneficial effects of two new compounds in reverting the MASLD-related molecular mechanisms. This study demonstrated that APPLIVER and ACTEOS compounds reduced TNF-α, a cytokine involved in the multiple steps process of MASH development. ACTEOS also showed a significant reduction in ROS generation and collagen production. The results suggest that APPLIVER and ACTEOS may be useful for the treatment of MASLD/MASH by mitigating the molecular mechanisms related to MASLD. The beneficial effects observed can be attributed to triterpenic acid and acteoside since they are the main components of APPLIVER and ACTEOS, respectively, but the contribution of other components present in the extracts cannot be excluded. Future studies could focus on assessing the effects of these compounds on other preclinical models of MASLD. An *in vivo* animal model, for example, can determine the compounds' bioavailability, safety, and efficacy before they can be utilized in the clinical MASLD/MASH setting.

The diagnosis of MASLD and fibrosis stage requires histological analysis, which has several limitations, making the development of alternative non-invasive diagnostic methods crucial. For the second part of this Ph.D. project, we identified and validated ficolin-2 (FCN-2) as a potential biomarker for fibrosis in the context of MASLD. Our study suggests that FCN-2, a plasma protein expressed by hepatocytes and secreted into the circulation, can serve as a potential biomarker for hepatic fibrosis. The present study showed a strong association between FCN-2 plasma level and fibrosis stage assessed by histological analysis. The plasma FCN-2 level was reduced in morbidly obese subjects with significant fibrosis and further reduced in cirrhosis, regardless of

fibrosis etiology. The plasma FCN-2 level was found to have good discriminative power in categorizing hepatic fibrosis, with an AUROC of 0.82 for diagnosis of significant fibrosis (F ≥ 2) and was superior to any other indexes tested (FIB-4, FORNS, and NFS). When combined with APRI and HDL in FCNscore, the plasma FCN-2 level yielded an excellent discriminative power with an AUC of 0.85. Based on the findings of the study, FCN-2 can be considered a potential non-invasive diagnostic biomarker for hepatic fibrosis, however, it remains to be validated in large independent cohorts. For future perspectives, the molecular mechanisms underlying the relationship between FCN-2 and MASLD pathogenesis, particularly fibrogenesis, can be elucidated through functional studies.

Obesity is a significant risk factor for MASLD, where the expansion of visceral adipose tissue contributes to numerous pathological events, including the dysregulation of adipocytokines. In the final phase of this Ph.D. project, we focused on identifying and characterizing a novel adipocytokine, involved in the development and progression of MASLD. Using a simple *in silico* analysis, omentin-1 has been identified as being differentially expressed between the VAT of obese versus obese MASH patients. Its role in MASLD using a variety of translational approaches has been investigated, including its beneficial effects in the MASLD-related inflammation, oxidative stress, ER stress, and insulin-glucose dysregulation. The present study suggests that a reduced level of omentin-1 is associated with MASLD development, probably via adipose tissue–liver crosstalk. Future perspectives should focus on identifying the specific receptor of omentin-1, which can serve as a pharmaceutical strategy and emerging therapy against MASLD through the development of omentin-1 analogs and omentin-1 receptor agonists. Additionally, investigating the crosstalk between the liver and VAT, and its relationship with omentin-1 action is crucial. Co-culture setup can be utilized to further elucidate the relationship between the hepatocytes and omentin-1 produced by VAT. Therefore, further research on the role of omentin-1 in MASLD is necessary, including larger, well-designed, multicentric, prospective, and longitudinal studies to elucidate its mechanisms and therapeutic potential, as well as its utility as a non-invasive biomarker.

REFERENCES

1. Younossi, Z.; Anstee, Q.M.; Marietti, M.; Hardy, T.; Henry, L.; Eslam, M.; George, J.; Bugianesi, E. Global Burden of NAFLD and NASH: Trends, Predictions, Risk Factors and Prevention. *Nat Rev Gastroenterol Hepatol* **2018**, *15*, 11–20, doi:10.1038/nrgastro.2017.109.
2. Ludwig, J.; Viggiano, T.R.; McGill, D.B.; Oh, B.J. Nonalcoholic Steatohepatitis: Mayo Clinic Experiences with a Hitherto Unnamed Disease. *Mayo Clin Proc* **1980**, *55*, 434–438.
3. Singh, S.P.; Anirvan, P.; Khandelwal, R.; Satapathy, S.K. Nonalcoholic Fatty Liver Disease (NAFLD) Name Change: Requiem or Reveille? *Journal of Clinical and Translational Hepatology* **2021**, *9*, 931–938, doi:10.14218/JCTH.2021.00174.
4. Puri, P.; Sanyal, A.J. Nonalcoholic Fatty Liver Disease: Definitions, Risk Factors, and Workup. *Clin Liver Dis (Hoboken)* **2012**, *1*, 99–103, doi:10.1002/cld.81.
5. Kim, C.H.; Younossi, Z.M. Nonalcoholic Fatty Liver Disease: A Manifestation of the Metabolic Syndrome. *Cleve Clin J Med* **2008**, *75*, 721–728, doi:10.3949/ccjm.75.10.721.
6. Eslam, M.; Sanyal, A.J.; George, J.; Sanyal, A.; Neuschwander-Tetri, B.; Tiribelli, C.; Kleiner, D.E.; Brunt, E.; Bugianesi, E.; Yki-Järvinen, H.; et al. MAFLD: A Consensus-Driven Proposed Nomenclature for Metabolic Associated Fatty Liver Disease. *Gastroenterology* **2020**, *158*, 1999-2014.e1, doi:10.1053/j.gastro.2019.11.312.
7. Lin, S.; Huang, J.; Wang, M.; Kumar, R.; Liu, Y.; Liu, S.; Wu, Y.; Wang, X.; Zhu, Y. Comparison of MAFLD and NAFLD Diagnostic Criteria in Real World. *Liver Int* **2020**, *40*, 2082–2089, doi:10.1111/liv.14548.
8. Fouad, Y.; Waked, I.; Bollipo, S.; Gomaa, A.; Ajlouni, Y.; Attia, D. What's in a Name? Renaming 'NAFLD' to 'MAFLD.' *Liver International* **2020**, *40*, 1254–1261, doi:10.1111/liv.14478.
9. Younossi, Z.M.; Rinella, M.E.; Sanyal, A.J.; Harrison, S.A.; Brunt, E.M.; Goodman, Z.; Cohen, D.E.; Loomba, R. From NAFLD to MAFLD: Implications of a Premature Change in Terminology. *Hepatology* **2021**, *73*, 1194, doi:10.1002/hep.31420.
10. Eslam, M.; Sarin, S.K.; Wong, V.W.-S.; Fan, J.-G.; Kawaguchi, T.; Ahn, S.H.; Zheng, M.-H.; Shiha, G.; Yilmaz, Y.; Gani, R.; et al. The Asian Pacific Association for the Study of the Liver Clinical Practice Guidelines for the Diagnosis and Management of Metabolic Associated Fatty Liver Disease. *Hepatol Int* **2020**, *14*, 889–919, doi:10.1007/s12072-020-10094-2.
11. Rinella, M.E.; Lazarus, J.V.; Ratziu, V.; Francque, S.M.; Sanyal, A.J.; Kanwal, F.; Romero, D.; Abdelmalek, M.F.; Anstee, Q.M.; Arab, J.P.; et al. A Multi-

Society Delphi Consensus Statement on New Fatty Liver Disease Nomenclature. *Journal of Hepatology* **2023**, *0*, doi:10.1016/j.jhep.2023.06.003.

12. Younossi, Z.M.; Koenig, A.B.; Abdelatif, D.; Fazel, Y.; Henry, L.; Wymer, M. Global Epidemiology of Nonalcoholic Fatty Liver Disease-Meta-Analytic Assessment of Prevalence, Incidence, and Outcomes. *Hepatology* **2016**, *64*, 73–84, doi:10.1002/hep.28431.
13. World Health Organization. Regional Office for Europe *WHO European Regional Obesity Report 2022*; World Health Organization. Regional Office for Europe, 2022; ISBN 978-92-890-5773-8.
14. Obesity and Overweight Available online: https://www.who.int/news-room/fact-sheets/detail/obesity-and-overweight (accessed on 2 September 2022).
15. Riazi, K.; Azhari, H.; Charette, J.H.; Underwood, F.E.; King, J.A.; Afshar, E.E.; Swain, M.G.; Congly, S.E.; Kaplan, G.G.; Shaheen, A.-A. The Prevalence and Incidence of NAFLD Worldwide: A Systematic Review and Meta-Analysis. *Lancet Gastroenterol Hepatol* **2022**, *7*, 851–861, doi:10.1016/S2468-1253(22)00165-0.
16. Rinella, M.E.; Neuschwander-Tetri, B.A.; Siddiqui, M.S.; Abdelmalek, M.F.; Caldwell, S.; Barb, D.; Kleiner, D.E.; Loomba, R. AASLD Practice Guidance on the Clinical Assessment and Management of Nonalcoholic Fatty Liver Disease. *Hepatology* **2023**, *77*, 1797, doi:10.1097/HEP.0000000000000323.
17. Zhou, F.; Zhou, J.; Wang, W.; Zhang, X.-J.; Ji, Y.-X.; Zhang, P.; She, Z.-G.; Zhu, L.; Cai, J.; Li, H. Unexpected Rapid Increase in the Burden of NAFLD in China From 2008 to 2018: A Systematic Review and Meta-Analysis. *Hepatology* **2019**, *70*, 1119–1133, doi:10.1002/hep.30702.
18. Liu, Y.; Zhong, G.-C.; Tan, H.-Y.; Hao, F.-B.; Hu, J.-J. Nonalcoholic Fatty Liver Disease and Mortality from All Causes, Cardiovascular Disease, and Cancer: A Meta-Analysis. *Sci Rep* **2019**, *9*, 11124, doi:10.1038/s41598-019-47687-3.
19. Ekstedt, M.; Hagström, H.; Nasr, P.; Fredrikson, M.; Stål, P.; Kechagias, S.; Hultcrantz, R. Fibrosis Stage Is the Strongest Predictor for Disease-Specific Mortality in NAFLD after up to 33 Years of Follow-Up. *Hepatology* **2015**, *61*, 1547–1554, doi:10.1002/hep.27368.
20. Friedman, S.L.; Neuschwander-Tetri, B.A.; Rinella, M.; Sanyal, A.J. Mechanisms of NAFLD Development and Therapeutic Strategies. *Nat Med* **2018**, *24*, 908–922, doi:10.1038/s41591-018-0104-9.
21. Ng, C.H.; Xiao, J.; Lim, W.H.; Chin, Y.H.; Yong, J.N.; Tan, D.J.H.; Tay, P.; Syn, N.; Foo, R.; Chan, M.; et al. Placebo Effect on Progression and Regression in NASH: Evidence from a Meta-Analysis. *Hepatology* **2022**, *75*, 1647–1661, doi:10.1002/hep.32315.
22. Sanyal, A.J.; Anstee, Q.M.; Trauner, M.; Lawitz, E.J.; Abdelmalek, M.F.; Ding, D.; Han, L.; Jia, C.; Huss, R.S.; Chung, C.; et al. Cirrhosis Regression Is Associated with Improved Clinical Outcomes in Patients with

Nonalcoholic Steatohepatitis. *Hepatology* **2022**, *75*, 1235–1246, doi:10.1002/hep.32204.

23. Wegermann, K.; Hyun, J.; Diehl, A.M. Molecular Mechanisms Linking Nonalcoholic Steatohepatitis to Cancer. *Clinical Liver Disease* **2021**, *17*, 6–10, doi:10.1002/cld.1006.
24. Sanyal, A.J.; Van Natta, M.L.; Clark, J.; Neuschwander-Tetri, B.A.; Diehl, A.; Dasarathy, S.; Loomba, R.; Chalasani, N.; Kowdley, K.; Hameed, B.; et al. Prospective Study of Outcomes in Adults with Nonalcoholic Fatty Liver Disease. *New England Journal of Medicine* **2021**, *385*, 1559–1569, doi:10.1056/NEJMoa2029349.
25. Bonsembiante, L.; Targher, G.; Maffeis, C. Non-Alcoholic Fatty Liver Disease in Obese Children and Adolescents: A Role for Nutrition? *Eur J Clin Nutr* **2022**, *76*, 28–39, doi:10.1038/s41430-021-00928-z.
26. Azzu, V.; Vacca, M.; Virtue, S.; Allison, M.; Vidal-Puig, A. Adipose Tissue-Liver Cross Talk in the Control of Whole-Body Metabolism: Implications in Nonalcoholic Fatty Liver Disease. *Gastroenterology* **2020**, *158*, 1899–1912, doi:10.1053/j.gastro.2019.12.054.
27. Pafili, K.; Kahl, S.; Mastrototaro, L.; Strassburger, K.; Pesta, D.; Herder, C.; Pützer, J.; Dewidar, B.; Hendlinger, M.; Granata, C.; et al. Mitochondrial Respiration Is Decreased in Visceral but Not Subcutaneous Adipose Tissue in Obese Individuals with Fatty Liver Disease. *Journal of Hepatology* **2022**, *77*, 1504–1514, doi:10.1016/j.jhep.2022.08.010.
28. EASL–EASD–EASO Clinical Practice Guidelines for the Management of Non-Alcoholic Fatty Liver Disease. *Journal of Hepatology* **2016**, *64*, 1388–1402, doi:10.1016/j.jhep.2015.11.004.
29. Ahmed, M.H.; Byrne, C.D. Obstructive Sleep Apnea Syndrome and Fatty Liver: Association or Causal Link? *World J Gastroenterol* **2010**, *16*, 4243–4252, doi:10.3748/wjg.v16.i34.4243.
30. Salvoza, N.C.; Giraudi, P.J.; Tiribelli, C.; Rosso, N. Sex Differences in Non-Alcoholic Fatty Liver Disease: Hints for Future Management of the Disease. *Explor Med.* **2020**, *1*, 51–74, doi:10.37349/emed.2020.00005.
31. Natalia Rosso; Stefano Bellentani Nonalcoholic Fatty Liver Disease: A Wide Spectrum Disease. In *Liver Diseases. Multidisciplinary Textbook*; Springer, 2020; pp. 273–284 ISBN 978-3-030-24431-6.
32. Day, C.P.; James, O.F.W. Steatohepatitis: A Tale of Two "Hits"? *Gastroenterology* **1998**, *114*, 842–845, doi:10.1016/S0016-5085(98)70599-2.
33. Tilg, H.; Moschen, A.R. Evolution of Inflammation in Nonalcoholic Fatty Liver Disease: The Multiple Parallel Hits Hypothesis. *Hepatology* **2010**, *52*, 1836–1846, doi:10.1002/hep.24001.
34. Godoy-Matos, A.F.; Silva Júnior, W.S.; Valerio, C.M. NAFLD as a Continuum: From Obesity to Metabolic Syndrome and Diabetes. *Diabetology & Metabolic Syndrome* **2020**, *12*, 60, doi:10.1186/s13098-020-00570-y.

35. Arroyave-Ospina, J.C.; Wu, Z.; Geng, Y.; Moshage, H. Role of Oxidative Stress in the Pathogenesis of Non-Alcoholic Fatty Liver Disease: Implications for Prevention and Therapy. *Antioxidants (Basel)* **2021**, *10*, 174, doi:10.3390/antiox10020174.
36. Pérez-Carreras, M.; Del Hoyo, P.; Martín, M.A.; Rubio, J.C.; Martín, A.; Castellano, G.; Colina, F.; Arenas, J.; Solis-Herruzo, J.A. Defective Hepatic Mitochondrial Respiratory Chain in Patients with Nonalcoholic Steatohepatitis. *Hepatology* **2003**, *38*, 999–1007, doi:10.1002/hep.1840380426.
37. Berson, A.; De Beco, V.; Lettéron, P.; Robin, M.A.; Moreau, C.; El Kahwaji, J.; Verthier, N.; Feldmann, G.; Fromenty, B.; Pessayre, D. Steatohepatitis-Inducing Drugs Cause Mitochondrial Dysfunction and Lipid Peroxidation in Rat Hepatocytes. *Gastroenterology* **1998**, *114*, 764–774, doi:10.1016/s0016-5085(98)70590-6.
38. Kawahara, H.; Fukura, M.; Tsuchishima, M.; Takase, S. Mutation of Mitochondrial DNA in Livers from Patients with Alcoholic Hepatitis and Nonalcoholic Steatohepatitis. *Alcohol Clin Exp Res* **2007**, *31*, S54-60, doi:10.1111/j.1530-0277.2006.00287.x.
39. Delli Bovi, A.P.; Marciano, F.; Mandato, C.; Siano, M.A.; Savoia, M.; Vajro, P. Oxidative Stress in Non-Alcoholic Fatty Liver Disease. An Updated Mini Review. *Frontiers in Medicine* **2021**, *8*.
40. Panic, A.; Stanimirovic, J.; Sudar-Milovanovic, E.; Isenovic, E.R. Oxidative Stress in Obesity and Insulin Resistance. *Explor Med.* **2022**, *3*, 58–70, doi:10.37349/emed.2022.00074.
41. Bañuls, C.; Rovira-Llopis, S.; Lopez-Domenech, S.; Diaz-Morales, N.; Blas-Garcia, A.; Veses, S.; Morillas, C.; Victor, V.M.; Rocha, M.; Hernandez-Mijares, A. Oxidative and Endoplasmic Reticulum Stress Is Impaired in Leukocytes from Metabolically Unhealthy vs Healthy Obese Individuals. *Int J Obes* **2017**, *41*, 1556–1563, doi:10.1038/ijo.2017.147.
42. Song, M.J.; Malhi, H. The Unfolded Protein Response and Hepatic Lipid Metabolism in Non-Alcoholic Fatty Liver Disease. *Pharmacol Ther* **2019**, *203*, 107401, doi:10.1016/j.pharmthera.2019.107401.
43. Chen, Z.; Tian, R.; She, Z.; Cai, J.; Li, H. Role of Oxidative Stress in the Pathogenesis of Nonalcoholic Fatty Liver Disease. *Free Radical Biology and Medicine* **2020**, *152*, 116–141, doi:10.1016/j.freeradbiomed.2020.02.025.
44. Angulo, P.; Kleiner, D.E.; Dam-Larsen, S.; Adams, L.A.; Bjornsson, E.S.; Charatcharoenwitthaya, P.; Mills, P.R.; Keach, J.C.; Lafferty, H.D.; Stahler, A.; et al. Liver Fibrosis, but No Other Histologic Features, Is Associated With Long-Term Outcomes of Patients With Nonalcoholic Fatty Liver Disease. *Gastroenterology* **2015**, *149*, 389-397.e10, doi:10.1053/j.gastro.2015.04.043.
45. Giraudi, P.J.; Barbero Becerra, V.J.; Marin, V.; Chavez-Tapia, N.C.; Tiribelli, C.; Rosso, N. The Importance of the Interaction between Hepatocyte and Hepatic Stellate Cells in Fibrogenesis Induced by Fatty Accumulation.

Experimental and Molecular Pathology **2015**, *98*, 85–92, doi:10.1016/j.yexmp.2014.12.006.

46. Barbero-Becerra, V.J.; Giraudi, P.J.; Chávez-Tapia, N.C.; Uribe, M.; Tiribelli, C.; Rosso, N. The Interplay between Hepatic Stellate Cells and Hepatocytes in an in Vitro Model of NASH. *Toxicology in Vitro* **2015**, *29*, 1753–1758, doi:10.1016/j.tiv.2015.07.010.
47. Wiering, L.; Subramanian, P.; Hammerich, L. Hepatic Stellate Cells: Dictating Outcome in Nonalcoholic Fatty Liver Disease. *Cell Mol Gastroenterol Hepatol* **2023**, *15*, 1277–1292, doi:10.1016/j.jcmgh.2023.02.010.
48. Chiyanika, C.; Wong, V.W.-S.; Wong, G.L.-H.; Chan, H.L.-Y.; Hui, S.C.N.; Yeung, D.K.W.; Chu, W.C.W. Implications of Abdominal Adipose Tissue Distribution on Nonalcoholic Fatty Liver Disease and Metabolic Syndrome: A Chinese General Population Study. *Clin Transl Gastroenterol* **2021**, *12*, e00300, doi:10.14309/ctg.0000000000000300.
49. Tilg, H.; Adolph, T.E.; Moschen, A.R. Multiple Parallel Hits Hypothesis in Nonalcoholic Fatty Liver Disease: Revisited After a Decade. *Hepatology* **2021**, *73*, 833–842, doi:10.1002/hep.31518.
50. Chao, H.-W.; Chao, S.-W.; Lin, H.; Ku, H.-C.; Cheng, C.-F. Homeostasis of Glucose and Lipid in Non-Alcoholic Fatty Liver Disease. *Int J Mol Sci* **2019**, *20*, 298, doi:10.3390/ijms20020298.
51. Kleiner, D.E.; Brunt, E.M.; Van Natta, M.; Behling, C.; Contos, M.J.; Cummings, O.W.; Ferrell, L.D.; Liu, Y.-C.; Torbenson, M.S.; Unalp-Arida, A.; et al. Design and Validation of a Histological Scoring System for Nonalcoholic Fatty Liver Disease. *Hepatology* **2005**, *41*, 1313–1321, doi:10.1002/hep.20701.
52. Sumida, Y.; Okanoue, T.; Nakajima, A.; Japan Study Group of NAFLD (JSG-NAFLD) Phase 3 Drug Pipelines in the Treatment of Non-Alcoholic Steatohepatitis. *Hepatol Res* **2019**, *49*, 1256–1262, doi:10.1111/hepr.13425.
53. Obeticholic Acid for the Treatment of Nonalcoholic Steatohepatitis: Expert Review of Gastroenterology & Hepatology: Vol 14, No 5 Available online: https://www.tandfonline.com/doi/full/10.1080/17474124.2020.1748498 (accessed on 24 April 2023).
54. Ratziu, V.; Harrison, S.A.; Francque, S.; Bedossa, P.; Lehert, P.; Serfaty, L.; Romero-Gomez, M.; Boursier, J.; Abdelmalek, M.; Caldwell, S.; et al. Elafibranor, an Agonist of the Peroxisome Proliferator-Activated Receptor-α and -δ, Induces Resolution of Nonalcoholic Steatohepatitis Without Fibrosis Worsening. *Gastroenterology* **2016**, *150*, 1147-1159.e5, doi:10.1053/j.gastro.2016.01.038.
55. Harrison, S.A.; Wong, V.W.-S.; Okanoue, T.; Bzowej, N.; Vuppalanchi, R.; Younes, Z.; Kohli, A.; Sarin, S.; Caldwell, S.H.; Alkhouri, N.; et al. Selonsertib for Patients with Bridging Fibrosis or Compensated Cirrhosis Due to NASH: Results from Randomized Phase III STELLAR Trials. *J Hepatol* **2020**, *73*, 26–39, doi:10.1016/j.jhep.2020.02.027.

56. Ratziu, V.; Sanyal, A.; Harrison, S.A.; Wong, V.W.-S.; Francque, S.; Goodman, Z.; Aithal, G.P.; Kowdley, K.V.; Seyedkazemi, S.; Fischer, L.; et al. Cenicriviroc Treatment for Adults With Nonalcoholic Steatohepatitis and Fibrosis: Final Analysis of the Phase 2b CENTAUR Study. *Hepatology* **2020**, *72*, 892–905, doi:10.1002/hep.31108.
57. Harrison, S.A.; Bashir, M.R.; Guy, C.D.; Zhou, R.; Moylan, C.A.; Frias, J.P.; Alkhouri, N.; Bansal, M.B.; Baum, S.; Neuschwander-Tetri, B.A.; et al. Resmetirom (MGL-3196) for the Treatment of Non-Alcoholic Steatohepatitis: A Multicentre, Randomised, Double-Blind, Placebo-Controlled, Phase 2 Trial. *Lancet* **2019**, *394*, 2012–2024, doi:10.1016/S0140-6736(19)32517-6.
58. Safadi, R.; Konikoff, F.M.; Mahamid, M.; Zelber-Sagi, S.; Halpern, M.; Gilat, T.; Oren, R.; FLORA Group The Fatty Acid-Bile Acid Conjugate Aramchol Reduces Liver Fat Content in Patients with Nonalcoholic Fatty Liver Disease. *Clin Gastroenterol Hepatol* **2014**, *12*, 2085-2091.e1, doi:10.1016/j.cgh.2014.04.038.
59. Devonas, M. Bench to Bedside — and Back to Bench Again Available online: https://www.christenseninstitute.org/blog/bench-to-bedside-and-back-to-bench-again/ (accessed on 5 October 2022).
60. Rosso, N.; Chavez-Tapia, N.C.; Tiribelli, C.; Bellentani, S. Translational Approaches: From Fatty Liver to Non-Alcoholic Steatohepatitis. *World J Gastroenterol* **2014**, *20*, 9038–9049, doi:10.3748/wjg.v20.i27.9038.
61. Musyuni, P.; Sharma, R.; Aggarwal, G. Optimizing Drug Discovery: An Opportunity and Application with Reverse Translational Research. *Health Sciences Review* **2023**, *6*, 100074, doi:10.1016/j.hsr.2022.100074.
62. Ramos, M.J.; Bandiera, L.; Menolascina, F.; Fallowfield, J.A. In Vitro Models for Non-Alcoholic Fatty Liver Disease: Emerging Platforms and Their Applications. *iScience* **2022**, *25*, 103549, doi:10.1016/j.isci.2021.103549.
63. Marin, V.; Rosso, N.; Dal Ben, M.; Raseni, A.; Boschelle, M.; Degrassi, C.; Nemeckova, I.; Nachtigal, P.; Avellini, C.; Tiribelli, C.; et al. An Animal Model for the Juvenile Non-Alcoholic Fatty Liver Disease and Non-Alcoholic Steatohepatitis. *PLoS One* **2016**, *11*, doi:10.1371/journal.pone.0158817.
64. Mašek, T.; Barišić, J.; Micek, V.; Starčević, K. Cafeteria Diet and High-Fructose Rodent Models of NAFLD Differ in the Metabolism of Important PUFA and Palmitoleic Acid without Additional Influence of Sex. *Nutrients* **2020**, *12*, 3339, doi:10.3390/nu12113339.
65. Jain, S.; Norinder, U.; Escher, S.E.; Zdrazil, B. Combining In Vivo Data with In Silico Predictions for Modeling Hepatic Steatosis by Using Stratified Bagging and Conformal Prediction. *Chem. Res. Toxicol.* **2021**, *34*, 656–668, doi:10.1021/acs.chemrestox.0c00511.
66. Giraudi, P.J.; Gambaro, S.E.; Arroyo, S.O.; Chackelevicius, C.M.; Giuricin, M.; Silvestri, M.; Macor, D.; Crocé, L.S.; Bonazza, D.; Soardo, G.; et al. A

Simple in Silico Strategy Identifies Candidate Biomarkers for the Diagnosis of Liver Fibrosis in Morbidly Obese Subjects. *Liver International* **2018**, *38*, 155–163, doi:10.1111/liv.13505.

67. Giraudi, P.J.; Salvoza, N.; Bonazza, D.; Saitta, C.; Lombardo, D.; Casagranda, B.; de Manzini, N.; Pollicino, T.; Raimondo, G.; Tiribelli, C.; et al. Ficolin-2 Plasma Level Assesses Liver Fibrosis in Non-Alcoholic Fatty Liver Disease. *Int J Mol Sci* **2022**, *23*, 2813, doi:10.3390/ijms23052813.
68. du Plessis, J.; van Pelt, J.; Korf, H.; Mathieu, C.; van der Schueren, B.; Lannoo, M.; Oyen, T.; Topal, B.; Fetter, G.; Nayler, S.; et al. Association of Adipose Tissue Inflammation With Histologic Severity of Nonalcoholic Fatty Liver Disease. *Gastroenterology* **2015**, *149*, 635-648.e14, doi:10.1053/j.gastro.2015.05.044.
69. Zareifi, D.S.; Chaliotis, O.; Chala, N.; Meimetis, N.; Sofotasiou, M.; Zeakis, K.; Pantiora, E.; Vezakis, A.; Matsopoulos, G.K.; Fragulidis, G.; et al. A Network-Based Computational and Experimental Framework for Repurposing Compounds toward the Treatment of Non-Alcoholic Fatty Liver Disease. *iScience* **2022**, *25*, 103890, doi:10.1016/j.isci.2022.103890.
70. Tsukada, S.; Parsons, C.J.; Rippe, R.A. Mechanisms of Liver Fibrosis. *Clinica Chimica Acta* **2006**, *364*, 33–60, doi:10.1016/j.cca.2005.06.014.
71. Giraudi, P.J.; Barbero Becerra, V.J.; Marin, V.; Chavez-Tapia, N.C.; Tiribelli, C.; Rosso, N. The Importance of the Interaction between Hepatocyte and Hepatic Stellate Cells in Fibrogenesis Induced by Fatty Accumulation. *Experimental and Molecular Pathology* **2015**, *98*, 85–92, doi:10.1016/j.yexmp.2014.12.006.
72. Olech, M.; Ziemichód, W.; Nowacka-Jechalke, N. The Occurrence and Biological Activity of Tormentic Acid—A Review. *Molecules* **2021**, *26*, 3797, doi:10.3390/molecules26133797.
73. Zhang, T.-T.; Yang, L.; Jiang, J.-G. Tormentic Acid in Foods Exerts Anti-Proliferation Efficacy through Inducing Apoptosis and Cell Cycle Arrest. *Journal of Functional Foods* **2015**, *19*, 575–583, doi:10.1016/j.jff.2015.09.061.
74. Villar, A.; Payá, M.; Hortigüela, M.D.; Cortes, D. Tormentic Acid, a New Hypoglycemic Agent from Poterium Ancistroides. *Planta Med* **1986**, 43–45, doi:10.1055/s-2007-969065.
75. Wang, A.; Luo, J.; Moore, W.; Alkhalidy, H.; Wu, L.; Zhang, J.; Zhen, W.; Wang, Y.; Clegg, D.J.; Bin Xu, null; et al. GPR30 Regulates Diet-Induced Adiposity in Female Mice and Adipogenesis in Vitro. *Sci Rep* **2016**, *6*, 34302, doi:10.1038/srep34302.
76. Zhao, J.; Liu, T.; Ma, L.; Yan, M.; Zhao, Y.; Gu, Z.; Huang, Y. Protective Effect of Acteoside on Immunological Liver Injury Induced by Bacillus Calmette-Guerin plus Lipopolysaccharide. *Planta Med* **2009**, *75*, 1463–1469, doi:10.1055/s-0029-1185796.

77. Lee, Y.; Cho, I.J.; Kim, J.W.; Lee, M.; Ku, S.K.; Choi, J.; Lee, H. Hepatoprotective Effects of Blue Honeysuckle on CCl4-induced Acute Liver Damaged Mice. *Food Sci Nutr* **2018**, *7*, 322–338, doi:10.1002/fsn3.893.
78. Soret, P.-A.; Magusto, J.; Housset, C.; Gautheron, J. In Vitro and In Vivo Models of Non-Alcoholic Fatty Liver Disease: A Critical Appraisal. *J Clin Med* **2020**, *10*, 36, doi:10.3390/jcm10010036.
79. Anfuso, B.; Tiribelli, C.; Adorini, L.; Rosso, N. Obeticholic Acid and INT-767 Modulate Collagen Deposition in a NASH in Vitro Model. *Sci Rep* **2020**, *10*, doi:10.1038/s41598-020-58562-x.
80. Chavez-Tapia, N.C.; Rosso, N.; Tiribelli, C. Effect of Intracellular Lipid Accumulation in a New Model of Non-Alcoholic Fatty Liver Disease. *BMC Gastroenterol* **2012**, *12*, 20, doi:10.1186/1471-230X-12-20.
81. 14:00-17:00 ISO 10993-5:2009 Available online: https://www.iso.org/cms/render/live/en/sites/isoorg/contents/data/standard/03/64/36406.html (accessed on 7 February 2022).
82. Oliver, J.C.; Bland, L.A.; Oettinger, C.W.; Arduino, M.J.; McAllister, S.K.; Aguero, S.M.; Favero, M.S. Cytokine Kinetics in an in Vitro Whole Blood Model Following an Endotoxin Challenge. *Lymphokine Cytokine Res* **1993**, *12*, 115–120.
83. Held, F.; Hoppe, E.; Cvijovic, M.; Jirstrand, M.; Gabrielsson, J. Challenge Model of TNFα Turnover at Varying LPS and Drug Provocations. *J Pharmacokinet Pharmacodyn* **2019**, *46*, 223–240, doi:10.1007/s10928-019-09622-x.
84. A Novel Recombinant Slow-Release TNF α-Derived Peptide Effectively Inhibits Tumor Growth and Angiogensis | Scientific Reports Available online: https://www.nature.com/articles/srep13595) (accessed on 21 January 2022).
85. Estratti Naturali. *ABR*.
86. Domitrović, R.; Potočnjak, I. A Comprehensive Overview of Hepatoprotective Natural Compounds: Mechanism of Action and Clinical Perspectives. *Arch Toxicol* **2016**, *90*, 39–79, doi:10.1007/s00204-015-1580-z.
87. Jiang, W.-P.; Huang, S.-S.; Matsuda, Y.; Saito, H.; Uramaru, N.; Ho, H.-Y.; Wu, J.-B.; Huang, G.-J. Protective Effects of Tormentic Acid, a Major Component of Suspension Cultures of Eriobotrya Japonica Cells, on Acetaminophen-Induced Hepatotoxicity in Mice. *Molecules* **2017**, *22*, 830, doi:10.3390/molecules22050830.
88. Monica R., L.; Marco, B.; Nicodemo G., P.; Antoine, S.; Francesco, M.; Rosa, T. Antiproliferative Activities on Renal, Prostate and Melanoma Cancer Cell Lines of Sarcopoterium Spinosum Aerial Parts and Its Major Constituent Tormentic Acid. *Anti-Cancer Agents in Medicinal Chemistry* **2013**, *13*, 768–776.
89. Ma, A.; Wang, Y.; Zhang, Q. Tormentic Acid Reduces Inflammation in BV-2 Microglia by Activating the Liver X Receptor Alpha. *Neuroscience* **2015**, *287*, 9–14, doi:10.1016/j.neuroscience.2014.12.005.

90. Lin, X.; Zhang, S.; Huang, R.; Tan, S.; Liang, S.; Wu, X.; Zhuo, L.; Huang, Q. Protective Effect of Tormentic Acid from Potentilla Chinensis against Lipopolysaccharide/d-Galactosamine Induced Fulminant Hepatic Failure in Mice. *International Immunopharmacology* **2014**, *19*, 365–372, doi:10.1016/j.intimp.2014.02.009.
91. Alipieva, K.; Korkina, L.; Orhan, I.E.; Georgiev, M.I. Verbascoside — A Review of Its Occurrence, (Bio)Synthesis and Pharmacological Significance. *Biotechnology Advances* **2014**, *32*, 1065–1076, doi:10.1016/j.biotechadv.2014.07.001.
92. Attia, Y.M.; El-Kersh, D.M.; Wagdy, H.A.; Elmazar, M.M. Verbascoside: Identification, Quantification, and Potential Sensitization of Colorectal Cancer Cells to 5-FU by Targeting PI3K/AKT Pathway. *Scientific Reports* **2018**, *8*, 16939, doi:10.1038/s41598-018-35083-2.
93. Burgos, C.; Muñoz-Mingarro, D.; Navarro, I.; Martín-Cordero, C.; Acero, N. Neuroprotective Potential of Verbascoside Isolated from Acanthus Mollis L. Leaves through Its Enzymatic Inhibition and Free Radical Scavenging Ability. *Antioxidants (Basel)* **2020**, *9*, doi:10.3390/antiox9121207.
94. Wong, V.W.-S.; Adams, L.A.; de Lédinghen, V.; Wong, G.L.-H.; Sookoian, S. Noninvasive Biomarkers in NAFLD and NASH — Current Progress and Future Promise. *Nat Rev Gastroenterol Hepatol* **2018**, *15*, 461–478, doi:10.1038/s41575-018-0014-9.
95. Pierantonelli, I.; Svegliati-Baroni, G. Nonalcoholic Fatty Liver Disease: Basic Pathogenetic Mechanisms in the Progression From NAFLD to NASH. *Transplantation* **2019**, *103*, e1, doi:10.1097/TP.0000000000002480.
96. Anfuso, B.; Giraudi, P.J.; Tiribelli, C.; Rosso, N. Silybin Modulates Collagen Turnover in an In Vitro Model of NASH. *Molecules* **2019**, *24*, doi:10.3390/molecules24071280.
97. Kakino, S.; Ohki, T.; Nakayama, H.; Yuan, X.; Otabe, S.; Hashinaga, T.; Wada, N.; Kurita, Y.; Tanaka, K.; Hara, K.; et al. Pivotal Role of TNF-α in the Development and Progression of Nonalcoholic Fatty Liver Disease in a Murine Model. *Horm Metab Res* **2018**, *50*, 80–87, doi:10.1055/s-0043-118666.
98. Jiang, W.-P.; Huang, S.-S.; Matsuda, Y.; Saito, H.; Uramaru, N.; Ho, H.-Y.; Wu, J.-B.; Huang, G.-J. Protective Effects of Tormentic Acid, a Major Component of Suspension Cultures of Eriobotrya Japonica Cells, on Acetaminophen-Induced Hepatotoxicity in Mice. *Molecules* **2017**, *22*, 830, doi:10.3390/molecules22050830.
99. Masarone, M.; Rosato, V.; Dallio, M.; Gravina, A.G.; Aglitti, A.; Loguercio, C.; Federico, A.; Persico, M. Role of Oxidative Stress in Pathophysiology of Nonalcoholic Fatty Liver Disease. *Oxid Med Cell Longev* **2018**, *2018*, doi:10.1155/2018/9547613.
100. Wang, Y.-L.; Sun, G.-Y.; Zhang, Y.; He, J.-J.; Zheng, S.; Lin, J.-N. Tormentic Acid Inhibits H2O2-Induced Oxidative Stress and Inflammation in Rat

Vascular Smooth Muscle Cells via Inhibition of the NF-KB Signaling Pathway. *Mol Med Rep* **2016**, *14*, 3559–3564, doi:10.3892/mmr.2016.5690.

101. Wu, C.-H.; Chen, C.-H.; Hsieh, P.-F.; Lee, Y.-H.; Kuo, W.W.-T.; Wu, R.C.-Y.; Hung, C.-H.; Yang, Y.-L.; Lin, V.C. Verbascoside Inhibits the Epithelial-Mesenchymal Transition of Prostate Cancer Cells through High-Mobility Group Box 1/Receptor for Advanced Glycation End-Products/TGF-β Pathway. *Environmental Toxicology* **2021**, *36*, 1080–1089, doi:https://doi.org/10.1002/tox.23107.
102. Stefanovic, B.; Hellerbrand, C.; Holcik, M.; Briendl, M.; Aliebhaber, S.; Brenner, D.A. Posttranscriptional Regulation of Collagen Alpha1(I) MRNA in Hepatic Stellate Cells. *Mol Cell Biol* **1997**, *17*, 5201–5209, doi:10.1128/mcb.17.9.5201.
103. Lin, X.; Li, Y.; Zhang, X.; Wei, Y.; Wen, S.; Lu, Z.; Huang, Q.; Wei, J. Tormentic Acid Inhibits Hepatic Stellate Cells Activation via Blocking PI3K/Akt/MTOR and NF-KB Signalling Pathways. *Cell Biochemistry and Function* **2021**, *39*, 77–87, doi:https://doi.org/10.1002/cbf.3564.
104. Xu, L.; Hui, A.Y.; Albanis, E.; Arthur, M.J.; O'Byrne, S.M.; Blaner, W.S.; Mukherjee, P.; Friedman, S.L.; Eng, F.J. Human Hepatic Stellate Cell Lines, LX-1 and LX-2: New Tools for Analysis of Hepatic Fibrosis. *Gut* **2005**, *54*, 142–151, doi:10.1136/gut.2004.042127.
105. Taimr, P.; Higuchi, H.; Kocova, E.; Rippe, R.A.; Friedman, S.; Gores, G.J. Activated Stellate Cells Express the TRAIL Receptor-2/Death Receptor-5 and Undergo TRAIL-Mediated Apoptosis. *Hepatology* **2003**, *37*, 87–95, doi:10.1053/jhep.2003.50002.
106. Bhatia, S.N.; Balis, U.J.; Yarmush, M.L.; Toner, M. Effect of Cell–Cell Interactions in Preservation of Cellular Phenotype: Cocultivation of Hepatocytes and Nonparenchymal Cells. *The FASEB Journal* **1999**, *13*, 1883–1900, doi:10.1096/fasebj.13.14.1883.
107. Grant, A.; Neuberger, J. Guidelines on the Use of Liver Biopsy in Clinical Practice. *Gut* **1999**, *45*, IV1–IV11, doi:10.1136/gut.45.2008.iv1.
108. Sterling, R.K.; Lissen, E.; Clumeck, N.; Sola, R.; Correa, M.C.; Montaner, J.; S Sulkowski, M.; Torriani, F.J.; Dieterich, D.T.; Thomas, D.L.; et al. Development of a Simple Noninvasive Index to Predict Significant Fibrosis in Patients with HIV/HCV Coinfection. *Hepatology* **2006**, *43*, 1317–1325, doi:10.1002/hep.21178.
109. Boyle, M.; Tiniakos, D.; Schattenberg, J.M.; Ratziu, V.; Bugianessi, E.; Petta, S.; Oliveira, C.P.; Govaere, O.; Younes, R.; McPherson, S.; et al. Performance of the PRO-C3 Collagen Neo-Epitope Biomarker in Non-Alcoholic Fatty Liver Disease. *JHEP Rep* **2019**, *1*, 188–198, doi:10.1016/j.jhepr.2019.06.004.
110. Younossi, Z.M.; Loomba, R.; Anstee, Q.M.; Rinella, M.E.; Bugianesi, E.; Marchesini, G.; Neuschwander-Tetri, B.A.; Serfaty, L.; Negro, F.; Caldwell, S.H.; et al. Diagnostic Modalities for Nonalcoholic Fatty Liver Disease,

Nonalcoholic Steatohepatitis, and Associated Fibrosis. *Hepatology* **2018**, *68*, 349–360, doi:10.1002/hep.29721.

111. Mardinoglu, A.; Boren, J.; Smith, U.; Uhlen, M.; Nielsen, J. Systems Biology in Hepatology: Approaches and Applications. *Nature Reviews Gastroenterology & Hepatology* **2018**, *15*, 365–377, doi:10.1038/s41575-018-0007-8.
112. Page, S.; Birerdinc, A.; Estep, M.; Stepanova, M.; Afendy, A.; Petricoin, E.; Younossi, Z.; Chandhoke, V.; Baranova, A. Knowledge-Based Identification of Soluble Biomarkers: Hepatic Fibrosis in NAFLD as an Example. *PLoS One* **2013**, *8*, e56009, doi:10.1371/journal.pone.0056009.
113. Hotta, K.; Kikuchi, M.; Kitamoto, T.; Kitamoto, A.; Ogawa, Y.; Honda, Y.; Kessoku, T.; Kobayashi, K.; Yoneda, M.; Imajo, K.; et al. Identification of Core Gene Networks and Hub Genes Associated with Progression of Non-Alcoholic Fatty Liver Disease by RNA Sequencing. *Hepatol. Res.* **2017**, doi:10.1111/hepr.12877.
114. Ryaboshapkina, M.; Hammar, M. Human Hepatic Gene Expression Signature of Non-Alcoholic Fatty Liver Disease Progression, a Meta-Analysis., Human Hepatic Gene Expression Signature of Non-Alcoholic Fatty Liver Disease Progression, a Meta-Analysis. *Sci Rep* **2017**, *7*, *7*, 12361–12361, doi:10.1038/s41598-017-10930-w, 10.1038/s41598-017-10930-w.
115. Uhlén, M.; Fagerberg, L.; Hallström, B.M.; Lindskog, C.; Oksvold, P.; Mardinoglu, A.; Sivertsson, Å.; Kampf, C.; Sjöstedt, E.; Asplund, A.; et al. Proteomics. Tissue-Based Map of the Human Proteome. *Science* **2015**, *347*, 1260419, doi:10.1126/science.1260419.
116. Younossi, Z.M.; Koenig, A.B.; Abdelatif, D.; Fazel, Y.; Henry, L.; Wymer, M. Global Epidemiology of Nonalcoholic Fatty Liver Disease-Meta-Analytic Assessment of Prevalence, Incidence, and Outcomes. *Hepatology* **2016**, *64*, 73–84, doi:10.1002/hep.28431.
117. Estes, C.; Anstee, Q.M.; Arias-Loste, M.T.; Bantel, H.; Bellentani, S.; Caballeria, J.; Colombo, M.; Craxi, A.; Crespo, J.; Day, C.P.; et al. Modeling NAFLD Disease Burden in China, France, Germany, Italy, Japan, Spain, United Kingdom, and United States for the Period 2016-2030. *J Hepatol* **2018**, *69*, 896–904, doi:10.1016/j.jhep.2018.05.036.
118. Godoy-Matos, A.F.; Silva Júnior, W.S.; Valerio, C.M. NAFLD as a Continuum: From Obesity to Metabolic Syndrome and Diabetes. *Diabetol Metab Syndr* **2020**, *12*, doi:10.1186/s13098-020-00570-y.
119. Polyzos, S.A.; Kountouras, J.; Mantzoros, C.S. Obesity and Nonalcoholic Fatty Liver Disease: From Pathophysiology to Therapeutics. *Metabolism Clinical and Experimental* **2019**, 16.
120. Machado, M.; Marques-Vidal, P.; Cortez-Pinto, H. Hepatic Histology in Obese Patients Undergoing Bariatric Surgery. *J Hepatol* **2006**, *45*, 600–606, doi:10.1016/j.jhep.2006.06.013.

121. Raimondo, G.; Saitta, C.; Lombardo, D.; Giraudi, P.J.; Rosso, N.; Ieni, A.; Lazzara, S.; Palmisano, S.; Bonazza, D.; Alibrandi, A.; et al. Occult Hepatitis B Virus Infection Predicts Non-Alcoholic Steatohepatitis in Severely Obese Individuals from Italy. *Liver Int* **2020**, *40*, 1601–1609, doi:10.1111/liv.14473.
122. Dulai, P.S.; Singh, S.; Patel, J.; Soni, M.; Prokop, L.J.; Younossi, Z.; Sebastiani, G.; Ekstedt, M.; Hagstrom, H.; Nasr, P.; et al. Increased Risk of Mortality by Fibrosis Stage in Nonalcoholic Fatty Liver Disease: Systematic Review and Meta-Analysis. *Hepatology* **2017**, *65*, 1557–1565, doi:10.1002/hep.29085.
123. Dai, Y.-N.; Tu, Y.-X.; Meng, D.; Chen, M.-J.; Zhang, J.-J.; Gong, Y.-H.; Tong, Y.-X.; Wang, M.-S.; Pan, H.-Y.; Huang, H.-J. Serum Proteomic Changes as Candidate Biomarkers of Intermediate Liver Fibrosis in Chronic Hepatitis B Infection. *OMICS: A Journal of Integrative Biology* **2019**, *23*, 167–179, doi:10.1089/omi.2018.0179.
124. Chen, T.; Hu, Y.; Ding, Q.; Yu, J.; Wang, F.; Luo, F.; Zhang, X.-L. Serum Ficolin-2 Concentrations Are Significantly Changed in Patients with Hepatitis B Virus Infection and Liver Diseases. *Virol. Sin.* **2015**, *30*, 249–260, doi:10.1007/s12250-015-3605-4.
125. Liu, J.; Ali, M.A.M.; Shi, Y.; Zhao, Y.; Luo, F.; Yu, J.; Xiang, T.; Tang, J.; Li, D.; Hu, Q.; et al. Specifically Binding of L-Ficolin to N -Glycans of HCV Envelope Glycoproteins E1 and E2 Leads to Complement Activation. *Cellular & Molecular Immunology* **2009**, *6*, 235–244, doi:10.1038/cmi.2009.32.
126. Kilpatrick, D.C.; Chalmers, J.D. Human L-Ficolin (Ficolin-2) and Its Clinical Significance. *J Biomed Biotechnol* **2012**, *2012*, doi:10.1155/2012/138797.
127. Thomsen, T.; Schlosser, A.; Holmskov, U.; Sorensen, G.L. Ficolins and FIBCD1: Soluble and Membrane Bound Pattern Recognition Molecules with Acetyl Group Selectivity. *Mol Immunol* **2011**, *48*, 369–381, doi:10.1016/j.molimm.2010.09.019.
128. Swierzko, A.S.; Atkinson, A.P.M.; Cedzynski, M.; Macdonald, S.L.; Szala, A.; Domzalska-Popadiuk, I.; Borkowska-Klos, M.; Jopek, A.; Szczapa, J.; Matsushita, M.; et al. Two Factors of the Lectin Pathway of Complement, l-Ficolin and Mannan-Binding Lectin, and Their Associations with Prematurity, Low Birthweight and Infections in a Large Cohort of Polish Neonates. *Mol Immunol* **2009**, *46*, 551–558, doi:10.1016/j.molimm.2008.07.025.
129. Harrison, S.A.; Ratziu, V.; Boursier, J.; Francque, S.; Bedossa, P.; Majd, Z.; Cordonnier, G.; Sudrik, F.B.; Darteil, R.; Liebe, R.; et al. A Blood-Based Biomarker Panel (NIS4) for Non-Invasive Diagnosis of Non-Alcoholic Steatohepatitis and Liver Fibrosis: A Prospective Derivation and Global Validation Study. *The Lancet Gastroenterology & Hepatology* **2020**, *5*, 970–985, doi:10.1016/S2468-1253(20)30252-1.
130. Hardy, T.; Wonders, K.; Younes, R.; Aithal, G.P.; Aller, R.; Allison, M.; Bedossa, P.; Betsou, F.; Boursier, J.; Brosnan, M.J.; et al. The European NAFLD Registry: A Real-World Longitudinal Cohort Study of

Nonalcoholic Fatty Liver Disease. *Contemp Clin Trials* **2020**, *98*, 106175, doi:10.1016/j.cct.2020.106175.

131. Cosentino, F.; Grant, P.J.; Aboyans, V.; Bailey, C.J.; Ceriello, A.; Delgado, V.; Federici, M.; Filippatos, G.; Grobbee, D.E.; Hansen, T.B.; et al. 2019 ESC Guidelines on Diabetes, Pre-Diabetes, and Cardiovascular Diseases Developed in Collaboration with the EASD: The Task Force for Diabetes, Pre-Diabetes, and Cardiovascular Diseases of the European Society of Cardiology (ESC) and the European Association for the Study of Diabetes (EASD). *European Heart Journal* **2020**, *41*, 255–323, doi:10.1093/eurheartj/ehz486.
132. Giraudi, P.J.; Gambaro, S.E.; Arroyo, S.O.; Chackelevicius, C.M.; Giuricin, M.; Silvestri, M.; Macor, D.; Crocé, L.S.; Bonazza, D.; Soardo, G.; et al. A Simple in Silico Strategy Identifies Candidate Biomarkers for the Diagnosis of Liver Fibrosis in Morbidly Obese Subjects. *Liver International* **2018**, *38*, 155–163, doi:10.1111/liv.13505.
133. Hepatology, T.L.G.& Obesity: Another Ongoing Pandemic. *The Lancet Gastroenterology & Hepatology* **2021**, *6*, 411, doi:10.1016/S2468-1253(21)00143-6.
134. Watanabe, T.; Watanabe-Kominato, K.; Takahashi, Y.; Kojima, M.; Watanabe, R. Adipose Tissue-Derived Omentin-1 Function and Regulation. In *Comprehensive Physiology*; John Wiley & Sons, Ltd, 2017; pp. 765–781 ISBN 978-0-470-65071-4.
135. de Oliveira dos Santos, A.R.; de Oliveira Zanuso, B.; Miola, V.F.B.; Barbalho, S.M.; Santos Bueno, P.C.; Flato, U.A.P.; Detregiachi, C.R.P.; Buchaim, D.V.; Buchaim, R.L.; Tofano, R.J.; et al. Adipokines, Myokines, and Hepatokines: Crosstalk and Metabolic Repercussions. *International Journal of Molecular Sciences* **2021**, *22*, 2639, doi:10.3390/ijms22052639.
136. Yang, R.-Z.; Lee, M.-J.; Hu, H.; Pray, J.; Wu, H.-B.; Hansen, B.C.; Shuldiner, A.R.; Fried, S.K.; McLenithan, J.C.; Gong, D.-W. Identification of Omentin as a Novel Depot-Specific Adipokine in Human Adipose Tissue: Possible Role in Modulating Insulin Action. *American Journal of Physiology-Endocrinology and Metabolism* **2006**, *290*, E1253–E1261, doi:10.1152/ajpendo.00572.2004.
137. Lee, J.-K.; Schnee, J.; Pang, M.; Wolfert, M.; Baum, L.G.; Moremen, K.W.; Pierce, M. Human Homologs of the Xenopus Oocyte Cortical Granule Lectin XL35. *Glycobiology* **2001**, *11*, 65–73, doi:10.1093/glycob/11.1.65.
138. de Souza Batista, C.M.; Yang, R.-Z.; Lee, M.-J.; Glynn, N.M.; Yu, D.-Z.; Pray, J.; Ndubuizu, K.; Patil, S.; Schwartz, A.; Kligman, M.; et al. Omentin Plasma Levels and Gene Expression Are Decreased in Obesity. *Diabetes* **2007**, *56*, 1655–1661, doi:10.2337/db06-1506.
139. Feng, W.-H.; Yuan, X.-W.; Tong, G.-Y.; Wang, W.-M.; Hu, Y.; Shen, S.-M.; Li, P.; Bi, Y.; Hu, J.; Shao, L.-L.; et al. Correlated Increase of Omentin-1 and

Adiponectin by Exenatide, Avandamet and Dietary Change in Diet-Induced Obese Rats. *Folia Biol (Praha)* **2013**, *59*, 217–224.
140. Greulich, S.; Chen, W.J.Y.; Maxhera, B.; Rijzewijk, L.J.; Meer, R.W. van der; Jonker, J.T.; Mueller, H.; Wiza, D.H. de; Floerke, R.-R.; Smiris, K.; et al. Cardioprotective Properties of Omentin-1 in Type 2 Diabetes: Evidence from Clinical and In Vitro Studies. *PLOS ONE* **2013**, *8*, e59697, doi:10.1371/journal.pone.0059697.
141. Kobayashi, H.; Uchimura, K.; Ishii, T.; Takahashi, K.; Mori, K.; Tsuchiya, K.; Furuya, F. Intelectin1 Ameliorates Macrophage Activation via Inhibiting the Nuclear Factor Kappa B Pathway. 8.
142. Bekaert, M.; Ouwens, D.M.; Hörbelt, T.; Van de Velde, F.; Fahlbusch, P.; Herzfeld de Wiza, D.; Van Nieuwenhove, Y.; Calders, P.; Praet, M.; Hoorens, A.; et al. Reduced Expression of Chemerin in Visceral Adipose Tissue Associates with Hepatic Steatosis in Patients with Obesity. *Obesity (Silver Spring)* **2016**, *24*, 2544–2552, doi:10.1002/oby.21674.
143. Page, M.J.; McKenzie, J.E.; Bossuyt, P.M.; Boutron, I.; Hoffmann, T.C.; Mulrow, C.D.; Shamseer, L.; Tetzlaff, J.M.; Akl, E.A.; Brennan, S.E.; et al. The PRISMA 2020 Statement: An Updated Guideline for Reporting Systematic Reviews. *BMJ* **2021**, *372*, n71, doi:10.1136/bmj.n71.
144. Home - GEO - NCBI Available online: https://www.ncbi.nlm.nih.gov/geo/ (accessed on 2 April 2023).
145. About GEO2R - GEO - NCBI Available online: https://www.ncbi.nlm.nih.gov/geo/info/geo2r.html (accessed on 2 April 2023).
146. UniProt Available online: https://www.uniprot.org/ (accessed on 2 April 2023).
147. The Human Protein Atlas Available online: https://www.proteinatlas.org/ (accessed on 2 April 2023).
148. Sattar, N.; Forrest, E.; Preiss, D. Non-Alcoholic Fatty Liver Disease. *BMJ* **2014**, *349*, g4596, doi:10.1136/bmj.g4596.
149. Tsuji, S.; Uehori, J.; Matsumoto, M.; Suzuki, Y.; Matsuhisa, A.; Toyoshima, K.; Seya, T. Human Intelectin Is a Novel Soluble Lectin That Recognizes Galactofuranose in Carbohydrate Chains of Bacterial Cell Wall. *J Biol Chem* **2001**, *276*, 23456–23463, doi:10.1074/jbc.M103162200.
150. Zhang, Y.-Y.; Zhou, L.-M. Omentin-1, a New Adipokine, Promotes Apoptosis through Regulating Sirt1-Dependent P53 Deacetylation in Hepatocellular Carcinoma Cells. *European Journal of Pharmacology* **2013**, *698*, 137–144, doi:10.1016/j.ejphar.2012.11.016.
151. Zhou, H.; Zhang, Z.; Qian, G.; Zhou, J. Omentin-1 Attenuates Adipose Tissue Inflammation via Restoration of TXNIP/NLRP3 Signaling in High-Fat Diet-Induced Obese Mice. *Fundamental & Clinical Pharmacology* **2020**, *34*, 721–735, doi:10.1111/fcp.12575.

152. Yamawaki, H.; Kuramoto, J.; Kameshima, S.; Usui, T.; Okada, M.; Hara, Y. Omentin, a Novel Adipocytokine Inhibits TNF-Induced Vascular Inflammation in Human Endothelial Cells. *Biochemical and Biophysical Research Communications* **2011**, *408*, 339–343, doi:10.1016/j.bbrc.2011.04.039.
153. Salvoza, N.; Bedin, C.; Saccani, A.; Tiribelli, C.; Rosso, N. The Beneficial Effects of Triterpenic Acid and Acteoside in an In Vitro Model of Nonalcoholic Steatohepatitis (NASH). *International Journal of Molecular Sciences* **2022**, *23*, 3562, doi:10.3390/ijms23073562.
154. Liu, T.; Zhang, L.; Joo, D.; Sun, S.-C. NF-KB Signaling in Inflammation. *Sig Transduct Target Ther* **2017**, *2*, 1–9, doi:10.1038/sigtrans.2017.23.
155. Sharma, G.; Prossnitz, E.R. G-Protein-Coupled Estrogen Receptor (GPER) and Sex-Specific Metabolic Homeostasis. *Adv Exp Med Biol* **2017**, *1043*, 427–453, doi:10.1007/978-3-319-70178-3_20.
156. Jorge-Galarza, E.; Medina-Urrutia, A.; Posadas-Sánchez, R.; Posadas-Romero, C.; Cardoso-Saldaña, G.; Vargas-Alarcón, G.; Caracas-Portilla, N.; González-Salazar, C.; Torres-Tamayo, M.; Juárez-Rojas, J.G. Adipose Tissue Dysfunction Increases Fatty Liver Association with Pre Diabetes and Newly Diagnosed Type 2 Diabetes Mellitus. *Diabetology & Metabolic Syndrome* **2016**, *8*, 73, doi:10.1186/s13098-016-0189-6.
157. Alcalá, M.; Calderon-Dominguez, M.; Bustos, E.; Ramos, P.; Casals, N.; Serra, D.; Viana, M.; Herrero, L. Increased Inflammation, Oxidative Stress and Mitochondrial Respiration in Brown Adipose Tissue from Obese Mice. *Sci Rep* **2017**, *7*, 16082, doi:10.1038/s41598-017-16463-6.
158. Asrih, M.; Jornayvaz, F.R. Inflammation as a Potential Link between Nonalcoholic Fatty Liver Disease and Insulin Resistance. *J Endocrinol* **2013**, *218*, R25-36, doi:10.1530/JOE-13-0201.
159. Furukawa, S.; Fujita, T.; Shimabukuro, M.; Iwaki, M.; Yamada, Y.; Nakajima, Y.; Nakayama, O.; Makishima, M.; Matsuda, M.; Shimomura, I. Increased Oxidative Stress in Obesity and Its Impact on Metabolic Syndrome Available online: https://www.jci.org/articles/view/21625/pdf (accessed on 25 October 2022).
160. Hotamisligil, G.S.; Arner, P.; Caro, J.F.; Atkinson, R.L.; Spiegelman, B.M. Increased Adipose Tissue Expression of Tumor Necrosis Factor-Alpha in Human Obesity and Insulin Resistance. *J Clin Invest* **1995**, *95*, 2409–2415, doi:10.1172/JCI117936.
161. Christodoulatos, G.S.; Antonakos, G.; Karampela, I.; Psallida, S.; Stratigou, T.; Vallianou, N.; Lekka, A.; Marinou, I.; Vogiatzakis, E.; Kokoris, S.; et al. Circulating Omentin-1 as a Biomarker at the Intersection of Postmenopausal Breast Cancer Occurrence and Cardiometabolic Risk: An Observational Cross-Sectional Study. *Biomolecules* **2021**, *11*, 1609, doi:10.3390/biom11111609.
162. Du, Y.; Ji, Q.; Cai, L.; Huang, F.; Lai, Y.; Liu, Y.; Yu, J.; Han, B.; Zhu, E.; Zhang, J.; et al. Association between Omentin-1 Expression in Human

Epicardial Adipose Tissue and Coronary Atherosclerosis. *Cardiovascular Diabetology* **2016**, *15*, 90, doi:10.1186/s12933-016-0406-5.

163. Tan, B.K.; Adya, R.; Farhatullah, S.; Lewandowski, K.C.; O'Hare, P.; Lehnert, H.; Randeva, H.S. Omentin-1, a Novel Adipokine, Is Decreased in Overweight Insulin-Resistant Women with Polycystic Ovary Syndrome: Ex Vivo and in Vivo Regulation of Omentin-1 by Insulin and Glucose. *Diabetes* **2008**, *57*, 801–808, doi:10.2337/db07-0990.
164. Nonnecke, E.B.; Castillo, P.A.; Akahoshi, D.T.; Goley, S.M.; Bevins, C.L.; Lönnerdal, B. Characterization of an Intelectin-1 (Itln1) Knockout Mouse Model. *Frontiers in Immunology* **2022**, *13*.
165. Buzzetti, E.; Pinzani, M.; Tsochatzis, E.A. The Multiple-Hit Pathogenesis of Non-Alcoholic Fatty Liver Disease (NAFLD). *Metab. Clin. Exp.* **2016**, *65*, 1038–1048, doi:10.1016/j.metabol.2015.12.012.
166. Spencer, N.Y.; Zhou, W.; Li, Q.; Zhang, Y.; Luo, M.; Yan, Z.; Lynch, T.J.; Abbott, D.; Banfi, B.; Engelhardt, J.F. Hepatocytes Produce TNF-α Following Hypoxia-Reoxygenation and Liver Ischemia-Reperfusion in a NADPH Oxidase- and c-Src-Dependent Manner. *American Journal of Physiology-Gastrointestinal and Liver Physiology* **2013**, *305*, G84–G94, doi:10.1152/ajpgi.00430.2012.
167. Kern, P.A.; Saghizadeh, M.; Ong, J.M.; Bosch, R.J.; Deem, R.; Simsolo, R.B. The Expression of Tumor Necrosis Factor in Human Adipose Tissue. Regulation by Obesity, Weight Loss, and Relationship to Lipoprotein Lipase. *J Clin Invest* **1995**, *95*, 2111–2119.
168. Zhong, X.; Li, X.; Liu, F.; Tan, H.; Shang, D. Omentin Inhibits TNF-α-Induced Expression of Adhesion Molecules in Endothelial Cells via ERK/NF-KB Pathway. *Biochemical and Biophysical Research Communications* **2012**, *425*, 401–406, doi:10.1016/j.bbrc.2012.07.110.
169. Hayden, M.S.; Ghosh, S. Regulation of NF-KB by TNF Family Cytokines. *Semin Immunol* **2014**, *26*, 253–266, doi:10.1016/j.smim.2014.05.004.
170. Imrie, D.; Sadler, K.C. Stress Management: How the Unfolded Protein Response Impacts Fatty Liver Disease. *Journal of Hepatology* **2012**, *57*, 1147–1151, doi:10.1016/j.jhep.2012.06.018.
171. Nakatsuka, A.; Wada, J.; Iseda, I.; Teshigawara, S.; Higashio, K.; Murakami, K.; Kanzaki, M.; Inoue, K.; Terami, T.; Katayama, A.; et al. Vaspin Is an Adipokine Ameliorating ER Stress in Obesity as a Ligand for Cell-Surface GRP78/MTJ-1 Complex. *Diabetes* **2012**, *61*, 2823–2832, doi:10.2337/db12-0232.
172. Heberle, H.; Meirelles, G.V.; Da Silva, F.R.; Telles, G.P.; Minghim, R. InteractiVenn: A Web-Based Tool for the Analysis of Sets through Venn Diagrams. *BMC Bioinformatics* **2015**, *16*, 169, doi:10.1186/s12859-015-0611-3.
173. Carswell, K.A.; Lee, M.-J.; Fried, S.K. Culture of Isolated Human Adipocytes and Isolated Adipose Tissue. *Methods Mol Biol* **2012**, *806*, 203–214, doi:10.1007/978-1-61779-367-7_14.

174. Mokrasch, L.C.; Teschke, E.J. Glutathione Content of Cultured Cells and Rodent Brain Regions: A Specific Fluorometric Assay. *Analytical Biochemistry* **1984**, *140*, 506–509, doi:10.1016/0003-2697(84)90201-X.

CHAPTER 7

RESEARCH DISSEMINATION

List of Publications

Salvoza N, Giraudi PJ, Gazzin S, Bonazza D, de Manzini N, Zanconari F, Palmisano S, Tiribelli C, Rosso N. The potential role of Omentin-1 in Obesity-Related Metabolic dysfunction-associated steatotic liver disease (MASLD): Evidence from translational studies (manuscript in preparation).

Salvoza N, Bedin C, Saccani A, Tiribelli C, Rosso N. The Beneficial Effects of Triterpenic Acid and Acteoside in an In Vitro Model of Nonalcoholic Steatohepatitis (NASH). International Journal of Molecular Sciences. 2022; 23(7):3562. https://doi.org/10.3390/ijms23073562

Giraudi PJ, **Salvoza N,** Bonazza D, Saitta C, Lombardo D, Casagranda B, de Manzini N, Pollicino T, Raimondo G, Tiribelli C, Palmisano S, Rosso N. Ficolin-2 Plasma Levels Assess Liver Fibrosis in Non-Alcoholic Fatty Liver Disease. International Journal of Molecular Sciences. 2022; 23(5):2813. https://doi.org/10.3390/ijms23052813

Salvoza N, Giraudi PJ, Tiribelli C, Rosso N. Natural Compounds for Counteracting Nonalcoholic Fatty Liver Disease (NAFLD): Advantages and Limitations of the Suggested Candidates. International Journal of Molecular Sciences. 2022; 23(5):2764. https://doi.org/10.3390/ijms23052764

Salvoza N, Giraudi Pj, Tiribelli C, Rosso N. Sex Differences in Non-Alcoholic Fatty Liver Disease: Hints for Future Management of the Disease. Explor Med. 2020;1:51–74. DOI: https://Doi.Org/10.37349/Emed.2020.0000

Poster Presentations

The potential role of Omentin-1 in Metabolic Associated Fatty Liver Disease (MAFLD): evidence from translational studies. "The International Liver Congress" by The European Association for the Study of the Liver (EASL). Vienna, Austria. June 21-24, 2023.

In silico identification and validation of plasma Ficolin-2 (FCN-2) as non-invasive biomarker of fibrosis in Non-alcoholic Fatty Liver Disease (NAFLD). "The

International Liver Congress" by The European Association for the Study of the Liver (EASL). London, United Kingdom. June 22-26, 2022.

Anti-oxidant, Anti-inflammatory, and Anti-fibrotic Properties of Triterpenic Acid and Acteoside in *In Vitro* Models of Non-Alcoholic Steatohepatitis (NASH). "International Conference on Fatty Liver". Vienna, Austria. February 17-22, 2022.

Anti-oxidant, Anti-inflammatory, and Anti-fibrotic Properties of Triterpenic Acids ABRTA22 (TA) and Phenylpropanoids ABRPP09 (PP) in *In Vitro* Models of Non-Alcoholic Steatohepatitis. "Digital NAFLD Summit" by the European Association for the Study of the Liver (EASL). Italy. September 16-17, 2021.

Alternative Compounds to Nonalcoholic Steatohepatitis (NASH) Treatment: In Vitro Evidence of Triterpenic Acids and Phenylpropanoids" "The Liver Meeting" by The American Association for the Study of the Liver Diseases. Digital Platform. November 12-15, 2021.

Anti-oxidant, Anti-Inflammatory, and Anti-fibrotic Properties of Triterpenic Acids ABRTA22 (TA) and Phenylpropanoids ABRPP09 (PP) in *In Vitro* Models of Non-Alcoholic Steatohepatitis. "The International Liver Congress" by The European Association for the Study of the Liver (EASL). Italy. June 23-26, 2021.

Oral Presentations

2022 World Research and Innovation Festival (A Virtual Conference). Organized by West Visayas State University (Philippines), Mahidol University (Thailand), and Universitas Islam Negeri (Indonesia). "Bench to Bedside and Back: Translational Models in studying Non-alcoholic Fatty Liver Disease (NAFLD)." October 17-19, 2022. Keynote Speaker.

St. Luke's Molecular Medicine Society's Webinar Series, Back to Basics: Benchside Research. "Translational Approach for the Study of Non-Alcoholic Fatty Liver Disease: A Wide Spectrum Disease". Philippines (via Online Meeting)." October 31, 2020. Keynote Speaker.